Biogeochemistry of denitrifying bioreactors to enhance phosphorus removal from agricultural subsurface drainage

A thesis

submitted in fulfilment of the requirement for the degree

of

Doctor of Philosophy in Environmental Science

at

The University of Waikato

By

M G N Perera

THE UNIVERSITY OF
WAIKATO
Te Whare Wānanga o Waikato

2024

Table of Contents

List of Figures

List of Tables

Abstract

Degradation of water quality due to nutrient over-enrichment has become a global environmental concern. In Aotearoa, agricultural pollution of freshwaters by nutrients is increasing. Therefore, strategies need to be implemented to minimize nutrient pollution in surface waters. Denitrifying bioreactors (DBRs) are a prominent edge-of-field treatment technology to mitigate surface water nitrate loadings from agricultural subsurface drainage. Recent studies have identified that subsurface drainage can also contribute to the loss of phosphorus from agricultural soil. Therefore, this thesis investigates the potential of DBRs to incorporate iron-based materials to sequester phosphorus and reduce pollution of waterways.

There is some evidence suggesting low-level phosphorus removal by woodchip bioreactors alone. However, it is inevitable that woodchips alone do not abiotically remove phosphorus due to the incompatibility between the surface charge of wood at neutral-to-acidic pH values. In this study, raw *pinus radiata*, and, thermally modified pyrolyzed woodchips were employed for surface modification, with view to enhancing P binding in DBRs.

We were mindful in the design of material functionalization to avoid complicated preparation steps, exotic or harmful reagents, and impractical particle sizes to ensure compatibility for large-scale applications in the agricultural landscape. Results indicated that the functionalization of wood media successfully inversed the surface charge, leading to a net positive charge within the favorable range for phosphorus adsorption under reactor-specific conditions (pH 5.5 − 6). The maximum adsorption capacity of functionalized wood and functionalized biochar corresponded to 65.8 mg g^{-1} and 31.4 mg g^{-1}, respectively, comparing well to values reported in the literature.

DBRs operate under varying hydraulic conditions, which results in variable flow rates, nutrient concentrations, redox status, pH, and many other variables that affect the operation of the bioreactor. The stability of iron hydr(oxide) composites is expected to be sensitive to some of these conditions, especially acidic and anaerobic conditions, which favor dissolution of iron hydr(oxide)s and therefore could adversely affect P removal. Furthermore, there are other likely products of reduced Fe^{2+} and orthophosphate (HPO_4^{2-}) that could form under the conditions anticipated. Therefore, the biogeochemical environment in the DBR was characterized to understand the stability of iron hydr(oxide)s and their ability to subsequently remove of phosphorus.

To date, there have been only limited investigations into the stability of iron hydr(oxide)s under real-world bioreactor conditions, and functionalisation studies often neglect the impact of oscillating redox conditions on the stability of Fe-based adsorbents. In light of this, bench-scale woodchip bioreactors were established, both with and without MnO_2, to evaluate the redox buffering capacity of MnO_2 with view to mitigating the reductive dissolution of iron oxide. This approach aimed to improve the retention of dissolved reactive phosphorus (DRP) on the introduced iron oxide surfaces. It was concluded that iron oxides effectively remove DRP and MnO_2 enhances nitrogen (N) removal, with slightly better performance observed in the treatment incorporating Fe oxides and MnO_2. Hence, it can be inferred that the addition of manganese and iron oxides proves advantageous as an amendment to the conventional woodchip substrate in DBRs to enhance nutrient removal.

This thesis has demonstrated that Fe-functionalized media can effectively remove DRP in agricultural drainage water. In addition, by incorporating MnO_2, Fe oxides can be stabilised under oscillating redox conditions, and therefore the combination of MnO_2 and Fe oxides could serve as a practical solution for DBRs to mitigate diffuse pollution in New Zealand. These findings offer insights for redesigning DBRs, providing a clearer understanding of the

dynamics of P removal in DBRs, and how functionalized media can be employed in the long term to remove phosphorus from agricultural drainage water, meeting water quality objectives while minimizing P releases.

Acknowledgements

I would like to express my sincere gratitude to my supervisors, Adam Hartland, Dorisel Torres-Rojas, Rupert Craggs, and Louis Schipper for their invaluable time, tremendous support, encouragement, and guidance throughout my PhD research. Adam, I extend my deepest thanks for your compassion, creative thinking, and research skills that have profoundly contributed to my growth as a researcher over the past four years. I appreciate the opportunity to be part of the research group and am grateful for my acceptance. I consider myself incredibly fortunate to have you as my chief supervisor.

Working with my co-supervisor, Dr. Dorisel Torres-Rojas, has been a great privilege, and I always felt like I had two chief supervisors. I am grateful for the wealth of knowledge I gained during our field visits and for your role in helping my development as an independent researcher. Thank you for your consistent support. Both of you have been a tremendous source of inspiration, and I am immensely thankful for the opportunities and guidance you provided.

I extend my appreciation to the research group Amir Mohomaddi, Sebastian Hopker, Thomas Corbett, Huma Saeed, and Mahdiyeh Salmanzadeh—for their exceptional support. Thank you for generously sharing your valuable knowledge, particularly in essential laboratory analysis skills. A special thanks to Linh, Harizah Hariz, Nandana Pathirage, and Isanka Diddeniya for your encouraging comments, support, and engaging conversations. Your contributions have greatly enriched my PhD journey.

I would like to acknowledge the Lincoln Agritech research group, Aldrin Rivas, Brian Moorhead, and Greg Barkle for their involvement in numerous field trips, assistance with sampling, and guidance on manuscript development. I am especially grateful to Greg Olsen at NIWA for his assistance with laboratory experiments during my time at NIWA.

A heartfelt thanks to my husband, Shehan, for his unwavering companionship and endless support. I feel fortunate to have you by my side, providing encouragement every step of the way.

I would also like to express my gratitude to my family, who, despite being thousands of miles away, have consistently encouraged me to pursue my passion and work towards my dreams. I am blessed to have your endless love and support.

Lastly, I extend my thanks to the National Institute of Water and Atmospheric Research (NIWA) for funding my PhD through the New Zealand Ministry of Business, Innovation, and Employment (MBIE) Endeavour Research Programme.

List of Abbreviations

Word/Acronym/ Abbreviation	Full description/ translation
Agricultural Drainage Water	A non-point (*diffuse*) source of polluted water that comes from surface ditches and subsurface drainpipes (tiles) consisting of high quantities of nutrients, sediments, organic particulates, and legumes
Denitrification	A process where nitrate-N is converted to inert N_2 gas by microbes
Denitrifying-Bioreactor	A saturated permeable bed of carbonaceous solids which water passes to promote microbial nitrate removal
Diffuse Nutrients	Nonpoint source nutrient pollution transferred to water bodies through various *diffuse* processes
DRP	Dissolved reactive phosphorus- the readily available fraction that can stimulate problem growths of algae and water plants
Eutrophication	Body of water becomes overly enriched with nutrients and minerals which induce excessive growth of algae
N	Nitrogen
NH_3	Ammonia
NH_4	Ammonium
Nitrification	A process where ammonium-N is converted to nitrite-N and nitrate-N by microbes
NIWA	National Institute of Water and Atmospheric Research
NPS-FM	National Policy Statement for Freshwater Management
P	Phosphorus
RMA	Resource Management Act 1991-the New Zealand law that governs all management of land and water resources
SRP	Soluble Reactive Phosphate
TN	Total Nitrogen
TP	Total Phosphorus
TSS	Total Suspended Solids
TDS	Total Dissolved Solids
UoW	University of Waikato
USEPA	United States Environmental Protection Agency

Chapter 1. Introduction, Thesis Aim, and Outline

1.1 Introduction

Degradation of water quality due to elevated nutrient loads in waterways has become a critical global environmental concern (Hutchins et al., 2018; Li et al., 2023; Sun et al., 2016; Janssen et al., 2017). Intensive agricultural practices have resulted in the leaching of excess nutrients into groundwater, as well as transport to surface waters via surface runoff and subsurface drainage (Hua et al., 2016). In New Zealand, agricultural nutrient pollution of freshwater is an ongoing concern (Hageman et al., 2019), but is difficult to deal with due to the non-point source or *diffuse* nature of this pollution. Where channelized, however, drainage water containing nitrogen (N) and phosphorus (P), can potentially be intercepted and treated to remove nuisance pollution (Parker et al., 1999).

An over-enrichment of P and N levels in water bodies often leads to increases in phytoplankton growth (i.e., eutrophication), and increased incidence of harmful algal blooms (Geng et al., 2022; Zhou et al., 2022). Over the last century, eutrophication has affected natural waters globally, leading to a widespread deterioration of water quality and loss of biodiversity, as well as posing risks to drinking water safety, food security, and public health (Jiang et al., 2022; Sun et al., 2022; Wu et al., 2017; Zhou et al., 2022). Therefore, reducing the inputs of N and P from agricultural drainage is key to minimizing eutrophication of New Zealand waterways (Abell et al., 2011; Ballantine & Davies-Colley, 2014).

Non-point source agricultural pollution is difficult to treat because it is widely dispersed and varies with season and weather conditions (Carpenter *et al.*, 1998). However, subsurface agricultural drainage can be categorized as a point source of pollution, which creates direct pathways for the transportation of nutrients from agricultural fields into

surface water bodies. One widely-adopted approach to treat subsurface drainage is woodchip bioreactor systems, which are an alternative method to existing on-farm treatment options (Blowes et al., 1994; Christianson et al., 2011; Schipper et al., 2010). Woodchip bioreactors are a promising technology, in which woodchips serve as a carbon source for microbial growth. Following a rapid loss of dissolved oxygen, anaerobic bacteria remove nitrate from water through a suite of redox reactions collectively termed *denitrification* (Mardani *et al.*, 2020). However, woodchip bioreactors do not generally remove P substantially (Jaynes *et al.*, 2008), reflecting the fact that P is not directly affected by redox reactions, such as denitrification. However, there is growing evidence that bioreactors remove phosphorus to a limited extent. Hence, there are clearly gains to be made for freshwater quality by re thinking bioreactor design to encompass the removal of P, which is often the main limiting nutrient in Aotearoa-New Zealand freshwater settings (Abell et al., 2011; McDowell et al., 2009).

Phosphorus removal technologies including chemical precipitation, biological accumulation, and adsorption, have been developed to remove P from freshwater systems. A variety of P adsorption materials including natural materials (e.g., calcite, limestone, zeolite), industrial by-products (e.g., steel slag, fly ash, residuals from drinking water treatment), and commercial synthetic products have been evaluated (Drizo *et al.*, 2002; Chardon *et al.*, 2012; Grace *et al.*, 2015; Lalley *et al.*, 2016; Soleimanifar *et al.*, 2016; Li *et al.*, 2018). Materials with a high content of calcium, aluminum, and iron bind with P through electrostatic attraction, precipitation, and ligand exchange, thereby immobilising it (Cucarella & Renman, 2009). Indeed, the addition of aluminum sulfate salts (colloquially known as alum dosing) is an actively applied approach in the Rotorua region of New Zealand, where P removal from lake tributaries is carried out as an intervention to minimize lake water quality decline (Eager, 2017).

Naturally occurring, iron(III) (hydr)oxide is a ubiquitous P *adsorbent* in aquatic ecosystems because of its wide distribution in soil and sediments and its positive surface charge at acidic-neutral pH values (Zhang *et al.*, 2019). In recent studies, particulate manganese oxides and iron oxides have found extensive use in constructed wetlands for sewage treatment due to their typically large specific surface areas involvement in redox cycling, and capacity to immobilise solutes through coprecipitation reactions (Cheng et al., 2022; Cheng et al., 2021; Song et al., 2016; Xie et al., 2018).

Because manganese oxide is energetically-close to NO_3 on the redox ladder (Rémazeilles & Refait), MnO_2 can theoretically participate in the process of denitrification by serving as a reducing agent. This process helps maintain an elevated redox potential, reduces the dissolution of iron oxide, and thereby facilitates the adsorption of phosphorus onto iron oxide surfaces. Therefore, this study considers the potential of iron-amended novel bioreactor media for the simultaneous removal of P and N from agricultural drainage water.

1.2 Thesis Aims and Objectives

The aim of this study was to investigate the geochemical conditions typical of woodchip bioreactors with a view to developing and deploying Fe-based P removal technologies. This was to be achieved through the study of the biogeochemistry of bioreactors encompassing microbial oxidation-reduction processes, mineral formation and dissolution, and adsorption reactions. The main objectives of this research were:

1) To determine the biogeochemistry of a typical woodchip bioreactor by characterizing redox zonation and mineral transformations using field monitoring informed by equilibrium geochemical modelling.

2) To evaluate the potential for phosphorus removal from agricultural drainage by iron hydr(oxide) functionalised woodchips through a series of laboratory batch experiments and mesocosm experiments.
3) To determine the potential for incorporation of iron hydr(oxide) functionalised woodchips into the reducing environment of woodchip bioreactors, and the potential for redox-buffering through manganese dioxide supplementation.

1.3 Thesis structure and outline

Throughout this thesis, the central role of redox chemistry and mineral solubility have been considered and used to design the laboratory and field experiments. Thus, this study provides insights into new aspects of bioreactor biogeochemistry, with the goal of advancing bioreactors as dual N- and P-removing systems. This thesis is organised into six chapters including; Introduction (Chapter 1), Literature Review (Chapter 2), Research Components (Chapters 3-5), and Conclusion (Chapter 6).

Chapter 1 is a general introduction describing P issues, mitigating technologies, and the overall aims and objectives of this body of work.

Chapter 2 is a literature review on P dynamics in agricultural drainage, the biogeochemistry of woodchip bioreactors, adsorption of P into Fe oxide surfaces, and redox processes involving manganese dioxide. Additionally, it outlines the methodology employed throughout the research including material synthesis, batch adsorption, column experiments, field sampling and analysis, PHREEQC modelling, and mesocosm (redox buffering) experiments.

Chapter 3 is a journal article published in *Science of the Total Environment* detailing the biogeochemistry of a bioreactor through two drainage seasons, with insights into the coupling of iron hydr(oxide) and P.

Chapter 4 is a journal article published in *Materials and Interfaces* which describes the synthesis method of the iron hydro(oxide) and its P removal performance in batch experiments and under flowing conditions.

Chapter 5 is a standalone chapter which is on the potential for P adsorption using functionalized materials in woodchip bioreactors.

Chapter 6 provides an overview of the study with suggestions for further research.

References

Abell, J. M., Özkundakci, D., Hamilton, D. P., & Miller, S. D. (2011). Relationships between land use and nitrogen and phosphorus in New Zealand lakes [Journal Article]. *Marine and Freshwater Research*, *62*(2), 162-175. https://doi.org/DOI:10.1071/MF10180

Ballantine, D. J., & Davies-Colley, R. J. (2014). Water quality trends in New Zealand rivers: 1989–2009. *Environmental Monitoring and Assessment*, *186*(3), 1939-1950. https://doi.org/10.1007/s10661-013-3508-5

Blowes, D. W., Robertson, W. D., Ptacek, C. J., & Merkley, C. (1994). Removal of agricultural nitrate from tile-drainage effluent water using in-line bioreactors. *Journal of Contaminant Hydrology*, *15*(3), 207-221. https://doi.org/https://doi.org/10.1016/0169-7722(94)90025-6

Cheng, C., He, Q., Zhang, J., Chai, H., Yang, Y., Pavlostathis, S. G., & Wu, H. (2022). New insight into ammonium oxidation processes and mechanisms mediated by manganese oxide in constructed wetlands. *Water Research*, *215*, 118251. https://doi.org/https://doi.org/10.1016/j.watres.2022.118251

Cheng, S., Qin, C., Xie, H., Wang, W., Zhang, J., Hu, Z., & Liang, S. (2021). Comprehensive evaluation of manganese oxides and iron oxides as metal substrate materials for constructed wetlands from the perspective of water quality and greenhouse effect. *Ecotoxicology and Environmental Safety*, *221*, 112451. https://doi.org/https://doi.org/10.1016/j.ecoenv.2021.112451

Christianson, L. E., Bhandari, A., & Helmers, M. J. (2011). Pilot-Scale Evaluation of Denitrification Drainage Bioreactors: Reactor Geometry and Performance. *Journal of Environmental Engineering*, *137*(4), 213-220. https://doi.org/doi:10.1061/(ASCE)EE.1943-7870.0000316

Geng, M., Zhang, W., Hu, T., Wang, R., Cheng, X., & Wang, J. (2022). Eutrophication causes microbial community homogenization via modulating generalist species. *Water Research*, *210*, 118003. https://doi.org/https://doi.org/10.1016/j.watres.2021.118003

Hageman, K. J., Aebig, C. H. F., Luong, K. H., Kaserzon, S. L., Wong, C. S., Reeks, T., Greenwood, M., Macaulay, S., & Matthaei, C. D. (2019). Current-use pesticides in New Zealand streams: Comparing results from grab samples and three types of passive samplers. *Environmental Pollution*, *254*, 112973. https://doi.org/https://doi.org/10.1016/j.envpol.2019.112973

Hua, G., Salo, M. W., Schmit, C. G., & Hay, C. H. (2016). Nitrate and phosphate removal from agricultural subsurface drainage using laboratory woodchip bioreactors and recycled steel byproduct filters. *Water Research*, *102*, 180-189. https://doi.org/https://doi.org/10.1016/j.watres.2016.06.022

Hutchins, M. G., Abesser, C., Prudhomme, C., Elliott, J. A., Bloomfield, J. P., Mansour, M. M., & Hitt, O. E. (2018). Combined impacts of future land-use and climate stressors on water resources and quality in groundwater and surface waterbodies of the upper Thames river basin, UK. *Science of The Total Environment*, *631-632*, 962-986. https://doi.org/https://doi.org/10.1016/j.scitotenv.2018.03.052

Janssen, A. B. G., de Jager, V. C. L., Janse, J. H., Kong, X., Liu, S., Ye, Q., & Mooij, W. M. (2017). Spatial identification of critical nutrient loads of large shallow lakes: Implications for Lake Taihu (China). *Water Research*, *119*, 276-287. https://doi.org/https://doi.org/10.1016/j.watres.2017.04.045

Jiang, X., Sun, X., Alahuhta, J., Heino, J., & Xie, Z. (2022). Responses of multiple facets of macroinvertebrate alpha diversity to eutrophication in floodplain lakes. *Environmental Pollution*, *306*, 119410. https://doi.org/https://doi.org/10.1016/j.envpol.2022.119410

Li, Y., Mi, W., Ji, L., He, Q., Yang, P., Xie, S., & Bi, Y. (2023). Urbanization and agriculture intensification jointly enlarge the spatial inequality of river water quality. *Science of The Total Environment*, *878*, 162559. https://doi.org/https://doi.org/10.1016/j.scitotenv.2023.162559

McDowell, R., Larned, S., & Houlbrooke, D. (2009). Nitrogen and phosphorus in New Zealand streams and rivers: control and impact of eutrophication and the influence of land management. *New Zealand Journal of Marine and Freshwater Research*, *43*(4), 985-995.

Parker, D., Schulte, D. D., & Eisenhauer, D. E. (1999). Seepage from earthen animal waste ponds and lagoons - An overview of research results and state regulations. *Transactions of the ASABE (American Society of Agricultural and Biological Engineers)*, *42*, 485-493. https://doi.org/10.13031/2013.13381

Rémazeilles, C., & Refait, P. (2007). On the formation of β-FeOOH (akaganéite) in chloride-containing environments. *Corrosion Science*, *49*(2), 844-857. https://doi.org/https://doi.org/10.1016/j.corsci.2006.06.003

Schipper, L. A., Robertson, W. D., Gold, A. J., Jaynes, D. B., & Cameron, S. C. (2010). Denitrifying bioreactors—An approach for reducing nitrate loads to receiving waters. *Ecological Engineering*, *36*(11), 1532-1543. https://doi.org/https://doi.org/10.1016/j.ecoleng.2010.04.008

Song, X., Wang, S., Wang, Y., Zhao, Z., & Yan, D. (2016). Addition of Fe2+ increase nitrate removal in vertical subsurface flow constructed wetlands. *Ecological Engineering*, *91*, 487-494. https://doi.org/https://doi.org/10.1016/j.ecoleng.2016.03.013

Sun, C., Wang, S., Wang, H., Hu, X., Yang, F., Tang, M., Zhang, M., & Zhong, J. (2022). Internal nitrogen and phosphorus loading in a seasonally stratified reservoir: Implications for eutrophication management of deep-water ecosystems. *Journal of*

Environmental Management, *319*, 115681. https://doi.org/https://doi.org/10.1016/j.jenvman.2022.115681

Sun, W., Xia, C., Xu, M., Guo, J., & Sun, G. (2016). Application of modified water quality indices as indicators to assess the spatial and temporal trends of water quality in the Dongjiang River. *Ecological Indicators*, *66*, 306-312. https://doi.org/https://doi.org/10.1016/j.ecolind.2016.01.054

Wu, Z., Liu, Y., Liang, Z., Wu, S., & Guo, H. (2017). Internal cycling, not external loading, decides the nutrient limitation in eutrophic lake: A dynamic model with temporal Bayesian hierarchical inference. *Water Research*, *116*, 231-240. https://doi.org/https://doi.org/10.1016/j.watres.2017.03.039

Xie, H., Yang, Y., Liu, J., Kang, Y., Zhang, J., Hu, Z., & Liang, S. (2018). Enhanced triclosan and nutrient removal performance in vertical up-flow constructed wetlands with manganese oxides. *Water Research*, *143*, 457-466. https://doi.org/https://doi.org/10.1016/j.watres.2018.05.061

Zhou, J., Leavitt, P. R., Zhang, Y., & Qin, B. (2022). Anthropogenic eutrophication of shallow lakes: Is it occasional? *Water Research*, *221*, 118728. https://doi.org/https://doi.org/10.1016/j.watres.2022.118728

Chapter 2. Literature Review

This chapter provides an overview of some relevant literature, with Fig. 2.1 illustrating the progression of the literature survey and its connection to the research data sections.

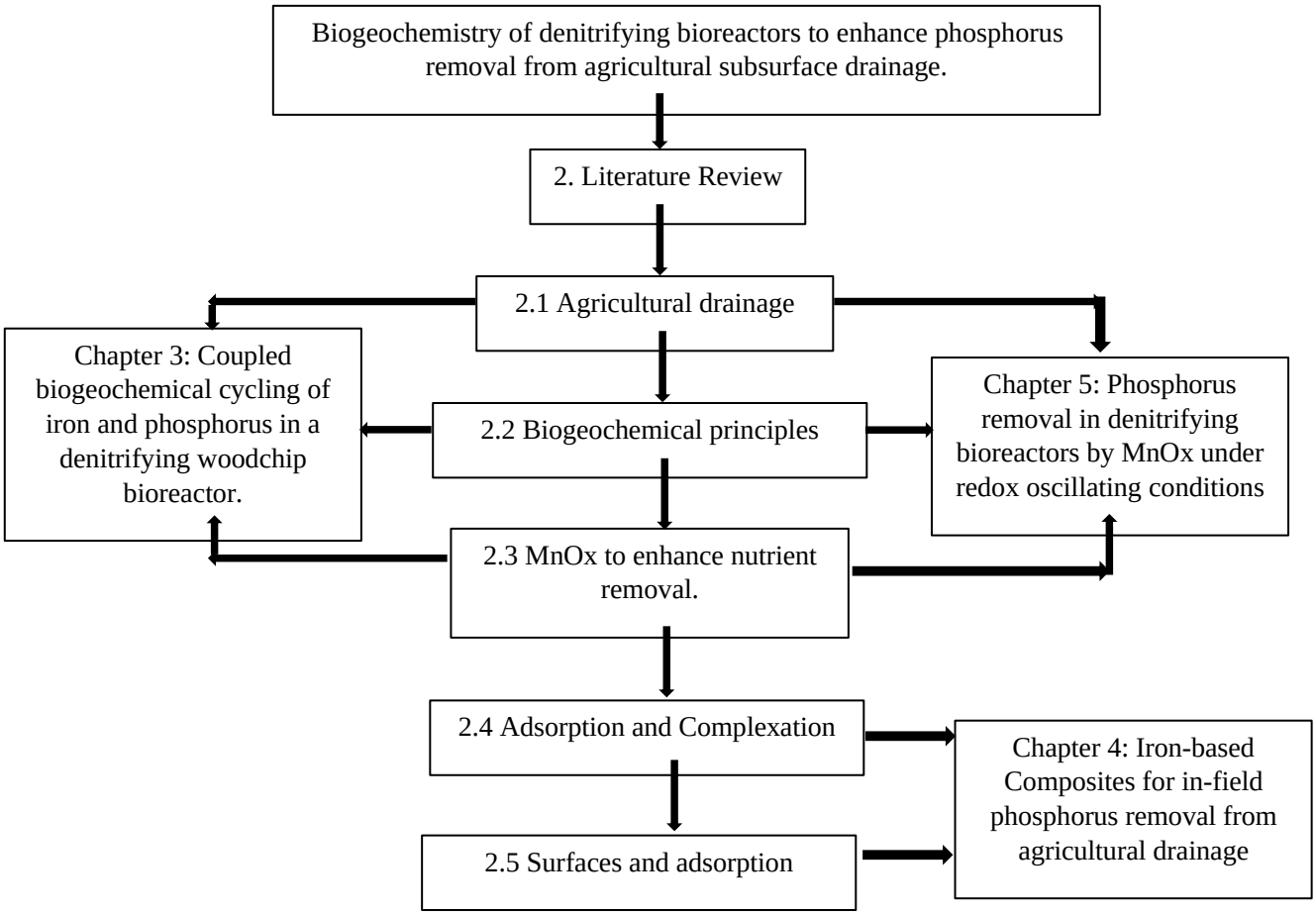

Figure 2. 1. Flow diagram of the literature review corresponding to the research papers.

2.1 Agricultural Drainage

2.1.1 Degradation of water quality

Currently, many countries and regions are experiencing water quality degradation (Hu et al., 2019; Peters & Meybeck, 2000). Water quality has a significant impact on the health of aquatic organisms within watersheds and on society as a whole due to its vital role in water resource management (Brabec et al., 2002; Karr, 1991). Water quality degradation is a complex problem

because it is influenced by different factors such as the source, climate, and hydrodynamic conditions (Schaffner et al., 2009; Elshemy et al., 2016; Robertson et al., 2018). However, human activities such as deforestation (An et al., 2008), agriculture (Zalidis et al., 2002), marine dumping (Williams, 1996), industrial discharge (Zhang et al., 2016), and radioactive waste discharges (Durham & Joshi, 1980) are the major causes of water pollution, and therefore these factors can be controlled by planned interventions.

In New Zealand, excess nutrients, sediments, pesticides, and pathogens affect the quality of freshwater ecosystems (Parliamentary Commissioner for the Environment, 2012). Of these water bodies, 32% are eutrophic, with 73% experiencing significant pressure from agricultural pollution. Over the last century, increasing nutrient loads, particularly total nitrogen and phosphorus in freshwaters have increased, to the point that they now exceeded guideline values specified in the Australian and New Zealand Guidelines for Freshwater and Marine Water Quality (ANZG), 2013–2017 data (Environmental Aotearoa 2019).

P is an essential element of plant growth and often limits primary production. In many countries, phosphorus-containing fertilizers are often applied to agricultural lands to improve crop production. Natural sources of P include the decomposition of rocks and minerals, sedimentation, erosion, atmospheric deposition, and inputs from living beings (Edahbi et al. 2018; Vikrant et al. 2018). P is found in environmental settings as either organic or inorganic compounds and has never been found as a free element due to its high reactivity (Carrillo et al., 2020). However, inorganic forms of phosphorus, such as orthophosphates are considered the most commonly present in agricultural drainage systems, due to their proximity to the sites of inorganic P fertiliser application. The largest P–entering channels from anthropogenic activities are industrial and municipal discharge, and agricultural effluent (Mohan et al. 2014; R. Li et al., 2018; Ogata et al., 2019). When phosphorus is present in excess, it leads to eutrophication, which causes the rapid growth of algae, hypoxia, and odor problems, resulting

in negative impacts on freshwater ecosystems and human health (i.e., esophageal cancer, methemoglobinemia) (Wang et al., 2021). Therefore, there is a need for effective treatment to remove nutrients before discharging them into waterways.

2.1.2 Agricultural activities and drainage water quality

Drainage activities are taking place in many agricultural regions around the world. In many regions, surface ditches and subsurface drains have constructed to remove excess water from the soil profile for the enhancement of the farming operations (Spaling and Smit, 1995). Installation of subsurface drainage systems are mainly considered for the poorly drained soils to prevent wet conditions and mitigate the excess moisture on crops. Subsurface drainage systems are widely popular in North America, Northwest Europe and Scotland and far less popular in Southeast Asia (Blann et al., 2009). However, the environmental impacts of agricultural drainage extend beyond farmlands, affecting the hydrology of catchments by varying runoff volumes (leading to flooding events), degrading water quality in waterways due to the presence of nutrients and other contaminants in agricultural runoff, and decreasing farmland biodiversity (Herzon and Helenius, 2008).

Agriculture is the major source of point and non-point (*diffuse*) P pollution to receiving waters in New Zealand (Wilcock *et al.*, 1999). Subsurface drainage or tile drainage networks which are designed to regulate farm surface runoff and subsurface water flows, are also a direct pathway for P to enter surface water (Jaynes *et al.*, 1999; Kay *et al.*, 2005; Washington *et al.*, 2018). In agro ecosystems the use of mineral fertilizers or manure inputs to the land cause P accumulation in topsoil (Sharpley & Tunney, 2000; SchjГënning *et al.*, 2004) which is subsequently mobilized through geochemical desorption, biological solubilization or physical detachment (i.e. erosion). The primary transportation pathways of P from agricultural fields to water bodies include surface runoff, shallow subsurface lateral movement, and engineered

drainage systems. Mobile P moves from the soil to surface waters through surface and subsurface pathways and is subjected to temporal variations and dynamics (Brazier *et al.*, 2005; Harris & Heathwaite, 2005). Further, the fractions of P found in drainage (orthophosphate, organic, particulate etc.) are likely to vary depending on factors such as physical flow rates and chemical properties of the soil, pH and dissolved P concentrations in the drainage water (Sallade & Sims, 1997b; Sallade & Sims, 1997a). A thorough understanding of the transportation pathways of nutrients from land to water is crucial for efficiently directing efforts towards mitigation measures.

The nutrient load in agricultural subsurface drainage is influenced by climatic factors, soil properties and management practices (Williams *et al.*, 2015 Randall & Goss, 2008 Randall & Mulla, 2001). Nutrient loads in tile drains vary with rainfall with dissolved reactive phosphorus (DRP) concentrations increasing during periods of elevated rainfall (Gentry *et al.*, 2007 King *et al.*, 2015). Soil texture influences nutrient loads in subsurface drainage by affecting water infiltration, denitrification, and P sorption processes (Plach *et al.*, 2018). Nutrient loads are also strongly impacted by fertilizer management practices.

In summary, the presence of excess P in aquatic systems has been identified as one of the main causes of eutrophication of freshwater bodies, which promotes nuisance algal growth and hence deteriorates water quality. Because even low concentrations (100 µg L^{-1}) of total phosphorus can result in eutrophication and algal blooms, techniques that enable the removal of P from agricultural drainage are an important complement to land management reform. Currently, diverse methods have been applied to capture nutrients from water media, including constructed wetlands, riparian buffer, and bioreactor methods. Among them, woodchip bioreactors appear most promising to be be engineered to remove P efficiently.

2.1.3 Management and treatment of nutrients in agricultural drainage

Worldwide, pollutant control for the protection of water quality is a high priority. Strict rules have been established in many countries to reduce the release of nutrients into surface waters. In New Zealand, the Resource Management Act (RMA) is the main government legislation relating to the management of land, air, and coastal environments (New Zealand Government 1991). The RMA has identified *diffuse* nutrients from agricultural drainage as one of the key water quality concerns. In addition, the National Policy Statement for Freshwater Management (NPS-FM) established on 1st July 2011, has the principal aim of authorizing policies that direct the government to manage water in an integrated and sustainable manner. All unitary and regional councils are required to establish a set of water quality standards for surface and groundwater in specified regions by the end of 2030 (National Policy Statement for Freshwater Management 2014). Among the compulsory standards, all councils must monitor the concentration of nutrients (primarily TN and TP) and periphyton biomass in water bodies (National Policy Statement for Freshwater Management 2014). Hence, *diffuse* nutrients from agricultural drainage input to freshwaters need to be managed and reduced in order to meet the required receiving water standards.

Global standards for freshwater quality can be quite variable. For phosphorus, the U.S.E.P.A. water quality criteria state that phosphates should not exceed 0.05 mg L^{-1} for streams that discharge into lakes or reservoirs and be no greater than 0.025 mg L^{-1} within a lake or reservoir, and 0.1 mg L^{-1} in streams or flowing waters that do not discharge into lakes or reservoirs (Taylor *et al.*, 1993). The World Health Organization (WHO, 1993) imposed a limit of 0.1 mg L^{-1} of phosphates for drinking water as well as 1 mg L^{-1} of total phosphates for wastewater effluent.

Waterway pollution from agricultural discharge can be controlled on–farm via lateral and in–stream methods. Lateral drainage management involves the construction of riparian buffer zones along the stream edge, whereas in–stream methods involve wetlands and denitrifying bioreactors (He *et al.*, 2020). Riparian zones have been identified as a promising technology that protects aquatic ecosystems from non–point source (NPS) pollutants by reducing pollutants through processes including filtration, precipitation, volatilization, adsorption, plant uptake, and various microbial processes (Li *et al.*, 2014; McKergow *et al.*, 2016). Plants in riparian zones enhance removal of nitrogen and phosphorus by utilizing the nutrients for growth (Matheson *et al.*, 2002; Collins *et al.*, 2013). Wetlands provide a variety of functions, including nutrient removal, biodiversity conservation, carbon sequestration, and acting as water flow stabilizers (Chen *et al.*, 2019; Jordan *et al.*, 2011). For instance, a constructed horizontal flow wetland can reduce TP concentration by 5.2 g P m^{-3} day^{-1} (Tanner *et al.*, 2012). Yet, primary issues associated with wetlands are timely monitoring, scientific management, protection, and restoration (Sims *et al.*, 2013; Reiss & Brown, 2007; Miller *et al.*, 2006). Furthermore, these nutrient mitigation methods are not widely employed by most farms in New Zealand, and they are not always practical to implement, as they are extremely sensitive to seasonal changes and variable nutrient loads.

Bioreactors are an alternative technology to mitigate *diffuse* agricultural pollution. Bioreactors have captured interest due to their simple design and installation, farmer–friendly operation, and low–cost technology. Woodchips are the most common substrate used in bioreactors (Christianson Laura *et al.*, 2011; Greenan *et al.*, 2009) and are estimated to have a life span of ten or more years (Robertson *et al.*, 2008). As a passive N removal method, bioreactors operate by diverting NO_3^- rich streams into a trench–like system where the water passes through a carbon (C) source, i.e., woodchips, before being released to receiving waters. The anoxic environment inside the bioreactor combined with an available electron donor from the C creates

ideal conditions for heterotrophic denitrification, a process where bacteria convert aqueous NO_3^- to inert di–nitrogen gas (N_2). Early research has demonstrated that bioreactors are capable of removing significant amounts of nitrate from agricultural drainage (Lepine *et al.*, 2016; von Ahnen *et al.*, 2016). However, many systems are not optimized for P removal.

A review of the literature reveals that nutrient removal rates vary among studies, for instance a woodchip bed system used for fish farm effluent was able to reduce nitrogen at a rate of 7.06 g-N m^{-3} d^{-1} and ortho–P was reduced 98% within 3 days of operation from an initial inlet concentration 0.28 mg-P L^{-1} (TP inlet 0.39 mg L^{-1}) (von Ahnen *et al*., 2016). In five different configurations of woodchip bioreactor coupled with wetlands, for the treatment of domestic wastewaters, reported nitrogen and phosphorus removal rates were 2.8−12.4 g- N m^{-3} d^{-1} and 0.19-0.23 g-P m^{-3} d^{-1} respectively (Tanner et al., 2012). A study examined a woodchip bioreactor containing a steel by-product filter (1.2 m of woodchip reactor coupled with 0.3 m of steel by−product reactor). This approach successfully removed between 10.1−21.6 g-N m^{-3} d^{-1} of nitrate and 0.25−0.89 g-P m^{-3} d^{-1} of phosphate (Hua et al., 2016b), demonstrating enhanced P removal from agricultural drainage water by bioreactors with iron addition. Phosphate removal using an iron-based filter could, therefore, be a suitable practice for agricultural drainage phosphate management.

2.2 Biogeochemical principles

In ecology and earth science, the biogeochemical cycle refers to how the essential elements, circulate through the lithosphere, hydrosphere, and biosphere. Generally, the biogeochemical cycle is an integration of biological, chemical, and physical processes that govern the environmental transfer of the elements.

Biogeochemical cycles are incredibly diverse, but we focus here on the acid−base and oxidation−reduction processes. Acid–base processes control weathering and solubility of minerals and influence biological processes and various aqueous phase reactions. An acid–base balance (or pH) can be easily disrupted by biogeochemical factors and anthropogenic influences (Charlson and Emerson, 2000). Likewise, the redox status of natural waters is the result of dynamic changes in biogeochemical cycles. However, from the most basic standpoint, there is a conceptual similarity between acid–base and oxidation–reduction reactions. Acids and bases are considered as proton donors and acceptors, and oxidizers and reductants are classified as electron acceptors and donors respectively. The central importance of redox and pH on aquatic processes is emphasized in the pourbaix (named after Marcel Pourbaix) diagram, in which these solution variables define the axes along which elemental speciation is presented (Fig. 2.3).

Geochemical cycles are natural phenomena, but agricultural and industrial activities have drastically perturbated these natural cycles. These changes influence ecosystems at all scales, ranging from microorganisms to the entire biosphere (Ahmadi et al., 2020).

2.2.2 Phosphorus biogeochemistry

P is an essential nutrient for all living organisms that participate in various biogeochemical cycles. On a geological scale, approximately 90–95% of the P in the Earth's crustal rocks is contained within apatite. Apatite exists in different forms, including hydroxylapatite (HAp), fluorapatite (FAp), and chlorapatite. Their chemical formulas correspond to $Ca_{10}(PO_4)_6(OH, F, Cl)_2$ (Li et al., 2017; Schlesinger & Bernhardt, 2020; Smil, 2000). Given the growing demand in agriculture, approximately 95% of extracted phosphorus is utilized as fertilizer in agricultural practices. As shown in Fig. 2.2, aside from being found in phosphate rock and phosphorite minerals, P is also found in aquatic ecosystems. The biogeochemical cycle of P predominantly consists of a sedimentary cycle which drives the regeneration of P over time (Reinhard et al., 2017; Steffen et al., 2015; Zhang, 2023). Hence, investigating the biogeochemical cycle of P, including the distribution, sources, and pathways of phosphate, is of great significance for further comprehension of the structure and functional characteristics of ecosystems.

The cycling of P is strongly associated with the adsorption of metal oxides in sediments (Krom & Berner, 1981; Lijklema, 1977). P can form stable oxides and complexes with iron (Fe), calcium (Ca), aluminium (Al) ions and trap inorganic phosphates. Further, the redox cycling of iron (Fe), manganese (Mn), arsenic (As), and sulfur (S), plays a crucial role in the mineralization of organic matter and the mobilization of internal P (Hu et al., 2022; Kraal et al., 2015; Xiao et al., 2023). For instance, P can be adsorbed onto iron and manganese (hydr)oxides under the oxic conditions (Sundby, 2006). However, under anoxic conditions, there is the potential for remobilization and release of P. This occurs through the reductive dissolution of iron and manganese oxides (Bose & Sharma, 2002). In reduced environmental settings, another governing process is sulfate reduction which leads to the oxidation of organic matter and the formation of H_2S. The production of H_2S can convert iron (hydr)oxides into insoluble iron sulfides (FeS_x), which, unlike iron (hydr)oxides, exhibit poor binding capacity

to phosphates (Reddy et al., 1999; Smolders et al., 2010). In the presence of NO_3^-, FeS_x can undergo oxidation back to iron (hydr)oxides, effectively immobilizing P within sediments (Smolders et al., 2010).

2.2.3 P uptake by PAOs (Polyphosphate Accumulating Organisms)

In aqueous environments, P exists in various forms depending on the pH and the oxidation conditions. P in the form of orthophosphate can be categorized as H_3PO_4, $H_2PO_4^-$, HPO_4^{2-} and PO_4^{3-} corresponding to aqueous solution pH ranges of < 2.15, 2.15 – 7.20, 7.20 – 12.33, and >12.33 respectively (vanLoon and Duffy, 2017; Chouyyok et al., 2010). In particular, only certain forms of phosphorus are available for biological uptake, while insoluble P tend to precipitate out of solution or adsorb onto surfaces. In addition to plants, a group of bacteria known as polyphosphate accumulating organisms (PAOs) utilize P and store it as intracellular polyphosphate (poly-P). This process involves intracellular polymers of polyphosphate, glycogen, and poly-β-hydroxyalkanoates (PHAs). Denitrifying PAOs (DPAOs) are able to utilize nitrate and nitrite as electron acceptors for the oxidation of PHAs (A. Oehmen et al., 2010). PAOs are capable of utilizing glycogen and poly–P within their cells to store carbon anaerobically, releasing phosphorus as orthophosphate in the process (Barnard et al., 2017). When the poly-P and glycogen are restored, it leads to the subsequent removal of P from the system, resulting in lowered orthophosphate levels in the aqueous solution. Studies by Adrian Oehmen et al., 2007; Yuan et al., 2012; Sun et al., 2020, have found that phosphorus removal by DPAOs is favored under anoxic conditions. These studies investigated phosphorus removal in a sludge system under oxic, anoxic, and anaerobic conditions over a period of 27 days. Another recent study has investigated that DPAOs have a competitive advantage for nitrate and

simultaneous phosphorus removal and denitrification at low DO concentrations (Zaman et al., 2021).

Fig. 2.2 shows the biochemical alterations of PAOs under the different conditions. PAOs are capable of utilizing the carbon polymers of polyhydroxyalkanoates (PHAs) as an energy source for P uptake and polyphosphate storage, biomass growth, and glycogen replenishment under aerobic conditions. Anaerobically, PAOs are able to take up the carbon sources of volatile fatty acids (VFAs) and store them in its intracellular as PHAs (Mino et al., 1998).

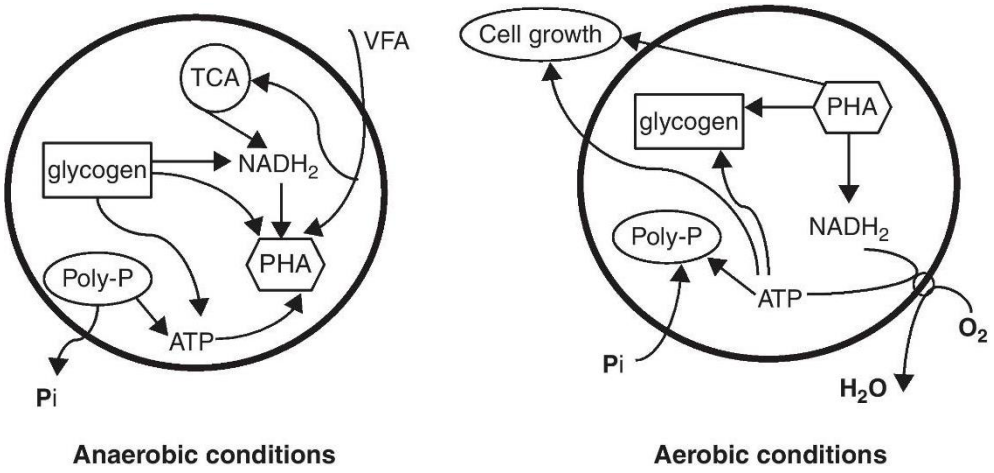

Figure 2. 2. Schematic diagrams of the P accumulation in PAOs under the anaerobic and aerobic conditions (adapted from (Yuan et al., 2012))

Many studies have investigated how operational factors such as pH, temperature, and dissolved oxygen (DO) concentrations can affect P removal by PAOs. Filipe et al., (2001) found that a higher pH of 7–7.5 is more effective for PAOs in terms of phosphorus (P) uptake, cell growth, and PHA oxidation, whereas these processes are inhibited at a lower pH of 6.5 under aerobic conditions. The enhancement of P removal has been reported when the pH increased from 6.8 to 7.25 under anaerobic conditions (Filipe et al., 2001). In contrast, an increased pH (below 8) could also induce biomineral precipitation, such as the formation of calcium phosphate, which needs to be considered (Maurer et al., 1999). In most biological reactions, temperature is another governing factor; higher temperatures have been observed to increase the rate of

biochemical transformations. However, several studies have found that the higher P removal at 5 ^{o}C than 20 ^{o}C, concluding that biomass growth of PAO is favourable at low temperatures (Brdjanovic et al., 1998; (Erdal, 2003). The DO concentration also appears to be another factor that has an impact on biological P removal. Griffiths et al., found a higher phosphorus (P) removal capacity at low dissolved oxygen (DO) concentrations (2.5–3.0 mg L^{-1}), whereas poor P removal performance was observed at high DO concentrations (4.5–5.9 mg L^{-1}). This is attributed to the higher abundance of PAOs at low DO levels. Furthermore, an increase in the abundance of PAOs has been observed in nitrite-limiting environments, proving that P uptake is inhibited when nitrite is present (Kuba and Loosdrechtt, 1996; Saito et al., 2004). In recent years, it is assumed that PAOs are the main agents of P removal in bioreactor systems, highlighting the need for further identification of the underlying mechanisms.

2.2.4 Microbial Processes

Microorganisms play an important role in facilitating many oxidation and reduction reactions of the major elements (C, H, N, O, S) in the natural environment. In most aerobic environments, oxygen acts as the primary oxidizing agent during biomass degradation. Under anaerobic conditions, organic matter is degraded via oxidation by oxygen-containing species in what can be viewed as a series of oxidant filtration reactions. Biomass degradation is the most common process of oxidation and can be expressed by the oxidation half reaction as:

$$2CH_2O \rightarrow CO_2 + 4H^+ + 4e^- \quad (1)$$

In the redox sequence, oxygen is the primary oxidant followed by nitrate and then sulphate (Table 2.1)

Table 2. 1. The sequence of electron acceptors and oxidizing reactions (ΔG^0 Gibbs free energy)

Biomass		**Nature's oxidizing agents**	**ΔG^0**
	Oxygen	$O_2 + 4H^+ + 4e^- \rightarrow 2H_2O$	–500 KJ
	Nitrate	$2NO_3^- + 12H^+ + 10e^- \rightarrow N_2 + 6H_2O$	–480 KJ
Minerals	Manganese oxide	$MnO_2 + 4H^+ + 2e^- \rightarrow Mn^{2+} + 2H_2O$	–341 KJ
	Iron hydrous oxide	$Fe(OH)_3 + 3H^+ + e^- \rightarrow Fe^{2+} + 3H_2O$	–115 KJ
	Sulfate	$SO_4^{2-} + 9H^+ + 8e^- \rightarrow HS^- + 2H_2O$	–102 KJ
	Self-oxidation	$CO_2 + 8H^+ + 8e^- \rightarrow CH_4 + 2H_2O$	–93 KJ

From Table 2.1, it can be inferred that redox reactions involving the coupling of organic matter oxidation to electron acceptor reductions, likewise impact acid–base chemistry via production and consumption of acid–base species. For instance, nitrate reduction leads to the generation of alkalinity via the overall reaction: it can quickly be seen that changes in redox potential (pE) and acid-base chemistry (pH) will impact the stability of minerals as a direct result of oxygen consumption and cascading redox reactions (Table 2.1).

2.2.5 Mineral stability

The pE–pH pourbaix diagrams give a quick impression of the possible equilibrium phases present in an aqueous system. pE is defined as negative logarithm of electron activity, which is analogue to pH ($-\log_{10}[H^+]$). Positive values of pE indicate oxidizing conditions whereas negative values of pE indicate reducing conditions. As a general rule, as water moves into and

through a bioreactor pE will decline. In Fig. 2.3, a hypothetical drainage water moves from neutral pH and high pE to lower pE (zone a to b), intersecting the Fe $(OH)_3$ / Fe^{2+} stability field.

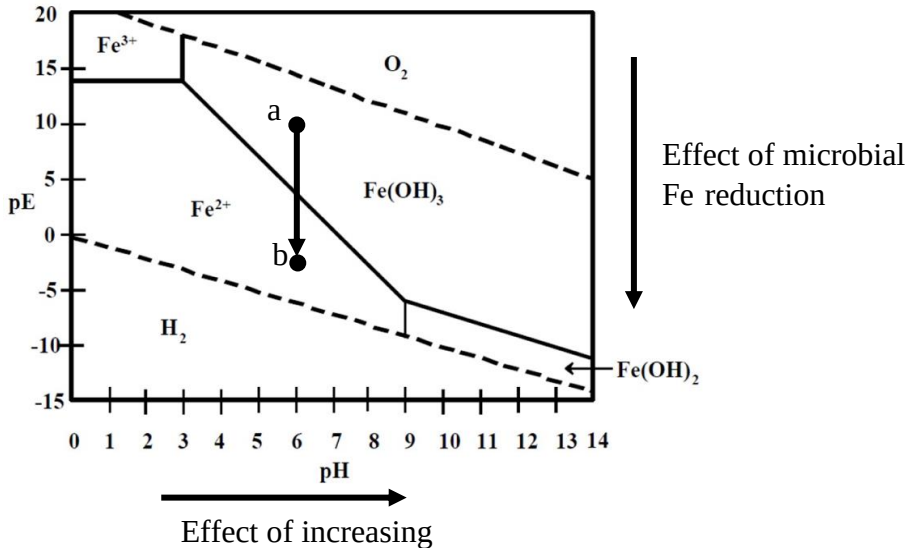

Figure 2. 3. pH-pE diagram for common Fe species

Fig 2.3 provides the visual representation of the oxidized and reduced species of Fe under varying environmental conditions. Ferric iron (Fe^{3+}) is a strong oxidizing agent, whereas, Fe^{2+} is a strong reducing agent at neutral – high pH. For the compounds of $Fe(OH)_3$ and $Fe(OH)_2$, the predominance area for a given oxidation state may disappear completely above or below a given pH. It is important to note that the phase boundaries given in Fig. 2.3 are only indicative and geochemical speciation modelling is needed to more accurately define the species distribution in a given system and settings.

While redox processes directly drive the behavior of Mn, Fe, and S, the biogeochemical behavior of non-redox active elements may be indirectly influenced by the mineral phases of manganese oxide and iron (hydr)oxide through adsorption/desorption reactions and the

formation and precipitation of secondary phases. For example, iron, manganese, and iron-manganese deposits occur in nearly all geomorphologic and tectonic environments in the ocean basins and form by processes of hydrogenetic precipitation from cold ambient seawater, hydrothermal fluids and sediment pore waters. Iron and manganese deposits occur in several different forms: nodules, crusts, cements, mounds and sediment-hosted strata bound layers. (Hein et al., 1997).

Iron compounds commonly exist in nature as iron hydr(oxide), Fe-bearing clay minerals, Fe carbonates and Fe sulphides. Iron (III) is soluble under highly acidic conditions, but precipitates under neutral pH environments. The surfaces of iron hydroxides catalyze many redox conversions. Of primary relevance, iron hydroxide minerals serve as electron acceptors for iron-reducing bacteria. (Dos Santos Afonso and Stumm, 1992). These microorganisms exist in freshwater and marine environments and oxidize organic compounds within their cytoplasm. In addition, microorganisms use extracellular reduction of poorly soluble iron minerals to gain energy for their growth (Macalady and Banfield, 2003). Reduction of Fe^{3+} minerals generates soluble Fe^{2+} and a wide range of secondary minerals, including vivianite ($Fe^{2+}_3(PO_4)_2.8H_2O$) and siderite ($FeCO_3$) minerals (both Fe^{2+} minerals), goethite (FeOOH) (a Fe^{3+} mineral) and magnetite (Fe_2O_3) (a mixed Fe^{2+}–Fe^{3+} mineral) (Liger et al., 1999) (Lloyd et al., 2000). Oxidation of Fe^{2+} may be completed by aerobic and anaerobic bacteria (Borch et al., 2010). In acidic environments, microbial Fe^{2+} oxidation is favorable, whereas under neutral pH conditions aerobic neutrophilic Fe^{2+} oxidizing organisms have to compete with chemical oxygenation of Fe^{2+}. Therefore, these organisms adapt to low levels of oxygen, typically occurring at oxic–anoxic interfaces (Druschel et al., 2008).

2.3 MnOx-induced nutrient removal

Manganese, another relatively common element at the Earth's surface, does not occur naturally in its pure state in surface environments, but is found in combination with other lelements. The

most abundant manganese minerals are pyrolusite (MnO_2), rhodocrosite ($MnCO_3$) and rhodonate ($MnSiO_3$). The behavior of iron and manganese in the environment is closely correlated to redox processes. Manganese oxides precipitate in a wide range of environmental redox reactions. For instance, birnessite (δ $-MnO_2$) tends to oxidize Se, Cr and As. Mn^{2+} oxidation is catalysed by a variety of bacteria and fungi (Miyata et al., 2006; Hastings and Emerson, 1986). Generally, the initial products of manganese oxidation are poorly crystalline, layered Mn^{4+} oxide minerals. Thus, the final form of mineral is often determined by the geochemical conditions during and after Mn^{2+} oxidation (Webb et al., 2005). Biologically mediated Mn^{2+} oxidation is the major source of environmental manganese oxides (Tebo et al., 2004; Hastings and Emerson, 1986). Reduced Mn^{2+} attract orthophosphate ions (HPO_4^-) from solution and enhance secondary mineral formation (eq. 2,3). Similarly, Fe minerals initially form in the less stable amorphous $Fe(OH)_3$ aqueous phase.

$$Mn^{4+} \rightarrow Mn^{2+} \quad (2)$$

$$Mn^{2+} + 2HPO_4^- \rightarrow Mn(HPO_4)_2 \quad (3)$$

The structure and reactivity of iron and manganese mineral surfaces in natural waters are further influenced by natural organic matter (NOM) and inorganic sorbates. Humic substances, known as polymeric organic compounds, can stimulate the microbial reduction of poorly soluble Fe(III) minerals by acting as electron connectors between the bacteria cell and the mineral (Rue et al., 2019). Further, reduced humic acids are able to transfer electrons to ferric iron and oxidized manganese species. Subsequently, the transfer of electrons from microbial oxidation processes to ferric iron could be an activity triggered by iron-reducing microorganisms, fermenting bacteria, sulfate–reducing, halo respiring and methanogenic microorganisms all occurring via humic acids as an electron shuttle (Kappler et al., 2004). Substantial adsorption of NOM, bicarbonate and phosphate to Fe(III) and Mn(IV) mineral

surfaces may inhibit the attachment of microorganisms and influence their surface properties with relevance to fully understanding adsorption and complexation reactions (Borch et al., 2007). Humic compounds further influence the biomineralization of iron and manganese minerals via complexation and solubilization of the metal ions and by sorption to the mineral surface, which leads to formation of less crystalline minerals (Eusterhues et al., 2008); (Jones et al., 2009). Crucially, phosphate interacts strongly with iron (hydr)oxides through surface complexation and, thereby alters Fe(III) reducibility, stability and mineralization pathways (Arai and Sparks, 2001). Phosphate increases the extent of iron reduction under certain conditions and promotes the formation of carbonate green rust (GR(CO_3^{2-}): [Fe_4^{2+} Fe_2^{3+} $(HO{-}12)^{2+}$.[CO_3^{2-}.$2H_2O$]$^{2-}$) and vivianite from magnetite (Kukkadapu et al., 2004).

2.3.1. MnOx intervention on the biogeochemical cycle

Manganese oxides are abundant in nature and can be found extensively in diverse environmental settings of seabeds, soil and sediments, rock dendrites, desert rock paint, and freshwater bodies (Remucal and Ginder−Vogel, 2014). Recently, manganese oxides have been widely introduced in constructed wetlands (CWs) to enhance ammonium (NH_4^+) oxidation (C. Cheng et al., 2022), sewage treatment (S. Cheng et al., 2021), and nutrient removal (Yang et al., 2019) due to their ability to participate in redox reactions. Additionally, it has been identified that the presence of Mn^{2+} in wastewater plays a significant role in the regulation of biological N and P removal processes (Shao et al., 2022).

Apart from biological P removal, adsorption within the filter media is the major P removal mechanism. This process is highly dependent on the characteristics of the materials, pH of the aqueous media, and the redox conditions. Woodchip bioreactors encompass a wide range of

redox conditions and microbial activities. The reducing conditions in the bioreactor can be a reason to inhibit P adsorption onto iron hydro(oxide) filter media. To address this issue, one possible solution is to introduce a strong oxidizing agent (i.e. Manganese oxide) to counteract the reducing conditions and thereby enhance the P adsorption process.

2.3.2 MnOx induced denitrification

MnO_x is a strong oxidizing agent with a high redox potential of 1.23 V, compared to 0.67 V for iron oxide. (Ding et al., 2015; Morse, 1988). Hence, MnO_x could be added to bioreactor systems to buffer the redox potential and inhibit iron oxide dissolution. Yang et al., 2019 has found that the 65 % P removal efficiency (initial TP 14 ± 0.9 mg L^{-1}) via magnesite (formation of solid Mg–phosphates – $Mg_3(PO_4)_2$ and $MgHPO_4$) and the 87% nitrogen removal efficiency (initial TN 40.40±1.40 mg L^{-1}) in a lab-scale constructed wetlands (CWs). 50 % of P removal was attributed to adsorption onto the manganese, with the remainder by plant (8%) and microbial uptake (6%) (Anschutz et al., 2000) whereas nitrogen enhances microbial activities. Thus, it seems that the addition of Mn increased the abundance of denitrifying bacteria resulting in enhanced denitrification. Many studies have reported that Mn oxides actively participated in the nitrogen cycle whereby ammonia is oxidized to nitrogen gas with manganese as the terminal electron acceptor (Bartlett et al., 2008); (Hulth et al., 1999; Aller et al., 1998; Anschutz et al., 2000). The reduced manganese (Mn^{2+}) effectively participates in redox cycle by allowing nitrate to be oxidised into nitrogen gas by facilitating denitrification.

Consequently, the DBRs have a great potential to generate similar nitrate removal pathways with the addition of Mn oxides. The removal of P with the presence of Mn oxide have been reported in the literature (Dong et al., 2012; Ong et al., 2010; Yang et al., 2019). However, the mechanisms of poising the oxidation by Mn are still unclear.

2.4 Adsorption and complexation

2.4.1 Adsorption mechanisms

Adsorption is a surface phenomenon involving the transfer of molecules, atoms or ions from the bulk fluid or gas phase onto a solid interface. By convention we define the substance being adsorbed as the *adsorbate* and the solid on which adsorption occurs as the *adsorbent*. A physical force or chemical bond is responsible for the adsorption. *Physisorption* refers to the adhesion between *adsorbate* and *adsorbent* via a physical mechanism, whereas adsorption due to chemical bonding is known as *chemisorption* (Patterson, 2009). In *physisorption*, weak forces such as electrostatic interactions and Van der Waals (dispersion) forces are involved. On the other hand, stronger chemical bonds, including covalent bonds are formed in *chemisorption*. *Chemisorption* is slower than *physisorption* and usually forms a so-called 'Monolayer' while *physisorption* involves the formation of multiple layers of the *adsorbate* on the surface of the *adsorbent* (Artioli, 2008).

Further, *chemisorption* involves various processes such as ionic exchange, surface complexation and precipitation. Ionic exchange takes place by selective replacement of positively or negatively charged ions on surfaces, the efficiency of which largely depends on the surface area and surface chemistry of the *adsorbent*. The electrostatic force between the charged surface and oppositely charged ions depends on solution pH and the point of zero charge (pH at which the net surface charge is equal to zero) of the *adsorbent*. Other mechanisms of adsorption include surface complexation and precipitation. Formation of complexes and structures associated with specific metal-ligand interactions is known as surface complexation. Precipitation is the formation of solids in a solution or on a surface during the adsorption process. The effects of these interactions for the overall process of adsorption is a critical consideration when determining the adsorption capacity (of an *adsorbent*) and predicting adsorption behavior (of the *adsorbate*). In most cases, the amount of a given substance attached

to a surface under experimental conditions is typically quantified using adsorption isotherms, such as the Langmuir and Freundlich equations (Tareq *et al.*, 2019).

2.4.2 Factors affecting adsorption

The mechanism of adsorption and the nature of the adsorption process is based on the intrinsic properties of the *adsorbent* including the *adsorbent's* hydrophilicity/hydrophobicity, the adsorption phase, temperature, pH, flow rate and concentrations of the reactants. Further, adsorption is significantly influenced by the surface area of the *adsorbent* in terms of porosity and particle size (Karimi *et al.*, 2019). There are many studies on synthetic and natural *adsorbents* (Zeng *et al.*, 2019; Soleimani *et al.*, 2019; Asere *et al.*, 2019). The availability and often superior performance of natural materials warrants their further investigation. Natural *adsorbents* comprise a range of minerals and biological materials often in intimate associations. The primary differences between synthetic and natural *adsorbents* are pore size, and surface properties (Karageorgiou *et al.*, 2007). Bio-based natural *adsorbents* have both hydrophilic and hydrophobic properties that interact with absorbates by polar and non-polar interactions (Huang *et al.*, 2008). Modification of *adsorbents* usually aims to enhance the surface area and porosity which both enhance adsorption. Hence, researchers are continuously working on modifying and optimizing existing *adsorbents*. The particle size of any *adsorbent* has a significant influence on the overall performance of the adsorption process. When the particle size is large, adsorption capacity reduces due to a lower surface area to volume ratio. Therefore, any potential *adsorbent* should possess a high surface area with active sites to bind the absorbate molecules. *Adsorbent* pore size and the molecular diameter of the *adsorbate* also play a significant role in the adsorption process. Thus, a larger pore size will enhance the adsorption efficiency particularly with respect to macromolecules (Sellner *et al.*, 2019). In addition, adsorption processes are highly dependent on temperature, ionic strength, and pH, and these parameters vary with the nature of different *adsorbents* and *adsorbates*. Moreover,

in flow through systems with variable flow the adsorption process is dynamic varying with flow rate and retention time.

2.4.3 Phosphate adsorption mechanisms

The rock cycle interacts with the hydrological cycle, which leads to the dissolution and weathering of minerals with water. Chemical weathering is one of the major processes dominating the global hydrogeochemical cycle of elements. Water interacts with rock leading to the weathering and dissolution of minerals which are transformed into secondary minerals formed in soils.

Phosphate is essential for life but is often scarce in natural systems. Generally, the sources of phosphate include the weathering of rocks and minerals, erosion, sedimentation and atmospheric deposition. In natural systems phosphate occurs as organic phosphate and inorganic orthophosphate or polyphosphates (Abu Shmeis, 2018). Orthophosphate species are common in water bodies, but the proportion of inorganic and organic P can be very system specific. Condensed phosphates are inorganic compounds that contain salts, metals or minerals like calcium (i.e. calcium phosphate) and are also pH sensitive. The solubility, and dynamics of phosphorus in water are a function of the interactions with other ions and are highly pH dependent. Mainly $H_2PO_4^-$ and HPO_4^{2-} species of orthophosphoric acid are present in the pH range of 5 to 9. In the range of pH 0 to 4.7 the, dominant P species are H_3PO_4 and $H_2PO_4^-$, in the pH range 4.7 to 9.7 are $H_2PO_4^-$ and HPO_4^{2-}, and pH values between 9.7 to 14 are HPO_4^{2-} and PO_4^{3-} (Fig 2.4).

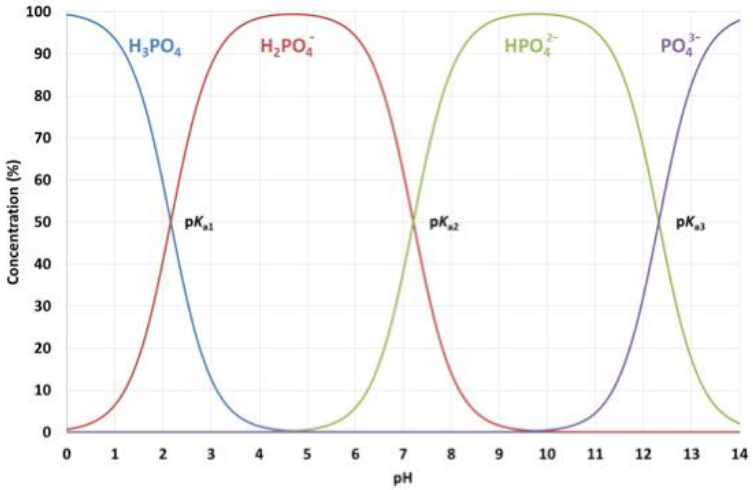

Figure 2. 4. Speciation of inorganic orthophosphoric acid as a function of pH (figure adapted from Karunanayake et al., (2019))

A systematic study of phosphate cycling and availability in different environmental conditions is vital for the understanding of phosphate removal. Phosphoric acid forms aqueous complexes with major cations of Ca^{2+}, Mg^{2+}, Al^{3+}, Fe^{2+}, and Fe^{3+} present in natural waters. At low pH, $FePO_4$ and $AlPO_4$ are the stable precipitates of phosphate. Furthermore, phosphate ions can become chemisorbed on the surfaces of iron (III) hydr(oxides). At higher pH phosphate concentrations at the water-sediment interface are buffered by the presence of hydroxyapatite ($Ca_5(PO_4)_3(OH)$), which influences P precipitation (Chang & Jackson, 1957).

The mechanism of phosphate removal by iron hydr(oxide)s can be expressed by the ligand exchange mechanism and electrostatic attraction (Yoon *et al.*, 2018). Similarly, the replacement of anions and hydroxyl by phosphate ions is referred to as the ligand exchange mechanism and is the principle removal mechanism operating on orthophosphoric at circumneutral pH.

It has previously been demonstrated that the pH of solution governs the phosphate removal efficiency. The relative contributions of different adsorption mechanisms also vary with pH which is closely related to factors such as the *adsorbent* net positive charge, free

hydroxides and the speciation of phosphate. Chitrakar *et al.*, (2006) reported the effect of pH on the adsorption of phosphate onto goethite (α-FeOOH) and akaganeite (β-FeOOH). The different ligand exchange mechanisms involved in phosphate adsorption to magnetite under varying pH is depicted in Fig. 2.5. Lower pH promotes the strength of electrostatic attraction between Fe hydroxide surfaces and orthophosphate. This is because iron hydr(oxide) functional groups are increasingly protonated and form -$FeOH_2^+$ or -Fe-O(H^+)-Fe under acidic conditions (pH~3) enabling the surface of iron hydr(oxide) particles to attract $H_2PO_4^-$ efficiently. However, phosphate adsorption becomes inhibited at pH~2, due to the formation of neutrally charged H_3PO_4 species and monovalent $H_2PO_4^-$; under which conditions the protonated *adsorbent* cannot adsorb neutral H_3PO_4 (Lin *et al.*, 2013). Moreover, iron minerals are soluble under acidic conditions. At higher pH, the net surface charge of iron minerals becomes negative via formation of -FeO^- ions. Thus, Fe surfaces create repulsion for phosphate ions and, hence inhibit phosphorus uptake. (Legodi & de Waal, 2007).

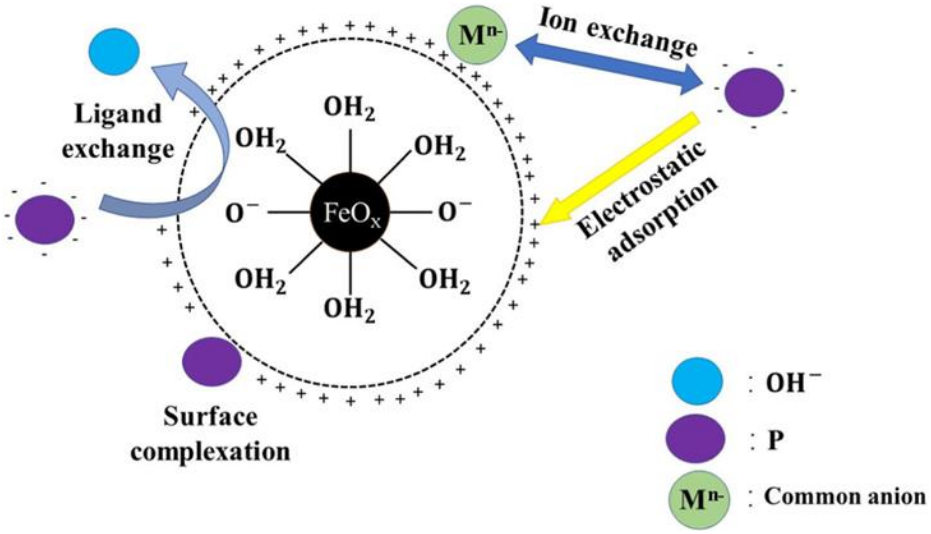

Figure 2. 5. Schematic description of phosphate adsorption onto magnetite particles under acidic conditions (adapted from Q. Wang, Z. Liao, D. Yao et al., (2021))

Various surface complexation models including non-electrostatic models, double-layer models, and triple-layer models have been developed to explain the adsorption mechanism at the solid-aqueous interface. Karunanayake *et al.*, (2019) illustrated the possible surface structures for *chemisorption* of phosphate to iron hydr(oxide) particles via surface complexation. The possible surface structures of phosphate adsorbed onto iron hydr(oxide) surfaces over the pH range of 3 to 12.8 are shown in Fig. 2.6. At low pH (3-6) structures 2,5,7 & 8 occur. At a pH of 7.5-7.9 only structure 3 occurs, while at pH 12.8 structure 4,6,9 and 10 occur. Structure 1 with hydroxyl groups is the 3D octahedral structure of magnetite.

When iron hydr(oxide) is in contact with a solution;

$$\equiv SOH + H^+ \leftrightarrow \equiv SOH_2^+ \quad (11)$$

$$\equiv SOH \leftrightarrow SO^- + H^+ \quad (12)$$

Here, $\equiv SOH$ represents the Fe surface.

Which surface complexation reaction occurs depends on pH and, can be expressed as follows:

$$\equiv SOH + H_3PO_4 \leftrightarrow SH_2PO_4 + H_2O \quad (13)$$

$$\equiv SOH + H_2PO_4^- \leftrightarrow SHPO_4^- + H_2O \quad (14)$$

$$\equiv SOH + HPO_4^{2-} \leftrightarrow SPO_4^{2-} + H_2O \quad (15)$$

$$\equiv SOH + PO_4^{3-} \leftrightarrow SOHPO_4^{3-} \quad (16)$$

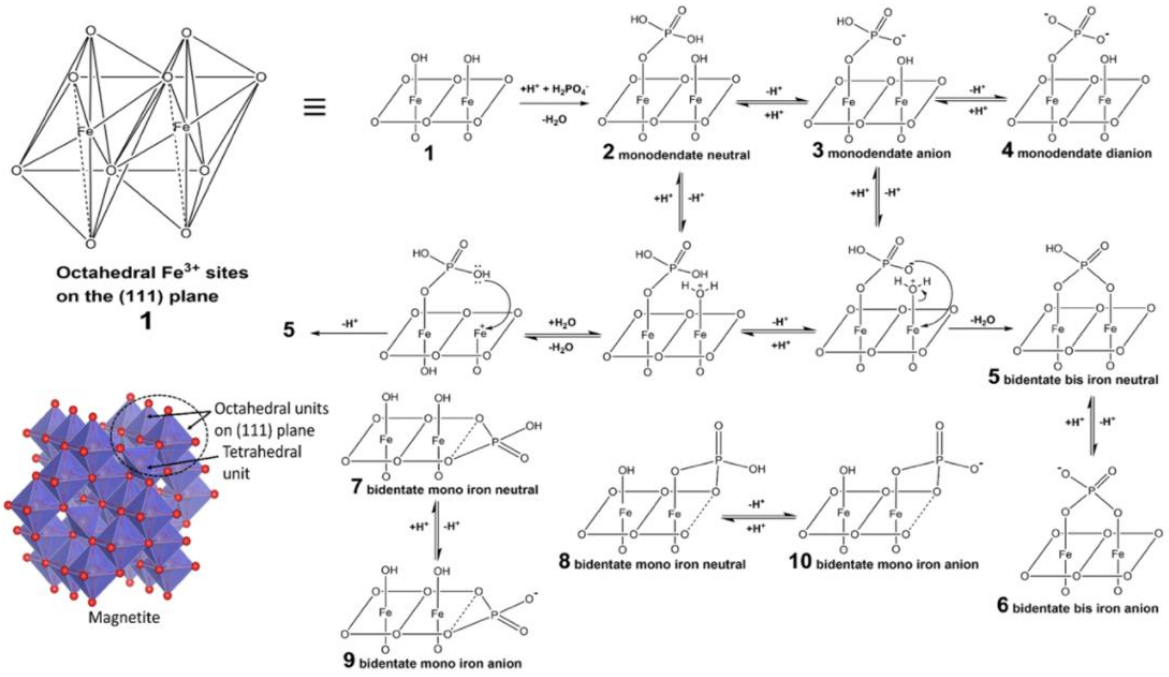

Figure 2. 6. Possible surface structures of iron hydr(oxide) and phosphate surface complexes. (figure adapted from Karunanayake et al., (2019))

2.4.4 Effect of ionic strength on P adsorption to Fe surfaces

In General, the adsorption capacity of an *adsorbent* is highly dependent on the adsorption conditions of pH and ionic strength. Ionic strength is a measure of the concentration of electrically charged species in a solution, the influence of which on adsorption varies with pH. (Barrow *et al.*, 1980). The effects of the electrolyte concentration are usually interpreted with respect to the type of complexes that the adsorbed ions can form with the surface. Ions of the electrolyte compete with the ions that form outer-sphere complexes at the adsorption sites, so adsorption of orthophosphate decreases when the electrolyte concentration increases. In contrast, electrolyte ions do not compete with orthophosphate forming inner-sphere complexes which are directly coordinated to surface groups. Additionally, increases in electrolyte concentration increase the formation of inner-sphere complexes and adsorption (Barrow *et al.*, 1980). This is because of the changes in the electric potential at the interface which decreases the electrostatic repulsion effects between the surface and anions and favors adsorption

(Hiemstra & Van Riemsdijk, 1999; Antelo *et al.*, 2005). Iron (III) is only adsorbed non-specifically (forming outer-sphere complexes), so Fe adsorption is much more affected by changing ionic strength than P adsorption. (Sparks, 2003).

2.4.5 Competing ions

The adsorption of anions to metal hydr(oxide) surfaces is important in balancing the concentration of anions in natural waters. The extent of adsorption is governed by the affinity of anions for surfaces and the relative concentration of anions. The selectivity sequences of anions for adsorption are:

For goethite Cl^-, NO_3^-, $SO_4^{2-} < CO_3^{2-}$, HPO_4^{2-}, and

For akaganeite Cl^-, $CO_3^{2-} < NO_3^- < SO_4^{2-} < HPO_4^{2-}$

These depend on the distribution coefficient K_d value (eq. 17) which is expressed as the relative affinity for a sorbate in solution to sorb to a particular solid.

$$K_d = \frac{Mass\ of\ adsorbate\ sorbed}{Mass\ of\ adsorbate\ in\ solution} \quad (17)$$

Generally, anions are effectively adsorbed on to solid surfaces through electrostatic interactions or formation of outer-sphere complexes. However, sulfate tends to compete with phosphate for adsorption sites. Nonetheless, phosphate interacts with iron hydr(oxide) via the formation of inner-sphere complexes within the coordination sphere of Fe(III) and is therefore relatively unaffected by the presence of monovalent and divalent anions (Khare *et al.*, 2005). However, the competing anion sequence with the presence of chlorides and bicarbonate follows sulfate > chloride > carbonate (Pan *et al.*, 2009).

2.4.6 Phosphate adsorption to engineered Fe surfaces

A variety of methods to remove phosphorus have been applied including chemical precipitation/crystallization, biological phosphorus removal, membrane separation, electrocoagulation, and adsorption. These methods have their own strengths and shortcomings, based on operational conditions and parameters. Among them, adsorption is often preferred due to cost-effectiveness, high efficiency and ease of operation by which the chemical sludge produced is small and the adsorbed phosphate can be easily recovered.

The main reactions are adsorption onto iron (hydr)oxides, calcite, Al(hydr)oxides and clay minerals. A variety of metal oxides, especially iron (hydr)oxides have been applied for the removal of phosphate in water. The adsorption of phosphate on different (hydr)oxides has been investigated in many articles (Table 2.2).

Table 2. 2. Fe *adsorbents* used for P removal (BET, Brunauer-Emmett-Teller)

Adsorbent	**Temp (^{0}C)**	**pH**	**Equilibration time**	**BET surface area (m^2/g)**	**pH_{pzc}**	**Pore size (nm)**	**Adsorption capacity (mg/g)**	**Adsorption capacity (mg/m^2)**	**Reference**
Nano-Fe_3O_4 modified biochar	25 35 45	3	2 min	312.6	6.6 9.1	16.7	91.3 91.0 90.0	0.3 0.3 0.3	(Karunanayake *et al.*, 2019)
Magnetite (iron hydr(oxide) waste)	-	-	1 h	75.8	6.6	11.6	11.8	0.2	(Shahid *et al.*, 2019)
Steel byproducts	20	7	6-24 h	-	-	-	1.3-5.8	-	(Hua *et al.*, 2016)
Recycled steel byproducts	20	5 7 9	1 min 3 min 10 min	-	-	-	3.5 8.4-10.4 22.7	-	(Sellner *et al.*, 2019)
Magnetite nanoparticles	25	3	24 h	-	8.0	40.0	5.2	-	(Daou *et al.*, 2007)
nFe-GAC (Granular activated carbon)	25	6.3	24 h	1024.0	6.9	4.0	100.0	0.1	(Zach-Maor *et al.*, 2011)

2.5 Surfaces and adsorption

Every structure, living or non-living, in nature, has a surface. The surface is a critical interface, which interacts with its surroundings, owing to characteristic physio-chemical properties. Surfaces that attract water and allow wetting are known as *hydrophilic*, whereas surfaces that repel water are termed *hydrophobic*. Generally, polar liquids (including water), interact strongly with hydrophilic surfaces, whereas non-polar liquids interact with hydrophobic surfaces. Polar liquids naturally contain polar molecules that create dipole moments resulting from the unequal distribution of electrons between atoms in covalent bonds. In contrast, non-polar solvents contain non-polar molecules that are composed of the atoms of equal or similar electronegativity in covalent bonds (Lag *et al.*, 2008).

An understanding of surface properties like hydrophilicity and hydrophobicity is correlated with the adsorption, catalysis and ion exchange capacities of materials. For instance, the electrostatic properties of particles govern the adsorption process via electrostatic interactions between surfaces and molecules. Electrostatic charge represents excess or deficiency of electrons on the particle surface (Salama, 2000). This leads to the development of an attractive force on oppositely charged ions, or a repulsive force on similarly charged ions (Lazarou & Aspragathos, 2012). The electrical double layer is an important concept in this regard because it describes the tendency for ions to be attracted to a surface as a result of chemical and electrochemical reactions (Park & Seo, 2011). The charge of the inner layer depends on the charge of the counterions adsorbed by the particle. Subsequently, the inner layer attracts ions of opposite polarity based on the charge (positive or negative) of the inner sphere and ions of like charge to the surface loosely bind to the second outer layer (Fig. 2.6) (Welker, 2012). Analogous to the electrical double layer concept, variable charge is electric charge on a surface that varies with the pH and electrolyte concentration. Nonbridging hydroxyls (M-OH)

coordinated with metals contribute mostly to variable charge surfaces (Laird & Koskinen, 2008). Positive and negative charge on these materials is generated from protonation and deprotonation of these hydroxyl functional groups present on their surfaces. Subsequently, oppositely charged ions can be adsorbed onto the charged surfaces. The surfaces of naturally occurring solids consist of functional groups such as −OH, −SH, −COOH. For instance, metal oxides in water acquire surface hydroxy groups, ≡S−OH for which the deprotonation step can be expressed as:

$$\equiv S{-}OH \rightleftharpoons \equiv S{-}O^{-} + H^{+} \quad (18)$$

Variable charge surfaces are strongly hydrophilic and easily form hydrogen bonds with water molecules (Wada & Kawabata, 1991). The protonation and the corresponding anion adsorption at relevant pH can be expressed as follows:

$$\equiv S{-}OH + A^{-} + H_2O \rightarrow (S{-}OH_2)\ A + OH^{-} \quad (19)$$

Thus, the charge formed by the corresponding anions or cations inhibit further adsorption as a result of repulsion forces or the neutralization of the primary double layer. Additionally, the concentration of the *adsorbate* in solution governs the extent of adsorption along with the governing chemical and physical properties of the system (e.g. pH, temperature, ionic strength, redox potential, competing ions).

Oxides or hydroxides of Si, Al, and Fe are abundant components in natural waters, soils, and sediments. Generally, surfaces of theses oxides are covered with surface hydroxyl groups when interacting with water, and hence the adsorption behavior of any material based on metal hydr(oxide) will be governed by the aforementioned phenomena.

2.5.1 Introduction to iron hydr(oxide) nanoparticles

In recent years, iron hydr(oxide)s have been a widely studied due to their unique chemical and physical properties including high adsorption capacity, magnetic properties, low-toxicity, and biocompatibility. Iron hydr(oxide)s are environmentally friendly and can be synthesized in large quantities at a low cost. Iron nanoparticles have been used extensively in the biomedical field. Iron hydr(oxide)s are used as sorbents for oil (Qiao *et al.*, 2019), wastewater heavy metals and dyes (Bhateria & Singh, 2019), and nutrients (Hua *et al.*, 2016b).

There are many categories of Iron (Fe)-based nanomaterials, such as magnetite (Fe_3O_4), hematite (Fe_2O_3), maghemite/lepidocrocite (γ- Fe_2O_3), goethite (α-FeOOH) and akaganeite (β-FeOOH) which are black, red, brown, yellow, brownish-yellow in colour respectively (Legodi & de Waal, 2007; Karunanayake *et al.*, 2019). It has been reported that (Fe)-based materials such as schwertmannite and Fe (III) oxyhydronite are known to occur but transformed into a more stable form of goethite. Many researchers investigate the adsorption onto goethite, which has become a model solid for adsorption studies. This is because goethite is one of the most common and stable crystalline iron hydr(oxides) in natural environments and is also a solid that can be prepared in a very reproducible way with particles of controlled size and geometry.

The chemical reactivity of iron hydr(oxide)s and the strong affinity of phosphorus-based ions toward metals or metal hydroxides have been extensively researched in numerous adsorption studies using different types of Fe(III) hydroxides (Table 2.4). Even though these studies deal with adsorption on goethite, akaganeite has been shown to have the highest capacity for phosphate adsorption. Akaganeite is a mesoporous material with a tunnel-shaped morphology resulting in high surface area and definite pore size distribution which assist with nanocrystal formation (Deliyanni *et al.*, 2007).

2.5.2 Synthesis of iron hydr(oxide) nanoparticles

Different methods are available for the synthesis of iron hydr(oxide) nanoparticles including chemical precipitation, co-precipitation, thermal decomposition, hydrothermal synthesis, and many other methods. A comparison of different synthesis methods based on preparation conditions, source, and different *adsorbents* is given in Table 2.3. Co-precipitation is the most widely used synthesis method because it is simple, cost–effective, and fast.

Optimizing the preparation process of iron-based *adsorbents* is necessary for any method to deposit the maximum amount of reactive surfaces of the substrate. This will allow for maximum adsorption and optimization of other physiochemical properties of the size, shape, and structure of nanoparticles. The physical, chemical and magnetic properties of nanoparticles are influenced by the type of salt used to form them, as well as the molar ratio of Fe^{3+}/ Fe^{2+}, pH, temperature and ionic strength of the media. For example, Iida *et al.*, (2007) used a molar ratio of 1:2 to reduce nanoparticle size by increasing the ion ratio resulting in the rapid crystallization of iron hydr(oxide)s.

Principally, an appropriate pH range is needed to precipitate Fe^{2+} and Fe^{3+}, higher pH results in higher precipitation of Fe^{3+} as compared with Fe^{2+} leading to the formation of ferric oxide. The alkaline medium also influences the deposition of the precipitate and formation of iron hydr(oxide) particles. Typically, sodium or ammonium hydroxides are used to create an alkaline medium, in particular and NH_4OH has been reported as the most effective precipitating agent (Morales *et al.*, 2019).

Table 2. 3. A comparison of different synthesis methods for iron hydr(oxide)

Synthesis method	**Preparation conditions**	**Source**	**Examples of adsorbents**	**Reference**
Coprecipitation	Chemical reaction of Fe^{3+} and Fe^{2+} salts in a basic solution. Iron salt solution treatment followed by alkaline solution.	Iron salts	Magnetic iron hydr(oxide) dolomite	(Yoon *et al.*, 2014)
Reverse coprecipitation	Chemical reaction of iron salt in an alkaline solution at pH ~9 to precipitate Fe^{3+}. Alkaline solution followed by iron salts	Mill scale	Magnetite particles	(Shahid *et al.*, 2019a) (Shahid & Choi, 2020)
Thermal decomposition	Materials formed from organometallic compounds. Organic solution phase used for stabilizing surfactants at a high temperature of 200-300 ^{0}C.	Tailing slurry	Iron hydr(oxide) tailings	(Zeng *et al.*, 2004)
Hydrothermal synthesis	Reactions of iron salts in alkaline solution under hydrothermal conditions (130-250 ^{0}C and 0.3-4 MPa).	Iron salts	Magnetite particles	(Cannio *et al.*, 2016) (Lassoued *et al.*, 2018)
Coprecipitation + hydrothermal treatment	Coprecipitation of iron salts in an alkaline solution at 70 ^{0}C. Hydrothermal treatment at 250 ^{0}C	Iron salts	Magnetite nanoparticles	(Daou *et al.*, 2007)
Adsorption	Agitation of Fe^{3+} salt solution with raw materials.	Eggshells and iron salt	Iron hydroxide–eggshell	(Mezenner & Bensmaili, 2009)
Microemulsion	Isotrophic synthesis using two immiscible liquids in the presence of surfactants.	Iron salts, surfactants	Iron nanoparticles	(Cheng *et al.*, 2011)

2.5.3 Surface modification of nanoparticles

When iron hydr(oxide) nanoparticles are dispersed in a fluid, they tend to aggregate as a result of their large surface area to volume ratio, creating issues of physical stability (Gupta & Gupta, 2005). In the case of bare magnetic nanoparticles, they tend to agglomerate due to strong magnetic dipolar interactions between and oxidation as a result of high chemical reactivity (Li *et al.*, 2008). Therefore, it is necessary to establish an effective strategy to improve chemical stability to protect bare iron hydr(oxide) nanoparticles from deterioration. The surface attachment of magnetic nanoparticles is a promising way to avoid aggregation between particles. To avoid aggregation, it is possible to create protecting shells with a layer of non-magnetic material (Simonsen *et al.*, 2018). Surface modification by means of coating is considered as an acceptable way to functionalize nanoparticles and to build up stability by forming colloidal dispersions. Recently, distinctive strategies including grafting organic species (surfactants, polymers, biomaterials) and coating with inorganic layers (silica, carbon, gold) have been investigated for the synthesis of high-quality magnetic nanoparticles in order to satisfy the requirements of high nutrient adsorption capacity, rapid recovery and reusability (Wu *et al.*, 2008). A comparison of different iron coated composite materials is shown in Table 2.4.

Table 2. 4. A comparison of the phosphate adsorption capacity of different composite materials

Description	**Surface area (m^2/g)**	**Particle size (nm)**	**pH**	**pH_{pzc}**	**P adsorption capacity (mg/g)**	**Reference**
Magnetite/pyrite nanocomposite	–	–	3	6.7	24.8	(Cai *et al.*, 2019)
Magnetite bio-activated carbon	520.2	0.6-5	7	–	21.2	(Han *et al.*, 2020)

Polyaminated Fe_3O_4 @ chitosan core-shell magnetic nanoparticles	74.7	11.1	4	10	50.8	(Fu *et al.*, 2020)
Hydrous zirconia coated magnetite	–	10-50	6.2 6.7-6.9	–	32.3 29.7	(Fang *et al.*, 2019)
Humic acid coated magnetite	–	–	6.6	–	28.9	(Rashid *et al.*, 2017)
Biochar coated magnetite	99.9	–	6.5	–	3.38	(Riddle *et al.*, 2018)
ferrihydrite–coated lanthanum–decorated magnetite	85.8	–	6.7	–	44.8	(Fu *et al.*, 2018)
Citric acid-coated magnetite	97.5	39.7	–	–	2.5	(Yu *et al.*, 2017)
Magnetite modified tuff grains	49	13.5	4	–	1.9	(Savić *et al.*, 2019)
Goethite coated kaolinite Goethite kaolinite mixture	39.6 34.2	– –	5 5	6.1 7.0	75.1 64.6	(Wei *et al.*, 2014)

2.5.4 Adsorbents for phosphorus removal

Considerable efforts have been made to accomplish high phosphate adsorption, using composite materials. A variety of materials have been employed for phosphorus uptake from aqueous solutions, including natural minerals, industrial by-products, and commercial synthetic products (Grace *et al.*, 2015). A comparison of phosphate adsorption capacity of *adsorbents* is shown in Table 2.5.

Recently, a variety of metal by-products have been investigated for the removal of phosphorus from water. The most common by-products are chips, wools, and turnings that are

produced during metal processing and steel manufacturing. These steel by-products have been used as effective adsorptive materials for phosphorus uptake due to their high iron content (Erickson *et al.*, 2012). Recycled steel by-products have been evaluated along with wood chip filters in subsurface drainage, demonstrating high level of phosphate removal (10-40 mg L^{-1}) (Hua *et al.*, 2016b).

Plant–based materials are widely used in adsorption and field-scale studies. These adsorption materials are preferred due to their biodegradability, recyclability, and abundance. However, modification of biomaterials via chemical and physical treatment is needed to enhance the properties of the wood as an *adsorbent*. Recently, magnetic bio sorbents have been reported as effective *adsorbents* for denitrification, phosphorus adsorption, and heavy metal removal (El-Sheikh *et al.*, 2019 ; Shah *et al.*, 2016).

Woodchips are widely used in denitrifying bioreactors to remove nitrate loads from agricultural drainage (Hua *et al.*, 2016a). Wood–based media have shown the ability to deliver long-term high nitrate removal with low maintenance in laboratory experiments (Robertson, 2010). Under field operating conditions, woodchip bioreactors have demonstrated high nitrate–removal efficiencies (Schipper *et al.*, 2010). However, woodchips do not substantially remove phosphorus largely because wood typically has a negative charge surface. Hence, woodchips have been modified in experimental studies to enhance phosphate removal (Li *et al.*, 2019), functionalization to inverse the surface charge of the wood, and thereby remove phosphrous (Wang *et al.*, 2017).

Table 2. 5. A comparison of the phosphate adsorption capacity of different adsorbents

Adsorbent	**pH**	**Particle size (nm)**	**Specific surface area (m^2/g)**	**P adsorption capacity (mg/g)**	**Reference**
Biochar	2.0	1.89	31.4	304.5	(Yin *et al.*, 2019)
Dolomite modified biochar	4.5	7.7	11.3	29.2	(Li *et al.*, 2019)
Dolomite	6.0	–	1.8	0.3	(Boeykens *et al.*, 2017)
Ochre	7.0	–	–	7.6	(Shepherd *et al.*, 2016)
Zirconium-modified zeolite	7.0	–	–	27.0	(Zhan *et al.*, 2017)
$CaCl_2$-treated zirconium-modified zeolite	7.0	–	–	14.0	(Zhan *et al.*, 2017)
pumice Mg^{2+} modified pumice	6.0	–	2.3 41.6	11.9 17.7	(Karimaian *et al.*, 2013)
Calcium-rich sepiolite	6.0	–	–	32.0	(Yin *et al.*, 2011)
Calcium decorated sludge carbon	–	20-50	15.7	116.8	(Kong *et al.*, 2018)
Modified fly ash	7.0	–	32.5	9.2	(Xu *et al.*, 2010)
Wheat straw	7.0	–	–	8.4	(Ma *et al.*, 2011)

References

Aalto, S. L., Suurnäkki, S., von Ahnen, M., Siljanen, H. M. P., Pedersen, P. B., & Tiirola, M. (2020). Nitrate removal microbiology in woodchip bioreactors: A case-study with full-scale bioreactors treating aquaculture effluents. *Science of The Total Environment*, *723*, 138093. https://doi.org/https://doi.org/10.1016/j.scitotenv.2020.138093

Abu Shmeis, R. M. (2018). Chapter One - Water Chemistry and Microbiology. In D. S. Chormey, S. Bakırdere, N. B. Turan, & G. Ö. Engin (Eds.), *Comprehensive Analytical Chemistry* (Vol. 81, pp. 1-56): Elsevier.

Ahmadi, E., Yousefzadeh, S., Mokammel, A., Miri, M., Ansari, M., Arfaeinia, H., . . . Mahvi, A. H. (2020). Kinetic study and performance evaluation of an integrated two-phase fixed-film baffled bioreactor for bioenergy recovery from wastewater and bio-wasted sludge. *Renewable and Sustainable Energy Reviews, 121*, 109674. doi:https://doi.org/10.1016/j.rser.2019.109674

Ajmal, Z., Muhmood, A., Usman, M., Kizito, S., Lu, J., Dong, R., & Wu, S. (2018). Phosphate removal from aqueous solution using iron oxides: Adsorption, desorption and regeneration characteristics. *Journal of Colloid and Interface Science, 528*, 145-155. doi:https://doi.org/10.1016/j.jcis.2018.05.084

Aller, R. C., Hall, P. O. J., Rude, P. D., & Aller, J. Y. (1998). Biogeochemical heterogeneity and suboxic diagenesis in hemipelagic sediments of the Panama Basin. *Deep Sea Research Part I: Oceanographic Research Papers, 45*(1), 133-165. doi:https://doi.org/10.1016/S0967-0637(97)00049-6

Anschutz, P., Sundby, B., Lefrançois, L., Luther, G. W., & Mucci, A. (2000). Interactions between metal oxides and species of nitrogen and iodine in bioturbated marine sediments. *Geochimica et Cosmochimica Acta, 64*(16), 2751-2763. doi:https://doi.org/10.1016/S0016-7037(00)00400-2

Antelo, J., Avena, M., Fiol, S., López, R., & Arce, F. (2005). Effects of pH and ionic strength on the adsorption of phosphate and arsenate at the goethite–water interface. *Journal of Colloid and Interface Science, 285*(2), 476-486. doi:https://doi.org/10.1016/j.jcis.2004.12.032

Arai, Y., & Sparks, D. L. (2001). ATR–FTIR Spectroscopic Investigation on Phosphate Adsorption Mechanisms at the Ferrihydrite–Water Interface. *Journal of Colloid and Interface Science, 241*(2), 317-326. doi:https://doi.org/10.1006/jcis.2001.7773

Artioli, Y. (2008). Adsorption. In S. E. Jørgensen & B. D. Fath (Eds.), *Encyclopedia of Ecology* (pp. 60-65). Oxford: Academic Press.

Asere, T. G., Stevens, C. V., & Du Laing, G. (2019). Use of (modified) natural adsorbents for arsenic remediation: A review. *Science of The Total Environment, 676*, 706-720. doi:https://doi.org/10.1016/j.scitotenv.2019.04.237

Barnard, J. L., Dunlap, P., & Steichen, M. (2017). Rethinking the Mechanisms of Biological Phosphorus Removal. *Water Environment Research, 89*(11), 2043-2054. doi:https://doi.org/10.2175/106143017X15051465919010

Barrow, N., Bowden, J., Posner, A., & Quirk, J. (1980). Describing the effects of electrolyte on adsorption of phosphate by a variable charge surface. *Soil Research, 18*(4), 395-404. doi:https://doi.org/10.1071/SR9800395

Bartlett, R., Mortimer, R. J. G., & Morris, K. (2008). Anoxic nitrification: Evidence from Humber Estuary sediments (UK). *Chemical Geology, 250*(1), 29-39. doi:https://doi.org/10.1016/j.chemgeo.2008.02.001

Bhateria, R., & Singh, R. (2019). A review on nanotechnological application of magnetic iron oxides for heavy metal removal. *Journal of Water Process Engineering, 31*, 100845. doi:https://doi.org/10.1016/j.jwpe.2019.100845

Blann, K. L., Anderson, J. L., Sands, G. R., & Vondracek, B. (2009). Effects of Agricultural Drainage on Aquatic Ecosystems: A Review. *Critical Reviews in Environmental Science and Technology, 39*(11), 909-1001. doi:10.1080/10643380801977966

Boeykens, S. P., Piol, M. N., Samudio Legal, L., Saralegui, A. B., & Vázquez, C. (2017). Eutrophication decrease: Phosphate adsorption processes in presence of nitrates.

Journal of Environmental Management, 203, 888-895. doi:https://doi.org/10.1016/j.jenvman.2017.05.026

Borch, T., Kretzschmar, R., Kappler, A., Cappellen, P. V., Ginder-Vogel, M., Voegelin, A., & Campbell, K. (2010). Biogeochemical Redox Processes and their Impact on Contaminant Dynamics. *Environmental Science & Technology, 44*(1), 15-23. doi:10.1021/es9026248

Borch, T., Masue, Y., Kukkadapu, R. K., & Fendorf, S. (2007). Phosphate Imposed Limitations on Biological Reduction and Alteration of Ferrihydrite. *Environmental Science & Technology, 41*(1), 166-172. doi:10.1021/es060695p

Brdjanovic, D., Logemann, S., M. van Loosdrecht, M. C., Hooijmans, C. M., J. Alaerts, G., & Heijnen, J. J. (1998). Influence of temperature on biological phosphorus removal: process and molecular ecological studies. *Water Research, 32*(4), 1035-1048. doi:https://doi.org/10.1016/S0043-1354(97)00322-9

Cai, W., Fu, F., Zhu, L., & Tang, B. (2019). Simultaneous removal of chromium(VI) and phosphate from water using easily separable magnetite/pyrite nanocomposite. *Journal of Alloys and Compounds, 803*, 118-125. doi:https://doi.org/10.1016/j.jallcom.2019.06.285

Cannio, M., Ponzoni, C., Gualtieri, M. L., Lugli, E., Leonelli, C., & Romagnoli, M. (2016). Stabilization and thermal conductivity of aqueous magnetite nanofluid from continuous flows hydrothermal microwave synthesis. *Materials Letters, 173*, 195-198. doi:https://doi.org/10.1016/j.matlet.2016.03.040

Carrillo, V., Fuentes, B., Gómez, G., & Vidal, G. (2020). Characterization and recovery of phosphorus from wastewater by combined technologies. *Reviews in Environmental Science and Bio/Technology, 19*(2), 389-418. https://doi.org/10.1007/s11157-020-09533-1

Chang, S., & Jackson, M. (1957). Solubility Product of Iron Phosphate 1. *Soil Sci. Soc. Am. J., 21*, 265.

Charlson, R. J., & Emerson, S. (2000). 16 - The Acid—Base and Oxidation—Reduction Balances of the Earth. In M. C. Jacobson, R. J. Charlson, H. Rodhe, & G. H. Orians (Eds.), *International Geophysics* (Vol. 72, pp. 421-438): Academic Press.

Cheng, C., He, Q., Zhang, J., Chai, H., Yang, Y., Pavlostathis, S. G., & Wu, H. (2022). New insight into ammonium oxidation processes and mechanisms mediated by manganese oxide in constructed wetlands. *Water Research, 215*, 118251. doi:https://doi.org/10.1016/j.watres.2022.118251

Cheng, S., Qin, C., Xie, H., Wang, W., Zhang, J., Hu, Z., & Liang, S. (2021). Comprehensive evaluation of manganese oxides and iron oxides as metal substrate materials for constructed wetlands from the perspective of water quality and greenhouse effect. *Ecotoxicology and Environmental Safety, 221*, 112451. doi:https://doi.org/10.1016/j.ecoenv.2021.112451

Cheng, X., Wu, B., Yang, Y., & Li, Y. (2011). Synthesis of iron nanoparticles in water-in-oil microemulsions for liquid-phase Fischer–Tropsch synthesis in polyethylene glycol. *Catalysis Communications, 12*(6), 431-435. doi:https://doi.org/10.1016/j.catcom.2010.11.011

Chitrakar, R., Tezuka, S., Sonoda, A., Sakane, K., Ooi, K., & Hirotsu, T. (2006). Phosphate adsorption on synthetic goethite and akaganeite. *Journal of Colloid and Interface Science, 298*(2), 602-608. doi:https://doi.org/10.1016/j.jcis.2005.12.054

Chouyyok, W., Wiacek, R. J., Pattamakomsan, K., Sangvanich, T., Grudzien, R. M., Fryxell, G. E., & Yantasee, W. (2010). Phosphate Removal by Anion Binding on Functionalized Nanoporous Sorbents. *Environmental Science & Technology, 44*(8), 3073-3078. doi:10.1021/es100787m

Daou, T. J., Begin-Colin, S., Grenèche, J. M., Thomas, F., Derory, A., Bernhardt, P., . . . Pourroy, G. (2007). Phosphate Adsorption Properties of Magnetite-Based Nanoparticles. *Chemistry of Materials, 19*(18), 4494-4505. doi:10.1021/cm071046v

Deliyanni, E., Peleka, E., & Lazaridis, N. (2007). Comparative Study of Phosphates Removal from Aqueous Solutions by Nanocrystalline Akaganéite and Hybrid Surfactant-akaganéite. *Sep. Purif. Technol., 52*, 478.

Deng, S., Li, D., Yang, X., Xing, W., Li, J., & Zhang, Q. (2016). Biological denitrification process based on the Fe(0)–carbon micro-electrolysis for simultaneous ammonia and nitrate removal from low organic carbon water under a microaerobic condition. *Bioresource Technology, 219*, 677-686. doi:https://doi.org/10.1016/j.biortech.2016.08.014

Ding, J., Su, M., Wu, C., & Lin, K. (2015). Transformation of triclosan to 2,8-dichlorodibenzo-p-dioxin by iron and manganese oxides under near dry conditions. *Chemosphere, 133*, 41-46. doi:https://doi.org/10.1016/j.chemosphere.2015.03.055

Dong, H., Qiang, Z., Li, T., Jin, H., & Chen, W. (2012). Effect of artificial aeration on the performance of vertical-flow constructed wetland treating heavily polluted river water. *Journal of Environmental Sciences, 24*(4), 596-601. doi:https://doi.org/10.1016/S1001-0742(11)60804-8

Dos Santos Afonso, M., & Stumm, W. (1992). Reductive dissolution of iron(III) (hydr)oxides by hydrogen sulfide. *Langmuir, 8*(6), 1671-1675. doi:10.1021/la00042a030

Druschel, G. K., Emerson, D., Sutka, R., Suchecki, P., & Luther, G. W. (2008). Low-oxygen and chemical kinetic constraints on the geochemical niche of neutrophilic iron(Aalto et al.) oxidizing microorganisms. *Geochimica et Cosmochimica Acta, 72*(14), 3358-3370. doi:https://doi.org/10.1016/j.gca.2008.04.035

Edahbi, M., Plante, B., Benzaazoua, M., Ward, M., & Pelletier, M. (2018). Mobility of rare earth elements in mine drainage: Influence of iron oxides, carbonates, and phosphates. *Chemosphere, 199*, 647-654. doi:https://doi.org/10.1016/j.chemosphere.2018.02.054

El-Sheikh, A. H., Al-Salamin, R. M., Alshamaly, H. S., Tahboub, D. a. M., Al-Degs, Y. S., Fasfous, I. I., . . . Abdelghani, J. I. (2019). Effect of varying deposition conditions of magnetite on sawdust on the physiochemical properties of the prepared composites. *Journal of Environmental Chemical Engineering, 7*(6), 103497. doi:https://doi.org/10.1016/j.jece.2019.103497

Erdal, U. (2003). The competition between PAOs and GAOs in EBPR systems at different temperatures and the effects on system performanace. *Wat. Sci. Tech., 47*(11), 1-8.

Erickson, A. J., Gulliver, J. S., & Weiss, P. T. (2012). Capturing phosphates with iron enhanced sand filtration. *Water Research, 46*(9), 3032-3042. doi:https://doi.org/10.1016/j.watres.2012.03.009

Eusterhues, K., Wagner, F. E., Häusler, W., Hanzlik, M., Knicker, H., Totsche, K. U., . . . Schwertmann, U. (2008). Characterization of Ferrihydrite-Soil Organic Matter Coprecipitates by X-ray Diffraction and Mössbauer Spectroscopy. *Environmental Science & Technology, 42*(21), 7891-7897. doi:10.1021/es800881w

Fang, W., Wang, Z., Xie, Q., Liu, Y., & Wu, D. (2019). Formation of Fe3O4@ZrO2 nanocomposite and its performance as a magnetic adsorbent for phosphate uptake: Influences of end-point pH and stirring rate during synthesis process. *Chemical Engineering Research and Design, 145*, 194-202. doi:https://doi.org/10.1016/j.cherd.2019.03.013

Filipe, C. D. M., Daigger, G. T., & Grady Jr, C. P. L. (2001). Effects of pH on the Rates of Aerobic Metabolism of Phosphate-Accumulating and Glycogen-Accumulating Organisms. *Water Environment Research, 73*(2), 213-222. doi:https://doi.org/10.2175/106143001X139191

Fu, C.-C., Tran, H. N., Chen, X.-H., & Juang, R.-S. (2020). Preparation of polyaminated Fe3O4@chitosan core-shell magnetic nanoparticles for efficient adsorption of phosphate in aqueous solutions. *Journal of Industrial and Engineering Chemistry, 83*, 235-246. doi:https://doi.org/10.1016/j.jiec.2019.11.033

Fu, H., Yang, Y., Zhu, R., Liu, J., Usman, M., Chen, Q., & He, H. (2018). Superior adsorption of phosphate by ferrihydrite-coated and lanthanum-decorated magnetite. *Journal of Colloid and Interface Science, 530*, 704-713. doi:https://doi.org/10.1016/j.jcis.2018.07.025

Grace, M. A., Healy, M. G., & Clifford, E. (2015). Use of industrial by-products and natural media to adsorb nutrients, metals and organic carbon from drinking water. *Science of The Total Environment, 518-519*, 491-497. doi:https://doi.org/10.1016/j.scitotenv.2015.02.075

Griffiths, P. C., Stratton, H. M., & Seviour, R. J. (2002). Environmental factors contributing to the "G bacteria" population in full-scale EBPR plants. *Water Science and Technology, 46*(4-5), 185-192. doi:10.2166/wst.2002.0583

Gupta, A. K., & Gupta, M. (2005). Synthesis and surface engineering of iron oxide nanoparticles for biomedical applications. *Biomaterials, 26*(18), 3995-4021. doi:https://doi.org/10.1016/j.biomaterials.2004.10.012

Hammes, F., & Verstraete*, W. (2002). Key roles of pH and calcium metabolism in microbial carbonate precipitation. *Reviews in Environmental Science and Biotechnology, 1*(1), 3-7. doi:10.1023/A:1015135629155

Han, T., Lu, X., Sun, Y., Jiang, J., Yang, W., & Jönsson, P. G. (2020). Magnetic bio-activated carbon production from lignin via a streamlined process and its use in phosphate removal from aqueous solutions. *Science of The Total Environment, 708*, 135069. doi:https://doi.org/10.1016/j.scitotenv.2019.135069

Harijan, D. K. L., & Chandra, V. (2017). Akaganeite nanorods decorated graphene oxide sheets for removal and recovery of aqueous phosphate. *Journal of Water Process Engineering, 19*, 120-125. doi:https://doi.org/10.1016/j.jwpe.2017.07.019

Hastings, D., & Emerson, S. (1986). Oxidation of manganese by spores of a marine bacillus: Kinetic and thermodynamic considerations. *Geochimica et Cosmochimica Acta, 50*(8), 1819-1824. doi:https://doi.org/10.1016/0016-7037(86)90141-9

Hein, J. R., Koschinsky, A., Halbach, P., Manheim, F. T., Bau, M., Kang, J.-K., & Lubick, N. (1997). Iron and manganese oxide mineralization in the Pacific. *Geological Society, London, Special Publications, 119*(1), 123. doi:10.1144/GSL.SP.1997.119.01.09

Herzon, I., & Helenius, J. (2008). Agricultural drainage ditches, their biological importance and functioning. *Biological Conservation, 141*(5), 1171-1183. doi:https://doi.org/10.1016/j.biocon.2008.03.005

Hiemstra, T., & Van Riemsdijk, W. H. (1999). Surface Structural Ion Adsorption Modeling of Competitive Binding of Oxyanions by Metal (Hydr)oxides. *Journal of Colloid and Interface Science, 210*(1), 182-193. doi:https://doi.org/10.1006/jcis.1998.5904

Hua, G., Salo, M. W., Schmit, C. G., & Hay, C. H. (2016). Nitrate and phosphate removal from agricultural subsurface drainage using laboratory woodchip bioreactors and recycled steel byproduct filters. *Water Research, 102*, 180-189. doi:https://doi.org/10.1016/j.watres.2016.06.022

Hua, G., Salo, M. W., Schmit, C. G., & Hay, C. H. (2016). Nitrate and phosphate removal from agricultural subsurface drainage using laboratory woodchip bioreactors and recycled steel byproduct filters. *Water Res, 102*, 180-189. doi:10.1016/j.watres.2016.06.022

Huang, H.-J., Ramaswamy, S., Tschirner, U. W., & Ramarao, B. V. (2008). A review of separation technologies in current and future biorefineries. *Separation and Purification Technology, 62*(1), 1-21. doi:https://doi.org/10.1016/j.seppur.2007.12.011

Hulth, S., Aller, R. C., & Gilbert, F. (1999). Coupled anoxic nitrification/manganese reduction in marine sediments. *Geochimica et Cosmochimica Acta, 63*(1), 49-66. doi:https://doi.org/10.1016/S0016-7037(98)00285-3

Iida, H., Takayanagi, K., Nakanishi, T., & Osaka, T. (2007). Synthesis of Fe3O4 nanoparticles with various sizes and magnetic properties by controlled hydrolysis. *Journal of Colloid and Interface Science, 314*(1), 274-280. doi:https://doi.org/10.1016/j.jcis.2007.05.047

Johnson, D. B., & Hallberg, K. B. (2005). Biogeochemistry of the compost bioreactor components of a composite acid mine drainage passive remediation system. *Science of The Total Environment, 338*(1), 81-93. doi:https://doi.org/10.1016/j.scitotenv.2004.09.008

Jones, A. M., Collins, R. N., Rose, J., & Waite, T. D. (2009). The effect of silica and natural organic matter on the Fe(Aalto et al.)-catalysed transformation and reactivity of Fe(III) minerals. *Geochimica et Cosmochimica Acta, 73*(15), 4409-4422. doi:https://doi.org/10.1016/j.gca.2009.04.025

Kappler, A., Benz, M., Schink, B., & Brune, A. (2004). Electron shuttling via humic acids in microbial iron(III) reduction in a freshwater sediment. *FEMS Microbiology Ecology, 47*(1), 85-92. doi:10.1016/S0168-6496(03)00245-9

Karageorgiou, K., Paschalis, M., & Anastassakis, G. N. (2007). Removal of phosphate species from solution by adsorption onto calcite used as natural adsorbent. *Journal of Hazardous Materials, 139*(3), 447-452. doi:https://doi.org/10.1016/j.jhazmat.2006.02.038

Karimaian, K. A., Amrane, A., Kazemian, H., Panahi, R., & Zarrabi, M. (2013). Retention of phosphorous ions on natural and engineered waste pumice: Characterization, equilibrium, competing ions, regeneration, kinetic, equilibrium and thermodynamic study. *Applied Surface Science, 284*, 419-431. doi:https://doi.org/10.1016/j.apsusc.2013.07.114

Karimi, S., Tavakkoli Yaraki, M., & Karri, R. R. (2019). A comprehensive review of the adsorption mechanisms and factors influencing the adsorption process from the perspective of bioethanol dehydration. *Renewable and Sustainable Energy Reviews, 107*, 535-553. doi:https://doi.org/10.1016/j.rser.2019.03.025

Karunanayake, A. G., Navarathna, C. M., Gunatilake, S. R., Crowley, M., Anderson, R., Mohan, D., . . . Mlsna, T. (2019). Fe3O4 Nanoparticles Dispersed on Douglas Fir Biochar for Phosphate Sorption. *ACS Applied Nano Materials, 2*(6), 3467-3479. doi:10.1021/acsanm.9b00430

Khare, N., Hesterberg, D., & Martin, J. D. (2005). XANES Investigation of Phosphate Sorption in Single and Binary Systems of Iron and Aluminum Oxide Minerals. *Environmental Science & Technology, 39*(7), 2152-2160. doi:10.1021/es049237b

Kong, L., Han, M., Shih, K., Su, M., Diao, Z., Long, J., . . . Peng, Y. (2018). Nano-rod Ca-decorated sludge derived carbon for removal of phosphorus. *Environmental Pollution, 233*, 698-705. doi:https://doi.org/10.1016/j.envpol.2017.10.099

Kuba, T., & Loosdrechtt, M. C. M. v. (1996). Effect of cyclic oxygen exposure on the activity of denitrifying phosphorus removing bacteria. *Water Science and Technology, 34*(1), 33-40. doi:https://doi.org/10.1016/0273-1223(96)00492-1

Kukkadapu, R. K., Zachara, J. M., Fredrickson, J. K., & Kennedy, D. W. (2004). Biotransformation of two-line silica-ferrihydrite by a dissimilatory Fe(III)-reducing bacterium: formation of carbonate green rust in the presence of phosphate1 1Associate editor: D. J. Vaughan. *Geochimica et Cosmochimica Acta, 68*(13), 2799-2814. doi:https://doi.org/10.1016/j.gca.2003.12.024

Lag, J., Hadas, A., Fairbridge, R. W., Muñoz, J. C. N., Pombal, X. P., Cortizas, A. M., . . . Jaynes, W. F. (2008). Hydrophilicity, Hydrophobicity. In W. Chesworth (Ed.), *Encyclopedia of Soil Science* (pp. 329-330). Dordrecht: Springer Netherlands.

Laird, D. A., & Koskinen, W. C. (2008). Chapter 21 - Triazine Soil Interactions. In H. M. LeBaron, J. E. McFarland, & O. C. Burnside (Eds.), *The Triazine Herbicides* (pp. 275-299). San Diego: Elsevier.

Lassoued, A., Lassoued, M. S., Dkhil, B., Ammar, S., & Gadri, A. (2018). Synthesis, photoluminescence and Magnetic properties of iron oxide (α-Fe2O3) nanoparticles through precipitation or hydrothermal methods. *Physica E: Low-dimensional Systems and Nanostructures, 101*, 212-219. doi:https://doi.org/10.1016/j.physe.2018.04.009

Lazarou, P., & Aspragathos, N. A. (2012). 2 - Planar micromanipulation on microconveyor platforms: recent developments. In J. P. Davim (Ed.), *Mechatronics and Manufacturing Engineering* (pp. 47-97): Woodhead Publishing.

Legodi, M. A., & de Waal, D. (2007). The preparation of magnetite, goethite, hematite and maghemite of pigment quality from mill scale iron waste. *Dyes and Pigments, 74*(1), 161-168. doi:https://doi.org/10.1016/j.dyepig.2006.01.038

Li, G.-y., Jiang, Y.-r., Huang, K.-l., Ding, P., & Chen, J. (2008). Preparation and properties of magnetic Fe3O4–chitosan nanoparticles. *Journal of Alloys and Compounds, 466*(1), 451-456. doi:https://doi.org/10.1016/j.jallcom.2007.11.100

Li, J., Li, B., Huang, H., Lv, X., Zhao, N., Guo, G., & Zhang, D. (2019). Removal of phosphate from aqueous solution by dolomite-modified biochar derived from urban dewatered sewage sludge. *Science of The Total Environment, 687*, 460-469. doi:https://doi.org/10.1016/j.scitotenv.2019.05.400

Li, R., Wang, J. J., Zhang, Z., Awasthi, M. K., Du, D., Dang, P., . . . Wang, L. (2018). Recovery of phosphate and dissolved organic matter from aqueous solution using a novel CaO-MgO hybrid carbon composite and its feasibility in phosphorus recycling. *Science of The Total Environment, 642*, 526-536. doi:https://doi.org/10.1016/j.scitotenv.2018.06.092

Liger, E., Charlet, L., & Van Cappellen, P. (1999). Surface catalysis of uranium(VI) reduction by iron(Aalto et al.). *Geochimica et Cosmochimica Acta, 63*(19), 2939-2955. doi:https://doi.org/10.1016/S0016-7037(99)00265-3

Lin, Y.-F., Chen, H.-W., Chen, Y.-C., & Chiou, C.-S. (2013). Application of magnetite modified with polyacrylamide to adsorb phosphate in aqueous solution. *Journal of the Taiwan Institute of Chemical Engineers, 44*(1), 45-51. doi:https://doi.org/10.1016/j.jtice.2012.09.005

Lloyd, J. R., Sole, V. A., Van Praagh, C. V. G., & Lovley, D. R. (2000). Direct and Fe(Aalto et al.)-Mediated Reduction of Technetium by Fe(III)-Reducing Bacteria. *Applied and Environmental Microbiology, 66*(9), 3743. doi:10.1128/AEM.66.9.3743-3749.2000

Ma, Z., Li, Q., Yue, Q., Gao, B., Li, W., Xu, X., & Zhong, Q. (2011). Adsorption removal of ammonium and phosphate from water by fertilizer controlled release agent prepared from wheat straw. *Chemical Engineering Journal, 171*(3), 1209-1217. doi:https://doi.org/10.1016/j.cej.2011.05.027

Macalady, J., & Banfield, J. F. (2003). Molecular geomicrobiology: genes and geochemical cycling. *Earth and Planetary Science Letters, 209*(1), 1-17. doi:https://doi.org/10.1016/S0012-821X(02)01010-5

Maurer, M., Abramovich, D., Siegrist, H., & Gujer, W. (1999). Kinetics of biologically induced phosphorus precipitation in waste-water treatment. *Water Research, 33*(2), 484-493. doi:https://doi.org/10.1016/S0043-1354(98)00221-8

Mezenner, N. Y., & Bensmaili, A. (2009). Kinetics and thermodynamic study of phosphate adsorption on iron hydroxide-eggshell waste. *Chemical Engineering Journal, 147*(2), 87-96. doi:https://doi.org/10.1016/j.cej.2008.06.024

Mino, T., van Loosdrecht, M. C. M., & Heijnen, J. J. (1998). Microbiology and biochemistry of the enhanced biological phosphate removal process. *Water Research, 32*(11), 3193-3207. doi:https://doi.org/10.1016/S0043-1354(98)00129-8

Miyata, N., Tani, Y., Maruo, K., Tsuno, H., Sakata, M., & Iwahori, K. (2006). Manganese(IV) Oxide Production by Acremonium sp. Strain KR21-2 and Extracellular Mn(Aalto et al.) Oxidase Activity. *Applied and Environmental Microbiology, 72*(10), 6467. doi:10.1128/AEM.00417-06

Mohan, D., Sarswat, A., Ok, Y. S., & Pittman, C. U. (2014). Organic and inorganic contaminants removal from water with biochar, a renewable, low cost and sustainable adsorbent – A critical review. *Bioresource Technology, 160*, 191-202. doi:https://doi.org/10.1016/j.biortech.2014.01.120

Morales, F., Márquez, G., Sagredo, V., Torres, T. E., & Denardin, J. C. (2019). Structural and magnetic properties of silica-coated magnetite nanoaggregates. *Physica B: Condensed Matter, 572*, 214-219. doi:https://doi.org/10.1016/j.physb.2019.08.007

Moreira, R. F. P. M., Vandresen, S., Luiz, D. B., José, H. J., & Puma, G. L. (2017). Adsorption of arsenate, phosphate and humic acids onto acicular goethite nanoparticles recovered from acid mine drainage. *Journal of Environmental Chemical Engineering, 5*(1), 652-659. doi:https://doi.org/10.1016/j.jece.2016.12.018

Morse, J. W. (1988). Stumm, W. [ed.]. 1987. Aquatic surface chemistry: Chemical processes at the particle-water interface. John Wiley & Sons, Inc., Somerset, New Jersey. 520 p. $69.95. *Limnology and Oceanography, 33*(2), 311-311. doi:https://doi.org/10.4319/lo.1988.33.2.0311

Oehmen, A., Carvalho, G., Freitas, F., & Reis, M. A. (2010). Assessing the abundance and activity of denitrifying polyphosphate accumulating organisms through molecular and chemical techniques. *Water Sci Technol, 61*(8), 2061-2068. doi:10.2166/wst.2010.976

Oehmen, A., Lemos, P. C., Carvalho, G., Yuan, Z., Keller, J., Blackall, L. L., & Reis, M. A. M. (2007). Advances in enhanced biological phosphorus removal: From micro to macro scale. *Water Research, 41*(11), 2271-2300. doi:https://doi.org/10.1016/j.watres.2007.02.030

Ogata, F., Nagai, N., Kishida, M., Nakamura, T., & Kawasaki, N. (2019). Interaction between phosphate ions and Fe-Mg type hydrotalcite for purification of wastewater. *Journal of Environmental Chemical Engineering, 7*(1), 102897. doi:https://doi.org/10.1016/j.jece.2019.102897

Ong, S.-A., Uchiyama, K., Inadama, D., Ishida, Y., & Yamagiwa, K. (2010). Performance evaluation of laboratory scale up-flow constructed wetlands with different designs and emergent plants. *Bioresource Technology, 101*(19), 7239-7244. doi:https://doi.org/10.1016/j.biortech.2010.04.032

Pan, B., Wu, J., Pan, B., Lv, L., Zhang, W., Xiao, L., . . . Zheng, S. (2009). Development of polymer-based nanosized hydrated ferric oxides (HFOs) for enhanced phosphate removal from waste effluents. *Water Research, 43*(17), 4421-4429. doi:https://doi.org/10.1016/j.watres.2009.06.055

Park, S.-J., & Seo, M.-K. (2011). Chapter 1 - Intermolecular Force. In S.-J. Park & M.-K. Seo (Eds.), *Interface Science and Technology* (Vol. 18, pp. 1-57): Elsevier.

Patterson, H. B. W. (2009). Chapter 2 - Adsorption. In G. R. List (Ed.), *Bleaching and Purifying Fats and Oils (Second Edition)* (pp. 53-67): AOCS Press.

Putt, R., Singh, M., Chinnasamy, S., & Das, K. C. (2011). An efficient system for carbonation of high-rate algae pond water to enhance CO2 mass transfer. *Bioresource Technology, 102*(3), 3240-3245. doi:https://doi.org/10.1016/j.biortech.2010.11.029

Qiao, K., Tian, W., Bai, J., Wang, L., Zhao, J., Du, Z., & Gong, X. (2019). Application of magnetic adsorbents based on iron oxide nanoparticles for oil spill remediation: A review. *Journal of the Taiwan Institute of Chemical Engineers, 97*, 227-236. doi:https://doi.org/10.1016/j.jtice.2019.01.029

Rashid, M., Price, N. T., Gracia Pinilla, M. Á., & O'Shea, K. E. (2017). Effective removal of phosphate from aqueous solution using humic acid coated magnetite nanoparticles. *Water Research, 123*, 353-360. doi:https://doi.org/10.1016/j.watres.2017.06.085

Remucal, C. K., & Ginder-Vogel, M. (2014). A critical review of the reactivity of manganese oxides with organic contaminants. *Environmental Science: Processes & Impacts, 16*(6), 1247-1266. doi:10.1039/C3EM00703K

Rickard, D. (2006). The solubility of FeS. *Geochimica et Cosmochimica Acta, 70*(23), 5779-5789. doi:https://doi.org/10.1016/j.gca.2006.02.029

Riddle, M., Cederlund, H., Schmieder, F., & Bergström, L. (2018). Magnetite-coated biochar as a soil phosphate filter: From laboratory to field lysimeter. *Geoderma, 327*, 45-54. doi:https://doi.org/10.1016/j.geoderma.2018.04.025

Robertson, W. D. (2010). Nitrate removal rates in woodchip media of varying age. *Ecological Engineering, 36*(11), 1581-1587. doi:https://doi.org/10.1016/j.ecoleng.2010.01.008

Rue, G. P., Darling, J. P., Graham, E., Tfaily, M. M., & McKnight, D. M. (2019). Dynamic changes in dissolved organic matter composition in a Mountain Lake under ice cover and relationships to changes in nutrient cycling and phytoplankton community composition. *Aquatic Sciences, 82*(1), 15. doi:10.1007/s00027-019-0687-3

Saito, T., Brdjanovic, D., & van Loosdrecht, M. C. M. (2004). Effect of nitrite on phosphate uptake by phosphate accumulating organisms. *Water Research, 38*(17), 3760-3768. doi:https://doi.org/10.1016/j.watres.2004.05.023

Salama, A. I. A. (2000). MECHANICAL TECHNIQUES: PARTICLE SIZE SEPARATION. In I. D. Wilson (Ed.), *Encyclopedia of Separation Science* (pp. 3277-3289). Oxford: Academic Press.

Sañudo-Wilhelmy, S. A., Tovar-Sanchez, A., Fu, F.-X., Capone, D. G., Carpenter, E. J., & Hutchins, D. A. (2004). The impact of surface-adsorbed phosphorus on phytoplankton Redfield stoichiometry. *Nature, 432*(7019), 897-901. doi:10.1038/nature03125

Savić, A. B., Čokeša, D., Lazarević, S., Jokić, B., Janaćković, D., Petrović, R., & Živković, L. S. (2016). Tailoring of magnetite powder properties for enhanced phosphate removal: Effect of PEG addition in the synthesis process. *Powder Technology, 301*, 511-519. doi:https://doi.org/10.1016/j.powtec.2016.06.028

Savić, A. B., Čokeša, D., Savić Biserčić, M., Častvan-Janković, I., Petrović, R., & Živković, L. S. (2019). Multifunctional use of magnetite-coated tuff grains in water treatment: Removal of arsenates and phosphates. *Advanced Powder Technology, 30*(8), 1687-1695. doi:https://doi.org/10.1016/j.apt.2019.05.020

Schipper, L. A., Robertson, W. D., Gold, A. J., Jaynes, D. B., & Cameron, S. C. (2010). Denitrifying bioreactors—An approach for reducing nitrate loads to receiving waters. *Ecological Engineering, 36*(11), 1532-1543. doi:https://doi.org/10.1016/j.ecoleng.2010.04.008

Sellner, B. M., Hua, G., & Ahiablame, L. M. (2019). Fixed bed column evaluation of phosphate adsorption and recovery from aqueous solutions using recycled steel byproducts. *Journal of Environmental Management, 233*, 595-602. doi:https://doi.org/10.1016/j.jenvman.2018.12.070

Shah, J., Jan, M. R., Khan, M., & Amir, S. (2016). Removal and recovery of cadmium from aqueous solutions using magnetic nanoparticle-modified sawdust: kinetics and adsorption isotherm studies. *Desalination and Water Treatment, 57*(21), 9736-9744. doi:10.1080/19443994.2015.1030777

Shahid, M. K., & Choi, Y. (2020). Characterization and application of magnetite Particles, synthesized by reverse coprecipitation method in open air from mill scale. *Journal of Magnetism and Magnetic Materials, 495*, 165823. doi:https://doi.org/10.1016/j.jmmm.2019.165823

Shahid, M. K., Kim, Y., & Choi, Y.-G. (2019a). Magnetite synthesis using iron oxide waste and its application for phosphate adsorption with column and batch reactors. *Chem. Eng. Res. Des., 148*, 169-179. doi:10.1016/j.cherd.2019.06.001

Shahid, M. K., Kim, Y., & Choi, Y.-G. (2019b). Magnetite synthesis using iron oxide waste and its application for phosphate adsorption with column and batch reactors. *Chemical Engineering Research and Design, 148*, 169-179. doi:https://doi.org/10.1016/j.cherd.2019.06.001

Shao, S., Zhong, J., Wang, C., Pan, D., & Wu, X. (2022). Performance of simultaneous nitrification–denitrification and denitrifying phosphorus and manganese removal by driving a single-stage moving bed biofilm reactor based on manganese redox cycling. *Bioresource Technology, 362*, 127846. https://doi.org/https://doi.org/10.1016/j.biortech.2022.127846

Shepherd, J. G., Sohi, S. P., & Heal, K. V. (2016). Optimising the recovery and re-use of phosphorus from wastewater effluent for sustainable fertiliser development. *Water Research, 94*, 155-165. doi:https://doi.org/10.1016/j.watres.2016.02.038

Simonsen, G., Strand, M., & Øye, G. (2018). Potential applications of magnetic nanoparticles within separation in the petroleum industry. *Journal of Petroleum Science and Engineering, 165*, 488-495. doi:https://doi.org/10.1016/j.petrol.2018.02.048

Soleimani, H., Mahvi, A. H., Yaghmaeian, K., Abbasnia, A., Sharafi, K., Alimohammadi, M., & Zamanzadeh, M. (2019). Effect of modification by five different acids on pumice stone as natural and low-cost adsorbent for removal of humic acid from aqueous solutions - Application of response surface methodology. *Journal of Molecular Liquids, 290*, 111181. doi:https://doi.org/10.1016/j.molliq.2019.111181

Spaling, H., & Smit, B. (1995). A conceptual model of cumulative environmental effects of agricultural land drainage. *Agriculture, Ecosystems & Environment, 53*(2), 99-108. doi:https://doi.org/10.1016/0167-8809(94)00566-W

Sparks, D. L. (2003). *Environmental soil chemistry* (2nd ed.. ed.). San Diego, Calif. London: San Diego, Calif. London : Academic.

Sun, Y., Peng, Y., Zhang, J., Li, X., Zhang, Q., & Zhang, L. (2020). Effect of endogenous metabolisms on survival and activities of denitrifying phosphorus removal sludge under various starvation conditions. *Bioresource Technology, 315*, 123839. doi:https://doi.org/10.1016/j.biortech.2020.123839

Tareq, R., Akter, N., & Azam, M. S. (2019). Chapter 10 - Biochars and Biochar Composites: Low-Cost Adsorbents for Environmental Remediation. In Y. S. Ok, D. C. W. Tsang, N. Bolan, & J. M. Novak (Eds.), *Biochar from Biomass and Waste* (pp. 169-209): Elsevier.

Tebo, B. M., Bargar, J. R., Clement, B. G., Dick, G. J., Murray, K. J., Parker, D., . . . Webb, S. M. (2004). BIOGENIC MANGANESE OXIDES: Properties and Mechanisms of Formation. *Annual Review of Earth and Planetary Sciences, 32*(1), 287-328. doi:10.1146/annurev.earth.32.101802.120213

vanLoon, G. W., & Duffy, S. J. (2017). *Environmental chemistry: a global perspective*: Oxford University Press.

Vikrant, K., Kim, K.-H., Ok, Y. S., Tsang, D. C. W., Tsang, Y. F., Giri, B. S., & Singh, R. S. (2018). Engineered/designer biochar for the removal of phosphate in water and wastewater. *Science of The Total Environment, 616-617*, 1242-1260. doi:https://doi.org/10.1016/j.scitotenv.2017.10.193

Wada, S.-I., & Kawabata, K. (1991). Ion adsorption on variable charge materials and thermodynamics of ion exchange. *Soil Science and Plant Nutrition, 37*(2), 191-200. doi:10.1080/00380768.1991.10415029

Wang, B., Wen, J.-L., Sun, S.-L., Wang, H.-M., Wang, S.-F., Liu, Q.-Y., . . . Sun, R.-C. (2017). Chemosynthesis and structural characterization of a novel lignin-based bio-sorbent and its strong adsorption for Pb (Aalto et al.). *Industrial Crops and Products, 108*, 72-80. doi:https://doi.org/10.1016/j.indcrop.2017.06.013

Wang, H., Li, Z., Peng, L., Tang, X., Lin, Y., Yang, D., Geng, J., Ren, H., & Xu, K. (2021). Performance evaluation and mechanism of nitrogen removal in a packed bed reactor using micromagnetic carriers at different carbon to nitrogen ratios. *Bioresource Technology, 341*, 125747. https://doi.org/https://doi.org/10.1016/j.biortech.2021.125747

Webb, S. M., Tebo, B. M., & Bargar, J. R. (2005). Structural characterization of biogenic Mn oxides produced in seawater by the marine bacillus sp. strain SG-1. *American Mineralogist, 90*(8-9), 1342-1357. doi:10.2138/am.2005.1669

Wei, S., Tan, W., Liu, F., Zhao, W., & Weng, L. (2014). Surface properties and phosphate adsorption of binary systems containing goethite and kaolinite. *Geoderma, 213*, 478-484. doi:https://doi.org/10.1016/j.geoderma.2013.09.001

Welker, R. W. (2012). Chapter 4 - Size Analysis and Identification of Particles. In R. Kohli & K. L. Mittal (Eds.), *Developments in Surface Contamination and Cleaning* (pp. 179-213). Oxford: William Andrew Publishing.

Wu, W., He, Q., & Jiang, C. (2008). Magnetic Iron Oxide Nanoparticles: Synthesis and Surface Functionalization Strategies. *Nanoscale Research Letters, 3*(11), 397. doi:10.1007/s11671-008-9174-9

Xu, K., Deng, T., Liu, J., & Peng, W. (2010). Study on the phosphate removal from aqueous solution using modified fly ash. *Fuel, 89*(12), 3668-3674. doi:https://doi.org/10.1016/j.fuel.2010.07.034

Xu, M., Bernards, M., & Hu, Z. (2014). Algae-facilitated chemical phosphorus removal during high-density Chlorella emersonii cultivation in a membrane bioreactor. *Bioresource Technology, 153*, 383-387. doi:https://doi.org/10.1016/j.biortech.2013.12.026

Yang, Y., Liu, J., Zhang, N., Xie, H., Zhang, J., Hu, Z., & Wang, Q. (2019). Influence of application of manganese ore in constructed wetlands on the mechanisms and improvement of nitrogen and phosphorus removal. *Ecotoxicology and Environmental Safety, 170*, 446-452. doi:https://doi.org/10.1016/j.ecoenv.2018.12.024

Yin, H., Yun, Y., Zhang, Y., & Fan, C. (2011). Phosphate removal from wastewaters by a naturally occurring, calcium-rich sepiolite. *Journal of Hazardous Materials, 198*, 362-369. doi:https://doi.org/10.1016/j.jhazmat.2011.10.072

Yin, Q., Liu, M., & Ren, H. (2019). Biochar produced from the co-pyrolysis of sewage sludge and walnut shell for ammonium and phosphate adsorption from water. *Journal of Environmental Management, 249*, 109410. doi:https://doi.org/10.1016/j.jenvman.2019.109410

Yoon, H.-S., Chung, K. W., Kim, C.-J., Kim, J.-H., Lee, H.-S., Kim, S.-J., . . . Lim, B.-C. (2018). Characteristics of phosphate adsorption on ferric hydroxide synthesized from a Fe2(SO4)3 aqueous solution discharged from a hydrometallurgical process. *Korean Journal of Chemical Engineering, 35*(2), 470-478. doi:10.1007/s11814-017-0287-7

Yoon, S.-Y., Lee, C.-G., Park, J.-A., Kim, J.-H., Kim, S.-B., Lee, S.-H., & Choi, J.-W. (2014). Kinetic, equilibrium and thermodynamic studies for phosphate adsorption to magnetic iron oxide nanoparticles. *Chemical Engineering Journal, 236*, 341-347. doi:https://doi.org/10.1016/j.cej.2013.09.053

Yu, Z., Zhang, C., Zheng, Z., Hu, L., Li, X., Yang, Z., . . . Zeng, G. (2017). Enhancing phosphate adsorption capacity of SDS-based magnetite by surface modification of citric acid. *Applied Surface Science, 403*, 413-425. doi:https://doi.org/10.1016/j.apsusc.2017.01.163

Yuan, Z., Pratt, S., & Batstone, D. J. (2012). Phosphorus recovery from wastewater through microbial processes. *Current Opinion in Biotechnology, 23*(6), 878-883. doi:https://doi.org/10.1016/j.copbio.2012.08.001

Zach-Maor, A., Semiat, R., & Shemer, H. (2011). Adsorption–desorption mechanism of phosphate by immobilized nano-sized magnetite layer: Interface and bulk interactions. *Journal of Colloid and Interface Science, 363*(2), 608-614. doi:https://doi.org/10.1016/j.jcis.2011.07.062

Zaman, M., Kim, M., & Nakhla, G. (2021). Simultaneous nitrification-denitrifying phosphorus removal (SNDPR) at low DO for treating carbon-limited municipal wastewater. *Science of The Total Environment, 760*, 143387. doi:https://doi.org/10.1016/j.scitotenv.2020.143387

Zeng, L., Li, X., & Liu, J. (2004). Adsorptive removal of phosphate from aqueous solutions using iron oxide tailings. *Water Research, 38*(5), 1318-1326. doi:https://doi.org/10.1016/j.watres.2003.12.009

Zeng, L., Liu, Q., Lu, M., Liang, E., Wang, G., & Xu, W. (2019). Modified natural loofah sponge as an effective heavy metal ion adsorbent: Amidoxime functionalized poly(acrylonitrile-g-loofah). *Chemical Engineering Research and Design, 150*, 26-32. doi:https://doi.org/10.1016/j.cherd.2019.07.021

Zhan, Y., Zhang, H., Lin, J., Zhang, Z., & Gao, J. (2017). Role of zeolite's exchangeable cations in phosphate adsorption onto zirconium-modified zeolite. *Journal of Molecular Liquids, 243*, 624-637. doi:https://doi.org/10.1016/j.molliq.2017.08.091

Zhang, H., Elskens, M., Chen, G., & Chou, L. (2019). Phosphate adsorption on hydrous ferric oxide (HFO) at different salinities and pHs. *Chemosphere, 225*, 352-359. doi:10.1016/j.chemosphere.2019.03.068

Zhao, Z., Song, X., Wang, W., Xiao, Y., Gong, Z., Wang, Y., Mei, M. (2016). Influences of iron and calcium carbonate on wastewater treatment performances of algae based reactors. *Bioresource Technology, 216*, 1-11. doi:https://doi.org/10.1016/j.biortech.2016.05.043

Chapter 3. Elucidating phosphorus removal dynamics in a denitrifying woodchip bioreactor

The manuscript has been published in:

G. N. Perera, D. T. Rojas, A. Rivas, G. Barkle, B. Moorhead, L. A. Schipper, et al

“Science of The Total Environment” 2024 Vol. 917 Pages 170478

Science of the Total Environment 917 (2024) 170478

Contents lists available at ScienceDirect

Science of the Total Environment

journal homepage: www.elsevier.com/locate/scitotenv

Elucidating phosphorus removal dynamics in a denitrifying woodchip bioreactor

Gimhani N. Perera [a,b], Dorisel Torres Rojas [a], Aldrin Rivas [c], Greg Barkle [d], Brian Moorhead [c], Louis A. Schipper [a], Rupert Craggs [b], Adam Hartland [a,c,*]

[a] Environmental Research Institute, School of Science, Faculty of Science and Engineering, University of Waikato, Kirikirioa Hamilton, New Zealand
[b] National Institute of Water and Atmospheric Research Ltd (NIWA), PO Box 11115, Kirikirioa Hamilton 3251, New Zealand
[c] Lincoln Agritech Ltd, Ruakura, Kirikirioa Hamilton 3214, New Zealand
[d] Land and Water Research Ltd, Kirikirioa Hamilton 3217, New Zealand

HIGHLIGHTS

- Denitrifying bioreactors receive phosphorus from allochthonous and autochthonous sources.
- Autochthonous phosphorus is generated by reduction of iron (hydr)oxides within reactors.
- Coupled iron-phosphorus cycles explain phosphorus source vs sink behaviour.
- Phosphorus removal rates can be of similar magnitude to nitrate removal rates.

GRAPHICAL ABSTRACT

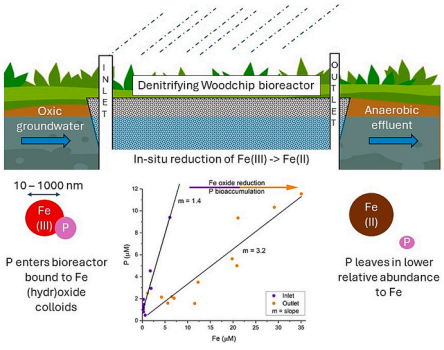

ARTICLE INFO

Editor: Yifeng Zhang

Keywords:
Phosphorus
Denitrifying woodchip bioreactor
Biological uptake
Biogeochemical cycles

ABSTRACT

Denitrifying woodchip bioreactors (DBRs) are an established nitrate mitigation technology, but uncertainty remains on their viability for phosphorus (P) removal due to inconsistent source-sink behaviour in field trials. We investigated whether iron (Fe) redox cycling could be the missing link needed to explain P dynamics in these systems. A pilot-scale DBR (Aotearoa New Zealand) was monitored for the first two drainage seasons (2017–2018), with supplemental in−field measurements of reduced solutes (Fe^{2+}, HS^-/H_2S) and their conjugate oxidised species (Fe^{3+}/SO_4^{2-}) made in 2021 to constrain within-reactor redox gradients. Consistent with thermodynamics, the dissolution of $Fe^{3+}_{(s)}$ to $Fe^{2+}_{(aq)}$ within the DBR sequentially followed O_2, NO_3^- and $MnO_{2(s)}$ reduction, but occurred before SO_4^{2-} reduction. Monitoring of inlet and outlet chemistry revealed tight coupling between Fe and P (inlet R^2 0.94, outlet R^2 0.85), but distinct dynamics between drainage seasons. In season one, outlet P exceeded inlet P (net P source), and coincided with elevated outlet Fe^{2+}, but at ~50 % lower P concentrations relative to inlet Fe:P ratios. In season 2 the reactor became a net P sink, coinciding with declining outlet Fe^{2+} concentrations (indicating exhaustion of $Fe^{3+}_{(s)}$ hydroxides and associated P). In order to characterize P removal under varying source dynamics (i.e. inflows vs *in-situ* P releases), we used the inlet Fe vs P relationship to

* Corresponding author. at: Environmental Research Institute, School of Science, Faculty of Science and Engineering, University of Waikato, Kirikirioa Hamilton, New Zealand.
E-mail address: adam.hartland@waikato.ac.nz (A. Hartland).

https://doi.org/10.1016/j.scitotenv.2024.170478
Received 3 October 2023; Received in revised form 23 January 2024; Accepted 24 January 2024
Available online 30 January 2024

estimate P binding to colloidal Fe (hydr)oxide surfaces under oxic conditions, and the outlet Fe^{2+} concentration to estimate *in-situ* P releases associated with Fe (hydr)oxide reduction. Inferred P-removal rates were highest early in season 1 ($k = 0.60$ g P m^3 d^{-1}; 75–100 % removal), declining significantly thereafter ($k = 0.01 \pm 0.02$ g P m^3 d^{-1}; ca. 3–67 % removal). These calculations suggest that microbiological P removal in DBRs can occur at comparable magnitudes to nitrate removal by denitrification, depending mainly on P availability and hydraulic retention efficiency.

1. Introduction

Denitrifying bioreactors (DBRs) are a widely employed edge−of−-field technology for the interception and removal of agricultural nitrate pollution (Blowes et al., 1994; Dougherty et al., 2020; Lepine et al., 2018). Phosphorus (P) also contributes significantly to nutrient loading in drainage, leading to eutrophication; but most DBR studies have focussed on nitrate (Schipper et al., 2010; Corbett et al., 2020), leaving an important gap in our understanding (Wu et al., 2023).

Woodchip bioreactors are known to leach P during initial commissioning (David et al., 2016). Subsequently, exhibiting consistent P removal in the order of 0.01 and 0.08 g P m^{-3} d^{-1} (Dougherty, 2018). While P removal has been documented in a few studies (Dougherty, 2018), there is conjecture regarding whether P removal in DBRs solely reflects biological accumulation, or whether other biogeochemical processes (e.g. adsorption, redox cycling) are involved (Sharrer et al., 2016; Sanchez Bustamante-Bailon et al., 2022; Wu et al., 2023).

To a first approximation, inconsistent P behaviour in DBRs occurs due to temporal variations in flow rates and the hydrochemistry of drainage waters, resulting from episodic flow dynamics and variable soil source chemistry. However, within-reactor biogeochemical and microbial processes are also likely to be relevant to P dynamics (Hartland et al., 2015). It is established that direct P bioaccumulation by microbes can occur in excess to requirements because bacteria utilize P and store it as intracellular polyphosphate (poly−P) (Oehmen et al., 2010). Indeed, faster P accumulation occurs under anaerobic conditions, which may favour P removal in DBRs compared to aerobic systems (Kerrn-Jespersen and Henze, 1993; Sun et al., 2020; Zaman et al., 2021), but these processes are understudied in woodchip DBRs and remain to be fully elucidated.

Biological P accumulation in DBRs may also be favoured because iron (hydr)oxides, the dominant P binding phase in aquatic systems, are unstable in anaerobic conditions (Sposito, 2004). Iron (hydr)oxides are ubiquitous in freshwater, soil, and sediment, and strongly bind orthophosphate (PO_4^{3-}) due to their large specific surface area and positive net surface charge at pH values <7 (Damasceno et al., 2023; Shahid et al., 2019). Hence, Fe (hydr)oxides are inevitably important vectors for P transfer into DBRs in agricultural settings; and Fe redox cycling is likely to affect P dynamics, because insoluble iron(III) (hydr)oxides undergo reductive dissolution under anaerobic conditions, simultaneously releasing P and soluble Fe^{2+} ions (Hartland et al., 2015).

In this paper, we investigated the biogeochemistry of a pilot-scale DBR (Tatuanui, Waikato, Aotearoa New Zealand) including all major element redox processes, with the goal of elucidating the reaction pathways controlling phosphorus. This work also contributes to ongoing research into the attenuation of P (and potentially other pollutants) in agricultural drainage through incorporation of novel substrates in woodchip DBRs.

2. Materials and methods

2.1. Water sampling

A pilot−scale denitrifying woodchip bioreactor located in Tatuanui of the Waikato region (Rivas et al., 2020a, 2020b), Aotearoa (New Zealand), was selected for this study. The primary substrate being pine woodchips, contained within a 58 m^3 bioreactor of trapezoidal shape (25 m^3 of saturated volume), with a basal area of 5 × 9 m, a surface area of 8.4 × 12.4 m, and depth of 1.2 m. The bioreactor was installed in 2017 and monitored throughout the 2017 and 2018 drainage seasons by researchers at Lincoln Agritech Ltd. Additional sampling and monitoring was conducted during the 2021 (July–October) drainage season, to better constrain the in−situ bioreactor redox conditions. Water samples were collected every two weeks during the first two drainage seasons, and on three occasions during the 2021 drainage season. Automatic monitoring devices and sensors were attached to the inlet and outlet wells to monitor the flow rate, NO_3^- concentration, temperature, and Electrical Conductivity (EC). An outlet weir recorded the flow through the bioreactor. Additional water quality measurements were made on manual (grab) samples following standard laboratory procedures (Rivas et al., 2020a, 2020b). Samples for laboratory analysis of bulk chemistry were collected in triplicate from the inlet, internal (mid) wells along the centre line of the bioreactor (C_1, C_2, C_3), and outlet, and filtered in-field using 0.45 μm syringe filters into 50 mL and 15 mL falcon tubes. The distances from the inlet well to the centre wells (C1, C2, C3), were approximately 2.15 m, 4.30 m, and 6.65 m, respectively; and the distance from the inlet well to the outlet well was approximately 8.65 m. These samples were collected using a flexible hose and syringe connected to a three−way valve to minimise exposure to oxygen. Samples were carefully handled to measure the concentration of reduced solutes in−field to constrain the Fe^{2+}/Fe^{3+} and HS^-/SO_4^{2-} redox couples. Samples for metal analysis were preserved using 2 % (*v*/v) double-distilled concentrated HNO_3 (Savillex DST − 1000 Acid Purification System; Eden Prairie, MN, USA) and were then stored on ice at ≤4 °C during transport.

2.2. Analytical chemistry

In−situ measurements of pH, temperature, DO (Dissolved Oxygen), ORP (Oxidation−Reduction Potential), Conductivity (EC), and TDS (Total Dissolved Solids) were made using a YSI ProODO probe (YSI incorporated, USA). Ferrous iron (Fe^{2+}) and hydrogen sulfide (HS^{2-}) concentrations were respectively determined by the ferrozine (Viollier et al., 2000) and methylene blue methods (Reese et al., 2011), using a portable UV−Vis spectrophotometer (HACH DR1900, USA). Offsite chemical analysis of water samples was performed at Waikato University. Total organic carbon (TOC) was measured on an OI Analytical Aurora 1030 W TOC analyser (Washington, USA), while nitrate (NO_3^-), sulphate (SO_4^{2-}), chloride (Cl^-), and fluoride (F^-) were analysed using an ICS−2000 Ion Chromatograph (Thermo Fisher, USA) using an isocratic method (5 mM KOH, 40 mins). Dissolved metals (Fe, and Mn) were determined by inductively coupled plasma mass spectrometry using an Agilent 8900 ICP − MS (Santa Clara, CA, United States), controlled by MassHunter Workstation Version 4.5 and connected to an SPS4 autosampler (Mohammadi et al., 2022). Phosphorus (ascorbic acid method) and ammonium (NH_4^+) concentrations were measured by UV spectrophotometry (Dynamica HALO VIS−20, UK). Finally, alkalinity was measured by using a universal digital titrator (HACH, USA) by titrating against pH with 0.15 N H_2SO_4 to the CO_2 equivalence point (pH 3.9). All the samples collected in 2021 were measured in triplicate and reported as the average and standard deviation. The statistical methods employed were Pearson's correlation analysis (Microsoft Excel Version 2311), and least squares regression (Grapher v22).

2.3. Hydrogeochemical simulations

The dataset for the year 2021 was simulated to determine the saturation indices of $Fe(OH)_3$ and FeS. However, the simulations could not be conducted for the data in 2017 and 2018 because the redox species (Fe^{2+} and HS^-) were not measured during routine monitoring. Prior to the hydro chemical simulations, input data were screened for gross errors using the charge balance error (CBE) metric, after which solutions were adjusted to charge neutrality within PHREEQC 3.0 (Parkhurst, 1995) by adding Cl^- and Na^+, since neither ion strongly affects the studied equilibria. Generally, the percent charge−balance error before adjustment was <5 %, reflecting a representative and accurate analysis of the studied solutions. PHREEQC scripts and the raw data used in these simulations are provided in the Supplementary Information (**Table S1**). Equilibrium speciation calculations based on the aforementioned monitoring data were also performed in PHREEQC 3.0, with particular attention paid to the accurate representation of the redox equilibrium along the reactors' length, to accurately determine the solubility of amorphous iron (hydr)oxides and the potential for formation of other reaction by-products (i.e., iron sulfide precipitates). Outputs from these simulations included the speciation of major and minor ions, saturation indices of amorphous $Fe(OH)_3$ and FeS precipitates, and could be extended in the future to include the interaction of the aqueous species with iron hydroxide surfaces (Charlton and Parkhurst, 2011; Dzombak and Morel, 1991). Hence, the general modelling framework employed here, allows for the calculation of saturation indices (a measure of mineral solubility) as constrained by in-field measurements of redox couples, and the distribution of aqueous species along the reactors' length (respecting the gradation from oxidising to reducing conditions).

3. Results

3.1. Bioreactor trends in redox-active species

Results of bioreactor monitoring over two consecutive drainage seasons are presented in Fig. 1 (**Table S2**), which shows the net change in N, Mn, Fe, P, and S between inlet and outlet ($\Delta_x = x_{out} - x_{in}$). These elements are included in this analysis because they constitute the main inorganic electron−accepting components involved in natural biogeochemical cycles (Stumm and Morgan, 1996).

In season 1, the reactor leached Mn, Fe and P. Concentrations of Fe, Mn and P declined exponentially from initial high values in season 1 and continued to decline into season 2. Outlet concentrations of Fe and P showed close covariation throughout season 1 ($R^2 = 0.86$), but then decoupled during season 2 ($R^2 = 0.11$). Over both periods, the reactor actively removed NO_3^-, but only minimal changes occurred in SO_4^{2-} concentrations between inlet and outlet, with the exception of higher sulfate removal under stagnant (no flow) conditions, toward the end of season 1.

Overall, the bioreactor was a nitrate and sulfate sink during both drainage seasons, but deviated from source−to−sink behaviour for P, over this period. Outlet manganese and iron concentrations were both highest following the commissioning of the bioreactor in 2017, then gradually diminished during the 2018 season. Throughout this period, iron and phosphorus remained tightly correlated (Fig. 2) at both inlet and outlet. Fe:P ratios were generally higher in inlet water compared to the outlet, where they remained correlated, but at a lower Fe:P ratio, indicating P loss (relative to Fe) along the flow path.

The hydrology of the bioreactor fluctuated significantly across the first two drainage seasons. Cumulative flows for 2017 (season 1) and 2018 (season 2) were 337 m^3 and 952 m^3, respectively; and peak flows were 28.8 m^3 day^{-1} and 100 m^3 day^{-1}, respectively (Rivas et al., 2020a, 2020b). The drainage seasons also differed substantially in their duration, with season 2 being much shorter than season 1, but with a cumulative drainage of ca. three times that of season 1. Accordingly, flashy (event) flows account for some of the observed dynamics in nutrient

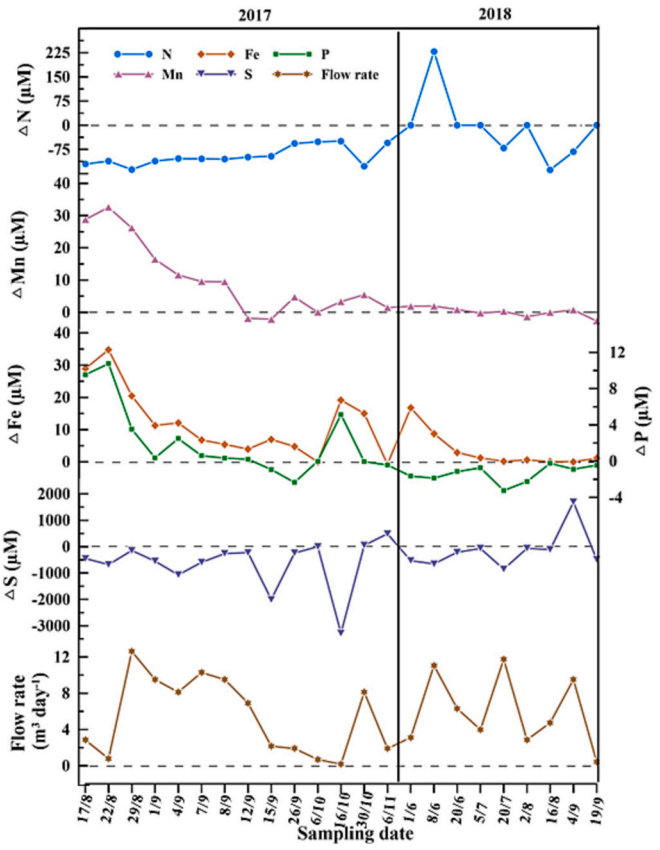

Fig. 1. Net change in N, Mn, Fe, S, and P (μM) (outlet−inlet) plotted with flow rate (m^3 d^{-1}) for the 2017 and 2018 drainage seasons.

removal. For example, the high outlet N concentration in season 2 corresponded to a high−flow event (0.23 mM; 11 m^3 day^{-1}), and conversely, an interval of pronounced S − removal was observed at low flows, when more reduced conditions were favoured in season 1 ($\Delta S = -3.28$ mM; 0.17 m^3 day^{-1} (Fig. 1)).

The results of PHREEQC modelling of the 2021 field data provide a more detailed picture of the underlying hydrogeochemical processes leading to shifts in the concentration of redox−active components between inlet and outlet. Fig. 2 shows the concentrations of nitrate, manganese, iron, and sulphate along the reactors' length, alongside derived saturation index values for common Fe minerals.

The hydrogeochemical simulations suggest that the consumption of all five major oxidizers (electron acceptors) present in the bioreactor influent (O_2, N(V), Mn(IV), Fe(III), S(VI)) were removed to some extent along the reactors' length, with Fe(III) and Mn(IV) reduction being shown by increases in the reaction products (Fe(II) and Mn(II)) (Fig. 2) (see **Table S3** for DO values). Consequently, the derived mineral saturation indices for Fe (hydr)oxides indicate oversaturated conditions in the inlet water ($SI_{Fe(OH)3} > 0$), but undersaturated conditions by the first centre well, trending to lower $SI_{Fe(OH)3}$ values in the downstream centre wells and the outlet of the bioreactor. Iron sulfide (SI_{FeS}) conversely remained undersaturated, despite increases in Fe^{2+} and HS^- (**Table S1**) along the flow path.

3.2. Changes in Fe and P dynamics with bioreactor age

Fig. 3 shows the correlation between Fe and P in the 2017 and 2018 monitoring data. Inlet samples in both season 1 and season 2 were characterised by steeper relationships (m = 1.449), compared to the outlet. In season 1, the correlation between Fe and P at the outlet was characterised by a much shallower slope (m = 0.3289) and higher Fe:P

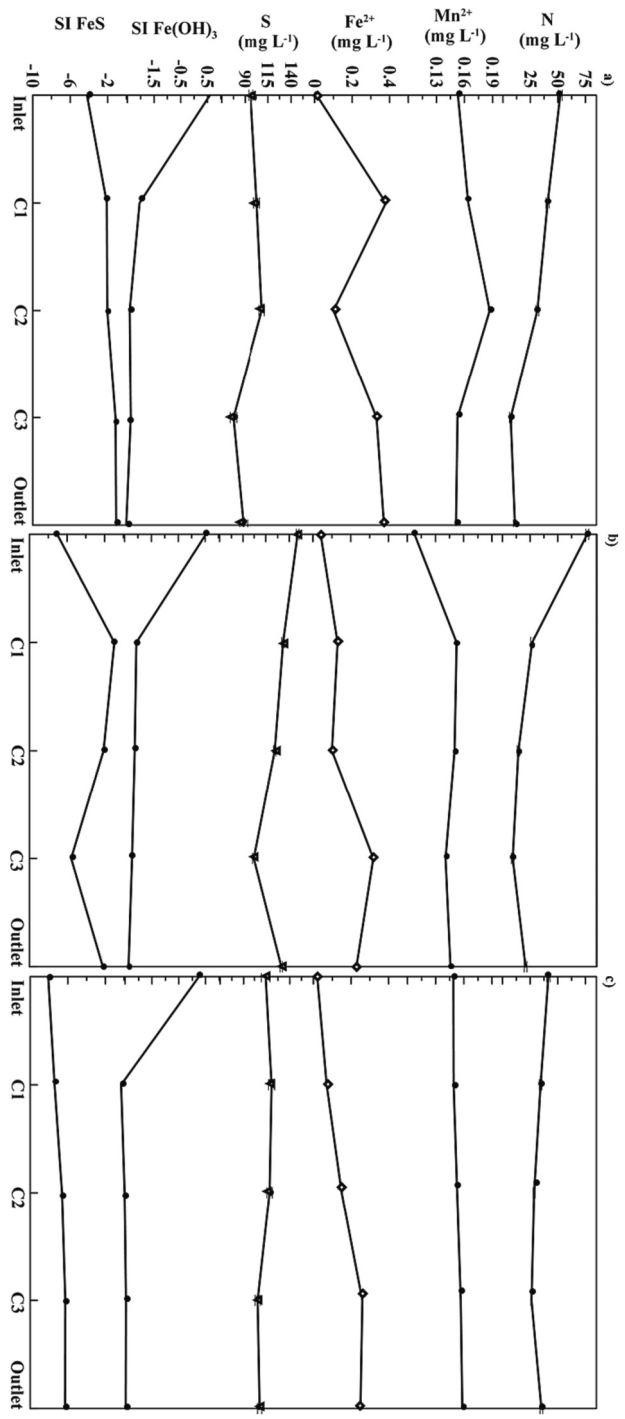

Fig. 2. Longitudinal trends in bioreactor hydrochemistry (data from the **2021 drainage season** 27th July, 17th Aug., 27th Sep). Results of hydrochemical simulations include saturation index (SI) values for two primary Fe minerals (amorphous iron hydroxide ($Fe(OH)_3$(a); and iron monosulfide (FeS)) and total N and S (SO_4^{2-}) concentrations plotted as a function of distance along the bioreactor alongside the products of Fe(III) and Mn(IV) reduction (Fe(II), Mn(II)).

ratios, consistent with P attenuation with respect to Fe within the DBR. However, in the subsequent season (2018), the outlet Fe and P were uncorrelated, indicating higher P retention within the reactor, and overall lower levels of Fe(III) reduction than observed in season 1.

4. Discussion

4.1. Redox biogeochemistry and denitrifying bioreactors

DBRs are engineered for denitrification. They provide a means to address diffuse nitrate pollution from the agricultural sector, and are most suitable where flow is channelled (i.e. by tile drainage). Once dissolved oxygen in drainage water is depleted, DBR's remove nitrate by supplying organic carbon as an energy source, thereby establishing a carbon-rich anaerobic environment for denitrifying microorganisms (Fan et al., 2022). Although recent studies have shown the potential for DBR's to remove phosphorus (Christianson et al., 2021; Povilaitis et al., 2020; Table 1), the underlying mechanisms of P removal remain to be fully described, limiting next-generation DBR designs that additionally target P removal. As shown by this study, beyond denitrification, a range of biogeochemical cycles operate in DBRs which correlate with P dynamics. In the following discussion, we explore the potential of redox transformations to explain P dynamics in DBRs. We also discuss the potential for Fe oxides to be harnessed to remediate P pollution.

4.2. Within−reactor trends in redox explain P dynamics

Denitrification is one of many possible reaction pathways between (oxidised) solutes and (reduced) organic carbon in DBRs (Blowes et al., 1994). A series of biogeochemical changes can be predicted based on the free−energy change of reaction (ΔG°) between reactants and products, in which oxidizers (electron acceptors) are removed sequentially, from most energetic ($O_2 > NO_3^-$), through the energetically−intermediate solids (MnO_2, $Fe(OH)_3$), to the least energetic and most abundant remaining oxidant (SO_4^{2-}) (**Fig. 3.b**). We note that terminal respiration of bicarbonate (C(IV)) to methane is generally avoided due to relatively high concentrations of sulfate (S(VI)) throughout the Tatuanui DBR, but may be more prevalent in less S-enriched settings. These reactions all proceed due to the ready supply of organic carbon, and the presence of microorganisms and dissolved/particulate electron acceptors in the water (Addy et al., 2016; Christianson et al., 2012; Thapa et al., 2023). Despite hydrologic variations, our results (**Fig. 2**) demonstrate that longitudinal changes in the Tatuanui DBR coherently followed the redox ladder (**Fig. 3.b**), after the initial rapid removal of oxygen between the inlet and first centre well (C1). In sequence, facultative bacteria then consumed nitrate, followed by manganese and iron oxides (forming Fe (II), Mn(II)), and finally sulphate, producing hydrogen sulfide, $H_2S_{(g)}$, which can commonly be smelt in DBR piezometers.

In principle, the progression of less energetic redox transformations (such as sulfate reduction; Fig. 3) within any DBR will be determined by carbon supply (assumed to be sufficient to maintain a long−term nitrate removal rate), nitrate supply, and the hydraulic residence time (HRT) of the water in the bioreactor (Schipper et al., 2010). Following oxygen and nitrate removal, the anaerobic DBR environment promotes dissimilatory manganese and iron reduction (where oxides are present), followed by the reduction of sulfate (Fig. 2). Hence, the detection of H_2S(g) in reactor piezometers, confirms that DBRs can naturally oscillate across a wide range of redox potentials depending on flow and nitrate supply (**Fig. 3**).

In the context of the redox ladder (Fig. 3), the observed emission of Fe(II) and Mn(II) from the outlet of the Tatuanui DBR in season 1, was therefore consistent with N-limitation and the gradual reduction of soil-derived Mn and Fe oxides likely incorporated either during reactor construction, leached from the 0.7 m topsoil above the uppermost woodchip layer (Rivas et al., 2023), or washed into the reactor during high flows (Fig. 1). Furthermore, because natural Fe (hydr)oxides adsorb and transport P (Saeed et al., 2018), but only the carrier phase (i.e. Fe (III) + e→ Fe(II)) becomes reduced, any inorganic P released via this process becomes available for other reactions, including cellular uptake. Therefore, the monitoring results presented here suggest that as the reactor aged, Fe (and Mn) oxides were removed by reductive dissolution, thereby generating P as a by−product in an analogous manner to

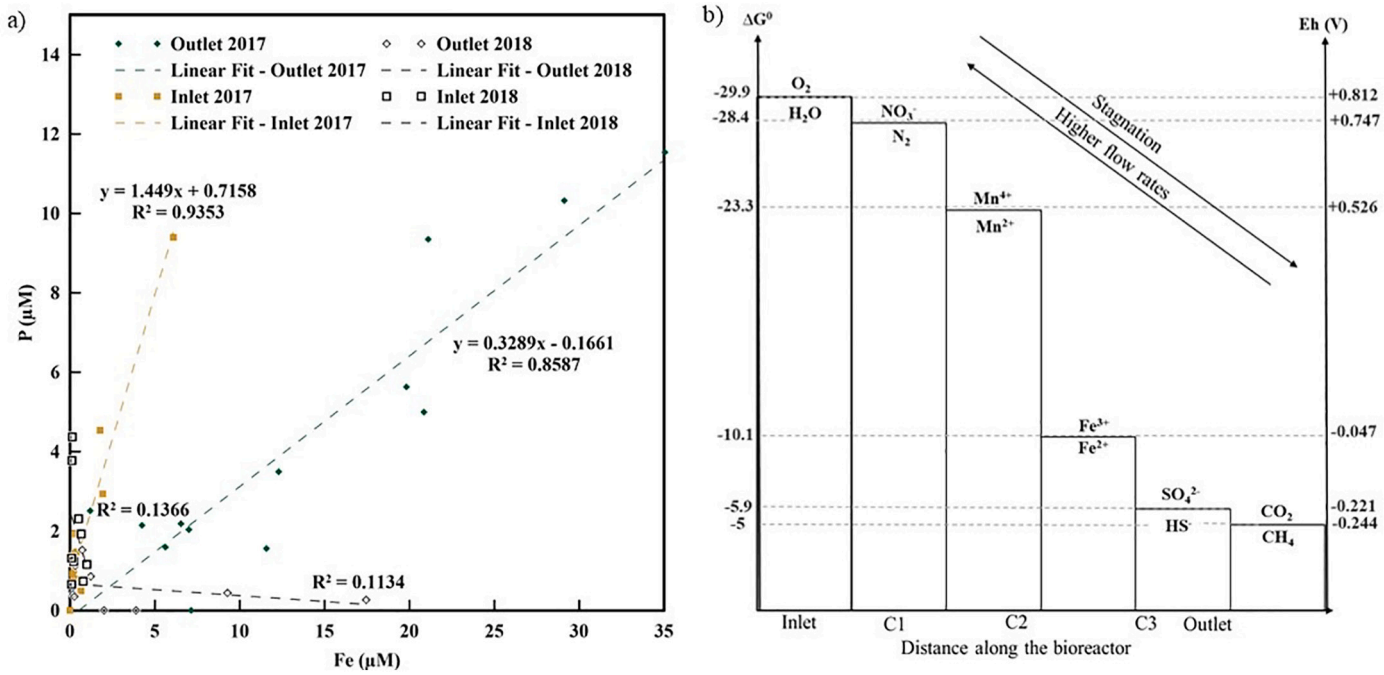

Fig. 3. a) Correlations between iron (Fe) and phosphorus (P) at the inlet and outlet of the Tatuanui bioreactor in the 2017 and 2018 drainage seasons. b) The redox ladder shown in the context of the Tatuanui DBR (ΔGo = Gibbs free energy change of reaction relative to the standard hydrogen electrode, Eh = redox potential in volts).

Table 1
Comparison of the P removal rates of the woodchip bioreactors.

Effluent	Bioreactor media	pH	DO (g m^3)	N-NO_3 removal rate (g m^3 d^{-1})	P removal rate (g m^3 d^{-1})	Reference
Agricultural drainage	Woodchips	5.6–7.1	0.0–0.2	0.7–1.6	0.6	Rivas et al. (2020a, 2020b)
Agricultural drainage	Sawdust			0.25	0	Schipper and Vojvodić-Vuković (2000)
Glasshouse	Woodchips and sawdust		0–15	10	0	Schipper et al. (2010)
Treated domestic	Woodchips and sawdust		0–15	11	0	
Treated dairy shed	Woodchips and sawdust		0–15	1.4	0	
Agricultural drainage	Woodchips with steel by products	6.1–6.8		10	0.3	Hua et al. (2016)
domestic wastewater	Woodchips and coconut husk	7	0.8–8.8	2.8–12	0.2	Tanner et al. (2012)
	Woodchips	6.6–7.2		40	0.4	Povilaitis et al. (2020)
Agriculture tile drainage	Woodchips and activated carbon			45	0	
	Woodchips and flaxseed cake			41	0	
Mine drainage	Woodchips and steel slag	7.5–8.4		8.0–18	8.8–48	Christianson et al. (2017)

arsenic releases common to reduced aquifer environments (Borch et al., 2010; Hartland et al., 2015).

Evidence for a range of redox transformations coupled to anaerobic carbon oxidation is provided by the loss of electron acceptors such as NO_3^- and SO_4^{2-}, or by the generation of reduction products such as Mn^{2+}, Fe^{2+}, and H_2S (Fig. 1). Unlike the mobile, soluble oxidants (NO_3^- and SO_4^{2-}), Fe and Mn are insoluble under oxidising conditions and therefore would be readily incorporated during reactor construction (i.e., from surrounding soils, or by attachment to wood chips). This explains why the outlet concentration of their reaction products (soluble Fe^{2+} and Mn^{2+} ions) exceeded the inlet concentration, decaying from initial highs following reactor commissioning, to reach consistently low concentrations by the second half of season 2 (Fig. 1).

4.3. Constraining P removal rates under varying source dynamics

Taking our analysis one step further, we can use the correlations reported here between Fe and P at the DBR inlet and outlet to evaluate P removal performance (due to biological P assimilation) under varying source dynamics. The steep Fe:P inlet ratio is consistent with the adsorption of P on colloidal iron oxides, which as widely observed elsewhere (Sposito, 2004), have large specific surface areas and correspondingly high P-adsorption capacities. Outlet concentrations of Fe and P also remained correlated throughout season 1, but the Fe:P ratio at the outlet was higher, suggesting preferential loss of P, relative to Fe along the flow path.

While Fe(II) cannot be considered truly conservative (e.g. because of potential formation of Fe(II) precipitates, adsorption and so on), if we assume that Fe^{2+} was minimally removed within the reactor (an assumption supported by negative $FeOH_3$ saturation index values (Fig. 2)), the outlet Fe concentrations can be used to estimate the equivalent autochthonous (i.e. *in-situ*) P supply to the reactor microorganisms (i.e. P that was originally associated with Fe (hydr)oxides incorporated during bioreactor construction, then subsequently released during Fe oxide dissolution). Using Eq. (1) (derivation of this equation is included in the supplementary information), we estimated the rate of biological P uptake within the Tatuanui DBR associated with Fe oxide dissolution (P removal rate $_{(FeOx)}$; Fig. 4) and compared this to the apparent P removal rate (P removal rate $_{(app)}$; Eq. (2)). The rates are then combined (Eq. (3)) to infer the overall P removal rate, accounting for

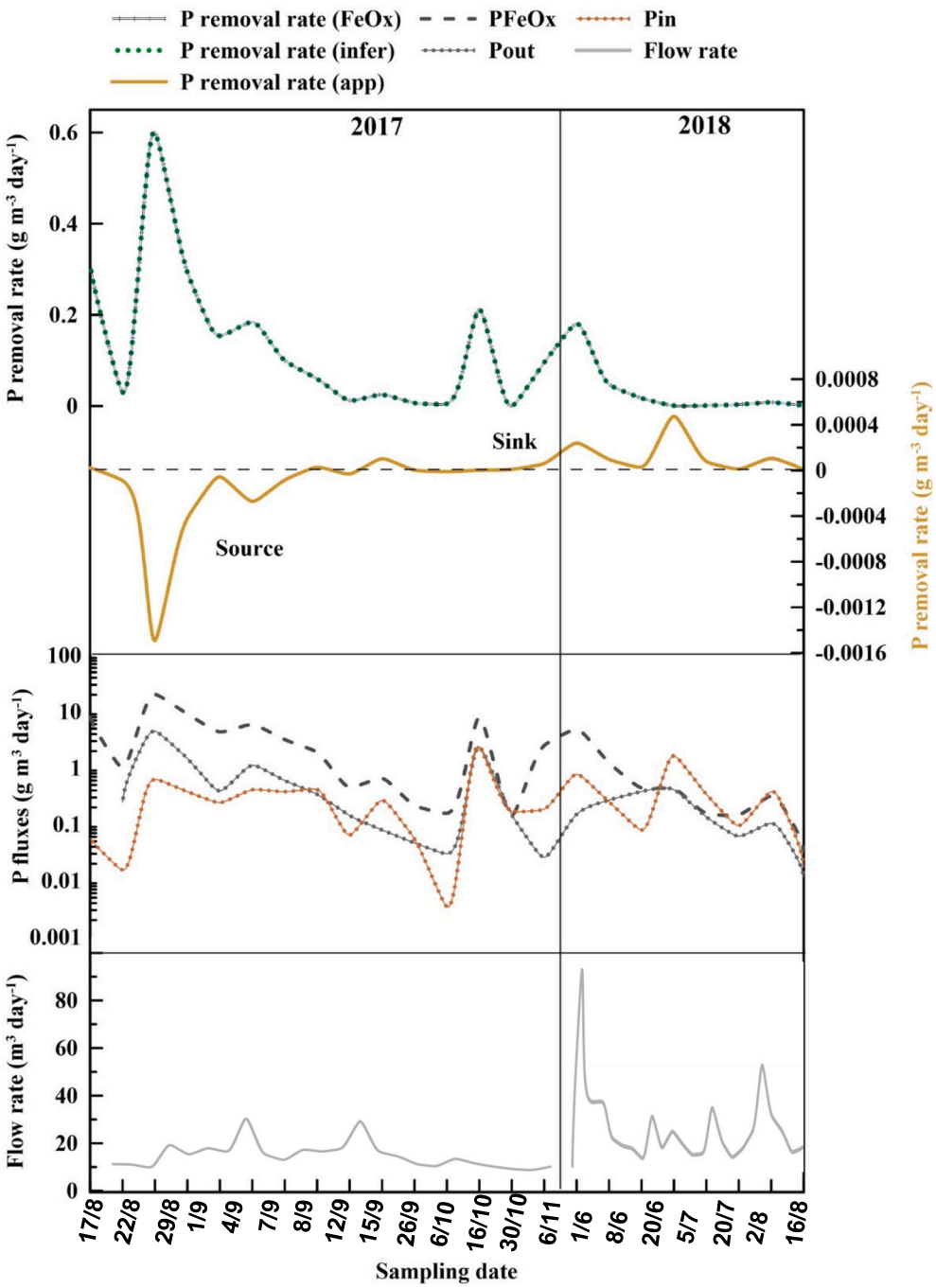

Fig. 4. Phosphorus (P) removal in the Tatuanui bioreactor across drainage seasons. Upper panel: apparent (P removal rate $_{(app)}$), iron (hydr)oxide associated (P removal rate $_{(FeOx)}$), and the overall inferred rate (P removal rate $_{(inf)}$). Middle panel: the corresponding observed and calculated P fluxes; lower panel: flow rate through the bioreactor.

allochthonous and autocthonous P sources (P removal rate $_{(inf)}$; Fig. 4). This analysis suggests that biological removal of P was highest following commissioning and was dominated by autocthonous P sources associated with iron (hydr)oxide dissolution. Inferred rates fluctuated throughout season 1, leading to pseudo steady−state removal in season 2, following exhaustion of Fe(III) (hydr)oxides (Fig. 4).

$$\text{P removal rate}_{(FeOx)} = \frac{[(Fe_{out}\ 1.449 + 0.7158) - P_{out}]Q}{V_s \varnothing} \quad (1)$$

$$\text{P removal rate}_{(app)} = \frac{[P_{in} - P_{out}]Q}{V_s \varnothing} \quad (2)$$

$$\text{P removal rate}_{(inf)} = \text{P removal rate}_{(app)} + \text{P removal rate}_{(FeOx)} \quad (3)$$

where Vs is the saturated volume of the bioreactor (m^3), $\varnothing$ is the effective or drainable porosity, and Q is the flow rate (m^3 day^{-1}). The drainable porosity and the saturated volume of the bioreactor were 46.2 % and 56.3 m^3, respectively (Rivas et al., 2020a, 2020b; Rivas et al., 2023). The equivalent inlet P concentration is estimated in Eq. (1), by substitution of the linear equation between inlet Fe and P (**Fig. 3**), based on the assumption that Fe entering the reactor inlet was present as insoluble Fe(III) hydro(oxides) and was representative of native soil-derived Fe oxides incorporated during reactor construction. We note that positive $Fe(OH)_3$(a) saturation index values were recovered for all

inlet solutions modelled in PHREEQC (Fig. 2)).

The assumptions made in the above analysis are further supported by PHREEQC modelling, which indicates that no P−bearing mineral phases were oversaturated within the reactor. Furthermore, the saturation index for amorphous $Fe(OH)_3$ remained negative (undersaturated) from the first mid−well (C1) to the outlet, i.e., indicating no formation of Fe (II) or Fe(III) species above the level needed to form insoluble products. Therefore, the dissolution of native iron hydr(oxide) minerals within the reactor (Fig. 2) is unlikely to have been reversed by either oxidation or formation of secondary/tertiary mineral phases between the site of Fe (III) reduction and the outlet. This modelling also indicates that P is likely to have remained as orthophosphate, or as organic P, once incorporated into biomass.

We hypothesise that during the process of dissolution of Fe (hydr) oxides in season 1 and season 2, P was preferentially retained through biological uptake. One implication of this hypothesis is that bioreactors may naturally shift from P−sources to P−sinks across their lifetimes, but with higher rates of P removal at the inception of drainage seasons due to the higher availability of insoluble Fe hydr(oxides), potentially indicating luxury uptake as microbiological communities become established (Khoshmanesh et al., 2002).

Several studies have demonstrated that the biological uptake of P by polyphosphate accumulating organisms, leads to P storage as intracellular polyphosphate polymers under both aerobic and anoxic conditions (Sathasivan, 2009). Specific microorganisms break down and release these polyphosphates under anaerobic conditions (Kerrn-Jespersen and Henze, 1993; Meinhold et al., 1999). However, in general, the rate of P uptake is considerably higher under anaerobic conditions than in aerobic conditions (Wu et al., 2023). Comeau et al. (1987) and Gerber et al. (1987) have suggested that nitrate may serve as an electron acceptor during P uptake reactions under anaerobic conditions, which may enhance P bioaccumulation rates in denitrifying bioreactors.

4.4. Potential for augmentation of denitrifying bioreactors with iron oxide surfaces to enhance P removal

As seen in other environments characterised by oscillating redox gradients (Saeed et al., 2018), natural Fe (and Mn) (hydr)oxides incorporated into woodchip bioreactors, become rapidly reduced under N − limiting conditions, leading to the release of P, previously adsorbed to Fe (hydr)oxide surfaces. We can anticipate that any colloidal or particulate iron oxides present in drainage water will also undergo dissolution within DBRs, producing Fe^{2+} ions and HPO_4^- among other secondary reaction products (at pH 5–6). This finding begs the question: can we harness these processes to enhance the removal of P from agricultural drainage water?

One approach is to use iron-based adsorbents for P removal. However, the evolution of redox chemistry in any DBR system will certainly have a major impact on the deployment of functionalized materials intended for P adsorption. Using PHREEQC 3.0 we calculated the saturation indices (SI) and the equilibrium speciation of all major and minor dissolved ions present in the Tatuanui bioreactor to evaluate the most effective positioning of a hypothetical P−sorbing substrate and to make recommendations for bioreactors more generally. Our results suggest that inlet water was commonly oversaturated with respect to amorphous Fe (hydr)oxide ($SI_{Fe(OH)3} > 0$), implying that introduced Fe−oxide−media would remain intact, and potentially grow through Fe precipitation if the media were placed close to the inlet. Conversely, the hypothetical media would be dissolved if positioned deeper within the bioreactor.

From a practitioner's standpoint, the introduction of Fe−based media in DBRs needs to be informed by an understanding of the potential for Fe oxide dissolution through dissimilatory Fe(III) reduction, and potential deterioration in media performance due to the formation and growth of biofilms on the surfaces of the functionalized media. Biofilms are complex systems composed of multicellular communities, organic and inorganic substances that grow on surfaces (Rao et al., 1997). There have been reports of biofilm formation under aphotic conditions that are analogous to conditions within DBRs. The formation of biofilms on any functionalized media (i.e., Fe−oxide−coated woodchips), could potentially inhibit P adsorption via changes in the electrostatic properties of solid surfaces, and possibly via wholesale changes in the functional chemistry of the biofilm−coated particles. While this remains an open question, our findings based on equilibrium speciation modelling indicate that Fe(III)-based materials would effectively capture additional iron from the influent, promoting the further growth and replenishment of introduced Fe (hydr)oxide surfaces, assuming Fe−media were placed at the inlet of the bioreactor.

To further illustrate this point, we simulated the effect of introducing iron oxides at different positions within the Tatuanui DBR based on the average composition of water at each position (Table 2). In Table 2, positive ΔFeT values indicate a net gain in the solid phase, and negative values indicate a net loss from the solid phase (i.e. dissolution). Based on the Tatuanui monitoring results, a net increase in $Fe(OH)_3$ is possible based on the inlet water reaching equilibrium with Fe oxides (placed at the inlet). For example, the net cumulative effect of Fe precipitation on introduced Fe−functionalized media (in proximity to the inlet of the studied system) could result in a gain of up to 10.9 g of mass and 1.39 cm^3 of volume based on a cumulative flow of 1000 m^3, assuming complete conversion of Fe to $Fe(OH)_3$ (s).

This exercise shows that iron-based composites would not be expected to withstand anaerobic conditions within the bioreactor, but would likely be retained if positioned in proximity to the reactor inlet due to higher dissolved oxygen levels (Tatuanui 2021 drainage season dataset).

5. Conclusions

We show that following denitrifying bioreactor commissioning, an initial period of phosphorus emission can occur. This initial period of P emission likely results from 1) the release of labile P from fresh wood chips (which declines rapidly as they age), and 2) the reductive dissolution of soil−derived iron (hydr)oxides. These autochthonous P sources resulted in net P emission throughout the initial phase of operation at the Tatuanui bioreactor. However, once both processes were exhausted, the denitrifying bioreactor became and remained, a net P sink. Furthermore, our analysis of Fe−P variations in the bioreactor supports the interpretation that P uptake rates scale with supply, with higher initial uptake of P in the reactor inferred during the phase of Fe (hydr) oxide dissolution. This analysis is extended to consider the potential for incorporating Fe−oxide based media within denitrifying bioreactors. We conclude that if positioned close to the reactor inlet, Fe−oxides should be preserved by the oxic conditions, and indeed may even grow, in effect potentially replenishing their P adsorption capacity over time.

CRediT authorship contribution statement

Gimhani N. Perera: Writing – original draft, Visualization, Validation, Software, Methodology, Investigation, Formal analysis, Data curation. **Dorisel Torres Rojas:** Writing – review & editing, Project

Table 2
Net predicted deviation in iron mass for iron−based composites within different bioreactor compartments (Tatuanui 2021 drainage season dataset).

Sampling wells	ΔFeT (μM)
Inlet	0.03
C1	−41.7
C2	−20.0
C3	−26.7
Outlet	−54.1

administration, Methodology, Investigation, Formal analysis, Conceptualization. **Aldrin Rivas:** Writing – review & editing, Supervision, Data curation. **Greg Barkle:** Writing – review & editing, Supervision. **Brian Moorhead:** Supervision, Resources, Methodology. **Louis A. Schipper:** Funding acquisition. **Rupert Craggs:** Supervision, Funding acquisition. **Adam Hartland:** Writing – review & editing, Visualization, Software, Project administration, Funding acquisition, Formal analysis, Conceptualization.

Declaration of competing interest

The authors declare no competing interests.

Data availability

Data and code provided in the supplementary information.

Acknowledgements

Primary funding for this research was provided by the Ministry for Business Innovation and Employment (MBIE) under Contract No. C01X1818, through the program "Te Waiora Joint Institute for Freshwater Management," a collaboration between the University of Waikato and NIWA. We would like to thank James Owers (Lincoln Agritech Ltd.) for assistance with bioreactor maintenance, Reza Moghaddam (University of Waikato) for fieldwork support, Annie Barker (University of Waikato) for help with laboratory analysis and Amir Mohammadi (University of Waikato) for guidance with fieldwork. This research was made possible by the Mourits family for allowing us to conduct our study on their farmland.

Appendix A. Supplementary data

Supplementary data to this article can be found online at https://doi.org/10.1016/j.scitotenv.2024.170478.

References

Addy, K., Gold, A.J., Christianson, L.E., David, M.B., Schipper, L.A., Ratigan, N.A., 2016. Denitrifying bioreactors for nitrate removal: a meta-analysis. J. Environ. Qual. 45 (3), 873–881.

Blowes, D.W., Robertson, W.D., Ptacek, C.J., Merkley, C., 1994. Removal of agricultural nitrate from tile-drainage effluent water using in-line bioreactors. J. Contam. Hydrol. 15 (3), 207–221. https://doi.org/10.1016/0169-7722(94)90025-6.

Borch, T., Kretzschmar, R., Kappler, A., Cappellen, P.V., Ginder-Vogel, M., Voegelin, A., Campbell, K., 2010. Biogeochemical redox processes and their impact on contaminant dynamics. Environ. Sci. Technol. 44 (1), 15–23. https://doi.org/10.1021/es9026248.

Charlton, S.R., Parkhurst, D.L., 2011. Modules based on the geochemical model PHREEQC for use in scripting and programming languages. Comput. Geosci. 37 (10), 1653–1663. https://doi.org/10.1016/j.cageo.2011.02.005.

Christianson, L., Bhandari, A., Helmers, M., Kult, K., Sutphin, T., Wolf, R., 2012. Performance evaluation of four field-scale agricultural drainage denitrification bioreactors in Iowa. Transactions of the ASABE 55 (6), 2163–2174. https://dr.lib.iastate.edu/handle/20.500.12876/1059.

Christianson, L.E., Lepine, C., Sibrell, P.L., Penn, C., Summerfelt, S.T., 2017. Denitrifying woodchip bioreactor and phosphorus filter pairing to minimize pollution swapping. Water Res. 121, 129–139. https://doi.org/10.1016/j.watres.2017.05.026.

Christianson, L.E., Cooke, R.A., Hay, C.H., Helmers, M.J., Feyereisen, G.W., Ranaivoson, A.Z., McMaine, J.T., McDaniel, R., Rosen, T.R., Pluer, W.T., Schipper, L. A., Dougherty, H., Robinson, R.J., Layden, I.A., Irvine-Brown, S.M., Manca, F., Dhaese, K., Nelissen, V., von Ahnen, M., 2021. Effectiveness of denitrifying bioreactors on water pollutant reduction from agricultural areas. Trans. ASABE 64 (2), 641–658. https://doi.org/10.13031/trans.14011.

Comeau, Y., Oldham, W.K., Hall, K.J., 1987. Dynamics of carbon reserves in biological dephosphatation of wastewater. In: Ramadori, R. (Ed.), Biological Phosphate Removal From Wastewaters. Pergamon, pp. 39–55. https://doi.org/10.1016/B978-0-08-035592-4.50010-9.

Corbett, T.D.W., Dougherty, H., Maxwell, B., Hartland, A., Henderson, W., Rys, G.J., Schipper, L.A., 2020. Utility of 'diffusive gradients in thin-films' for the measurement of nitrate removal performance of denitrifying bioreactors. Sci. Total Environ. 718, 135267 https://doi.org/10.1016/j.scitotenv.2019.135267.

Damasceno, B.S., da Silva, A.F.V., Ferreira, M.C., de Melo, A.N., Leite, D.M.G., de Araújo, A.C.V., 2023. A facile and eco-friendly hydrothermal synthesis of magnetic graphite nanocomposite and its application in water purification. Colloids Surf. A Physicochem. Eng. Asp. 670, 131528 https://doi.org/10.1016/j.colsurfa.2023.131528.

David, M.B., Gentry, L.E., Cooke, R.A., Herbstritt, S.M., 2016. Temperature and substrate control woodchip bioreactor performance in reducing tile nitrate loads in east-central Illinois. J. Environ. Qual. 45 (3), 822–829. https://doi.org/10.2134/jeq2015.06.0296.

Dougherty, H. (2018). Hydraulic Evaluation of a Denitrifying Bioreactor With Baffles Urbana, IL: University of Illinois.] Master thesis.

Dougherty, H., Cooke, R.A.C., Bhattarai, R., Christianson, L., 2020. Design flow and nitrate removal evaluation of a wide denitrifying bioreactor with baffles. Ecol. Eng. 158, 106068 https://doi.org/10.1016/j.ecoleng.2020.106068.

Dzombak, D.A., Morel, F.M.M., 1991. Surface Complexation Modeling: Hydrous Ferric Oxide. Wiley. https://books.google.co.nz/books?id=LGBtoHNUbWwC.

Fan, Y., Essington, M., Jagadamma, S., Zhuang, J., Schwartz, J., Lee, J., 2022. The global significance of abiotic factors affecting nitrate removal in woodchip bioreactors. Sci. Total Environ. 848, 157739 https://doi.org/10.1016/j.scitotenv.2022.157739.

Gerber, A., De Villiers, R., Mostert, E., Van Riet, C., 1987. The phenomenon of simultaneous phosphate uptake and release, and its importance in biological nutrient removal. In: Biological Phosphate Removal from Wastewaters. Elsevier, pp. 123–134. https://doi.org/10.1016/B978-0-08-035592-4.50016-X.

Hartland, A., Larsen, J.R., Andersen, M.S., Baalousha, M., O'Carroll, D., 2015. Association of arsenic and phosphorus with iron nanoparticles between streams and aquifers: implications for arsenic mobility. Environ. Sci. Technol. 49 (24), 14101–14109. https://doi.org/10.1021/acs.est.5b03506.

Hua, G., Salo, M.W., Schmit, C.G., Hay, C.H., 2016. Nitrate and phosphate removal from agricultural subsurface drainage using laboratory woodchip bioreactors and recycled steel byproduct filters. Water Res. 102, 180–189. https://doi.org/10.1016/j.watres.2016.06.022.

Kerrn-Jespersen, J.P., Henze, M., 1993. Biological phosphorus uptake under anoxic and aerobic conditions. Water Res. 27 (4), 617–624. https://doi.org/10.1016/0043-1354(93)90171-D.

Khoshmanesh, A., Hart, B.T., Duncan, A., Beckett, R., 2002. Luxury uptake of phosphorus by sediment bacteria. Water Res. 36 (3), 774–778. https://doi.org/10.1016/S0043-1354(01)00272-X.

Lepine, C., Christianson, L., Davidson, J., Summerfelt, S., 2018. Woodchip bioreactors as treatment for recirculating aquaculture systems' wastewater: a cost assessment of nitrogen removal. Aquac. Eng. 83, 85–92. https://doi.org/10.1016/j.aquaeng.2018.09.001.

Meinhold, J., Arnold, E., Isaacs, S., 1999. Effect of nitrite on anoxic phosphate uptake in biological phosphorus removal activated sludge. Water Res. 33 (8), 1871–1883. https://doi.org/10.1016/S0043-1354(98)00411-4.

Mohammadi, A., Corbett, T., French, A., Lehto, N.J., Hadfield, J., Jarman, P., Sandwell, D., Shokri, A., Schipper, L., Hartland, A., 2022. Application of diffusive gradients in thin films for monitoring groundwater quality. ACS ES&T Water 2 (4), 518–526. https://doi.org/10.1021/acsestwater.1c00279.

Oehmen, A., Carvalho, G., Freitas, F., Reis, M.A., 2010. Assessing the abundance and activity of denitrifying polyphosphate accumulating organisms through molecular and chemical techniques. Water Sci. Technol. 61 (8), 2061–2068. https://doi.org/10.2166/wst.2010.976.

Parkhurst, D. L. (1995). *User's guide to PHREEQC, a computer program for speciation, reaction-path, advective-transport, and inverse geochemical calculations* [Report] (95–4227). (Water-Resources Investigations Report, Issue. U. S. G. Survey. http://pubs.er.usgs.gov/publication/ wri954227.

Povilaitis, A., Matikienė, J., Vismontienė, R., 2020. Effects of three types of amendments in woodchip-denitrifying bioreactors for tile drainage water treatment. Ecol. Eng. 158, 106054 https://doi.org/10.1016/j.ecoleng.2020.106054.

Rao, T.S., Rani, P.G., Venugopalan, V.P., Nair, K.V.K., 1997. Biofilm formation in a freshwater environment under photic and aphotic conditions. Biofouling 11 (4), 265–282. https://doi.org/10.1080/08927019709378336.

Reese, B.K., Finneran, D.W., Mills, H.J., Zhu, M.-X., Morse, J.W., 2011. Examination and refinement of the determination of aqueous hydrogen sulfide by the methylene blue method. Aquat. Geochem. 17, 567–582.

Rivas, A., Barkle, G., Stenger, R., Moorhead, B., Clague, J., 2020a. Nitrate removal and secondary effects of a woodchip bioreactor for the treatment of subsurface drainage with dynamic flows under pastoral agriculture. Ecol. Eng. 148, 105786 https://doi.org/10.1016/j.ecoleng.2020.105786.

Rivas, A., Singh, R., Horne, D.J., Roygard, J., Matthews, A., Hedley, M.J., 2020b. Contrasting subsurface denitrification characteristics under temperate pasture lands and its implications for nutrient management in agricultural catchments. J. Environ. Manag. 272, 111067 https://doi.org/10.1016/j.jenvman.2020.111067.

Rivas, A., Barkle, G., Sarris, T., Park, J., Kenny, A., Maxwell, B., Stenger, R., Moorhead, B., Schipper, L., Clague, J., 2023. Improving accuracy of quantifying nitrate removal performance and enhancing understanding of processes in woodchip bioreactors using high-frequency data. Sci. Total Environ. 880, 163289 https://doi.org/10.1016/j.scitotenv.2023.163289.

Saeed, H., Hartland, A., Lehto, N.J., Baalousha, M., Sikder, M., Sandwell, D., Mucalo, M., Hamilton, D.P., 2018. Regulation of phosphorus bioavailability by iron nanoparticles in a monomictic lake. Sci. Rep. 8 (1), 17736. https://doi.org/10.1038/s41598-018-36103-x.

Sanchez Bustamante-Bailon, A.P., Margenot, A., Cooke, R.A.C., Christianson, L.E., 2022. Phosphorus removal in denitrifying woodchip bioreactors varies by wood type and water chemistry. Environ. Sci. Pollut. Res. Int. 29 (5), 6733–6743. https://doi.org/10.1007/s11356-021-15835-w.

Sathasivan, A. (2009). Biological phosphorus removal processes for wastewater treatment. *Water and wastewater treatment technologies. Oxford (UK): encyclopedia of life support systems (EOLSS)*, 1-23.

Schipper, L.A., Vojvodić-Vuković, M., 2000. Nitrate removal from groundwater and denitrification rates in a porous treatment wall amended with sawdust. Ecol. Eng. 14 (3), 269–278.

Schipper, L.A., Robertson, W.D., Gold, A.J., Jaynes, D.B., Cameron, S.C., 2010. Denitrifying bioreactors—an approach for reducing nitrate loads to receiving waters. Ecol. Eng. 36 (11), 1532–1543. https://doi.org/10.1016/j.ecoleng.2010.04.008.

Shahid, M.K., Kim, Y., Choi, Y.-G., 2019. Magnetite synthesis using iron oxide waste and its application for phosphate adsorption with column and batch reactors. Chem. Eng. Res. Des. 148, 169–179. https://doi.org/10.1016/j.cherd.2019.06.001.

Sharrer, K.L., Christianson, L.E., Lepine, C., Summerfelt, S.T., 2016. Modeling and mitigation of denitrification 'woodchip' bioreactor phosphorus releases during treatment of aquaculture wastewater. Ecol. Eng. 93, 135–143. https://doi.org/10.1016/j.ecoleng.2016.05.019.

Sposito, G., 2004. The Surface Chemistry of Natural Particles. Oxford University Press.

Stumm, W., Morgan, J.J., 1996. Aquatic Chemistry: Chemical Equilibria and Rates in Natural Waters. Wiley. https://books.google.co.nz/books?id=xvZOAAAAMAAJ.

Sun, Y., Peng, Y., Zhang, J., Li, X., Zhang, Q., Zhang, L., 2020. Effect of endogenous metabolisms on survival and activities of denitrifying phosphorus removal sludge under various starvation conditions. Bioresour. Technol. 315, 123839 https://doi.org/10.1016/j.biortech.2020.123839.

Tanner, C.C., Sukias, J.P.S., Headley, T.R., Yates, C.R., Stott, R., 2012. Constructed wetlands and denitrifying bioreactors for on-site and decentralised wastewater treatment: comparison of five alternative configurations. Ecol. Eng. 42, 112–123. https://doi.org/10.1016/j.ecoleng.2012.01.022.

Thapa, U., Ahiablame, L., Kjaersgaard, J., Hay, C., 2023. Field evaluation of four denitrifying woodchip bioreactors for nitrogen removal in eastern South Dakota, United States. Sci. Total Environ. 855, 158740 https://doi.org/10.1016/j.scitotenv.2022.158740.

Viollier, E., Inglett, P.W., Hunter, K., Roychoudhury, A.N., Van Cappellen, P., 2000. The ferrozine method revisited: Fe(II)/Fe(III) determination in natural waters. Appl. Geochem. 15 (6), 785–790. https://doi.org/10.1016/S0883-2927(99)00097-9.

Wu, T., Yang, S.-S., Zhong, L., Pang, J.-W., Zhang, L., Xia, X.-F., Yang, F., Xie, G.-J., Liu, B.-F., Ren, N.-Q., Ding, J., 2023. Simultaneous nitrification, denitrification and phosphorus removal: what have we done so far and how do we need to do in the future? Sci. Total Environ. 856, 158977 https://doi.org/10.1016/j.scitotenv.2022.158977.

Zaman, M., Kim, M., Nakhla, G., 2021. Simultaneous nitrification-denitrifying phosphorus removal (SNDPR) at low DO for treating carbon-limited municipal wastewater. Sci. Total Environ. 760, 143387 https://doi.org/10.1016/j.scitotenv.2020.143387.

Chapter 4. Iron–based composites for in–field phosphorus removal from agricultural drainage

The manuscript has been published in:

G. N. Perera, D. T. Rojas, S. N. Höpker, G. Olsen, R. Craggs and A. Hartland

Surfaces and Interfaces 2024 Vol. 51 Pages 104566

Surfaces and Interfaces 51 (2024) 104566

Contents lists available at ScienceDirect

Surfaces and Interfaces

journal homepage: www.sciencedirect.com/journal/surfaces-and-interfaces

Iron−based composites for in−field phosphorus removal from agricultural drainage

Gimhani N. Perera [a,b], Dorisel Torres Rojas [a], Sebastian N Höpker [a], Greg Olsen [b], Rupert Craggs [b], Adam Hartland [a,c,*]

[a] Environmental Research Institute, School of Science, Faculty of Science and Engineering, University of Waikato, Kirikirioa Hamilton, New Zealand
[b] National Institute of Water and Atmospheric Research Ltd (NIWA), PO Box 11115, Kirikirioa Hamilton 3251, New Zealand
[c] Lincoln Agritech Ltd, Ruakura, Kirikirioa Hamilton 3214, New Zealand

ARTICLE INFO

Keywords:
Adsorption
Agricultural drainage
Iron oxide composite
Phosphorus removal
Denitrifying bioreactors

ABSTRACT

Elevated phosphorus and nitrogen concentrations in agricultural drainage are responsible for widespread declines in water quality across freshwater and marine receiving environments worldwide. Removal of P at source is particularly important because its tight biogeochemical cycling with iron (Fe), leads to preferential *P*−retention (over N) across the aquatic continuum, particularly in lake basins. This paper introduces new Fe−C−based composites (Fe(III)oxide/akaganite) designed for use in edge-of-field mitigations such as denitrifying bioreactors, with the goal of intercepting and retaining P on−farm. Our Fe−functionalised media had a net positive charge in the favourable range for P adsorption under the typical pH conditions encountered in denitrifying bioreactors (pH 5.5 − 6). Although functionalized wood (Fe-WC) had significantly higher P adsorption capacity than functionalised biochar (Fe-PyOM), 65.8 mg g^{-1} and 31.4 mg g^{-1}, respectively; this was of comparable magnitude to powdered akaganite (107 mg g^{-1}), despite large differences in particle size. Batch and column adsorption experiments indicate a multi−layer adsorption mechanism for P removal on Fe−PyOM and Fe−WC, which was further investigated using XPS, confirming dominant electrostatic P binding by Fe-functionalised media below pH 6, but an increasing importance of ligand exchange (Fe-O-P) at pH 8, particularly for Fe-PyOM. Based on the prevailing geochemistry of influent solutions to DBRs (pe ~ -8, pH ~ 6), we suggest that Fe−PyOM may be able to continuously adsorb P over a long timespans without requiring replenishment, due to its higher surface area, stability, and multiple P binding mechanisms.

1. Introduction

Degradation of water quality by diffuse nutrient pollution has prompted extensive research into nitrate removal from agricultural drainage, leading to a proliferation of studies investigating denitrifying bioreactors (DBRs), saturated buffers, and other edge−of−field strategies [1,2]. Surprisingly, less attention has been paid to phosphorus removal in edge−of−field solutions like bioreactors [3], but the scope of this research area is increasingly expanding to include P, and more broadly, to understand how DBRs can be engineered, or augmented, to maximise nutrient removal, whilst minimising deleterious emissions (i.e. pollution swapping).

Woodchips are the most common substrate used in bioreactors [4,5] and are estimated to have a functional life span of ten or more years over which they supply carbon (C), the substrate fuelling denitrifying microorganisms [6]. Aside from fuelling denitrification, woodchips confer few additional advantages, and do not act to remove phosphorus, largely because wood has a negative surface charge at the (circumneutral to acidic) pH values typical of near−surface freshwater environments [7]. This incompatibility in the interfacial properties of woodchips, therefore, inhibits P adsorption and attenuation in DBRs. Interestingly, wood that contains higher proportions of metals such as Fe, Al, Mg, and Ca, has been shown to capture P in small quantities, leading to small but proportionally high (84 %) removal of dissolved reactive phosphorus (DRP) at the typically low levels characteristic of agricultural drainage 0.61−0.78 mg l^{-1} (Sanchez [8]). Hence, woodchips may have some intrinsic capacity to remove DRP, but the total P adsorption capacity is likely to be small.

Wood and other bio-media have previously been modified in experimental studies to enhance P removal [9,10]. In particular,

* Corresponding author.
E-mail address: adam.hartland@waikato.ac.nz (A. Hartland).

https://doi.org/10.1016/j.surfin.2024.104566
Received 1 May 2024; Received in revised form 29 May 2024; Accepted 1 June 2024
Available online 28 June 2024

pyrolyzed organic matter (PyOM), or 'biochar' has proven to be an excellent substrate for nanomaterials due to its large specific surface area and porous structure [11,12]. These studies aimed to use functionalization strategies to invert the surface charge of woodchips, favouring electrostatic attraction between P and wood surfaces [13]. This study follows numerous others [14,15,16] to evaluate natural and synthetic adsorbents in laboratory and field studies, but with attention to important, practical constraints. For example, practicality dictates that materials need to be based on locally−abundant and culturally acceptable materials [17,18], and using particle sizes which allow for fluid−flow in often turbid conditions. Therefore, in designing the research presented, we were cognizant to avoid complicated preparation steps, exotic or harmful reagents, and infeasible particle sizes, to ensure compatibility for large−scale applications in the agricultural landscape.

Previous research has demonstrated that the oxides and hydroxides of metals including Ca, La, Zr, Al, Zn, and Fe have a range of phosphorus removal properties due to the strong affinity of phosphate ions for specific complexation with *O*−containing surface groups [10,19]. Recently, iron−based adsorbents have attracted attention for phosphorus removal because iron (hydr)oxide is chemically stable in oxygenated waters [20], environmentally compatible, cost−effective, and abundant [10]. Moreover, iron−hydroxides are positively charged under circumneutral−to−acidic pH values, making them an obvious choice for P removal from agricultural drainage with a typical pH of 5.5 − 8 [21].

In this study, we introduce a novel, green synthesis approach to fabricating composite materials (akaganeite, Fe−functionalized wood, and Fe−functionalized biochar) for phosphorus removal. Our strategy provides a low-cost, efficient, and environmentally friendly approach for phosphorus remediation in DBRs supporting broader initiatives in water purification and environmental conservation. Standard characterisation was followed by batch tests for surface charge and adsorption characteristics, and XPS analysis to evaluate changes in Fe mineralogy following P adsorption. Finally, column experiments were used to evaluate phosphorus uptake under flowing conditions, to ensure performance under comparable conditions to typical denitrifying bioreactors.

2. Methods and materials

2.1. Materials

The radiata pine (*pinus radiata*) woodchips were obtained from local plantation forest sources similar to those used in the bioreactor located in Tatuanui, New Zealand. The PyOM was obtained from Massey University Biochar Research Centre in New Zealand. NaOH, NaCl, $FeCl_3$, NH_4OH were purchased from Sigma Aldrich. All chemical reagents used in this investigation were of analytical grade (AR).

2.2. Pre-treatment of woodchips

Radiata pine (*pinus radiata*) woodchips were rinsed thoroughly using deionized water and dried at 60 °C for 3 days before sieving to a target particle size of 2 − 2.8 mm. Woodchips were then pre-treated following standard methods [22]. Briefly, woodchips were soaked in 0.5 M sodium hydroxide at a solid to liquid ratio of 1:10 (mass basis) to dissolve lignin and cellulose and stirred for 10 min at 70 °C under a vacuum to assist penetration of the solvent. Thus, pre−treated woodchips were then rinsed with deionized water to remove lignin and cellulose.

2.3. Synthesis of Fe-WC and Fe-PyOM

Functionalization of woodchips and PyOM followed a modified procedure based on Ramasahayam et al. [23]. Pre-treated woodchips and non-pre-treated PyOM were immersed in a solution of 1 M iron (III) chloride (Sigma Aldrich, ACS grade) dissolved in saturated sodium chloride (NaCl) solution (solid to liquid ratio 1:10 [mass basis]) and stirred for 3 hrs under vacuum. The iron (III) chloride solution was then decanted, and the materials then dried at 60 °C for 24 hrs. The treated materials were then immersed in 5 M ammonium hydroxide (NH_4OH) solution and the pH adjusted to 9 − 10 while stirring, and then left for 3 hrs to precipitate iron (hydr)oxides. The solution was left to settle overnight, and the newly functionalized materials were rinsed thoroughly with DI water until the pH reached ca. 7. Functionalized materials were then dried at 60 °C for 24 hrs.

2.4. Synthesis of akaganeite

In this work, akaganeite was prepared via the reverse co-precipitation technique whereby a 1 M Iron (III) chloride solution (Sigma Aldrich, ACS grade) saturated with NaCl was added dropwise to a 5 M ammonium hydroxide solution at room temperature. The solution was stirred magnetically during the addition of $Fe(III)Cl_3$ [24]. The pH was then raised with 2 M NaOH until a precipitate formed (pH~8.5) and the suspension was further stirred for 1 h. The precipitate was separated by centrifugation, washed with deionized water until reaching neutral pH, and finally dried in an oven at 60 ºC for 48 h.

2.5. Determination of point of zero charge (pH_{pzc}) of the sorbents

The raw and functionalized materials were evaluated for the point of zero charge (pH_{pzc}) using a pH titration procedure [25]. This involved placing 20 mL of 0.1 M sodium chloride solution into Erlenmeyer flasks and adjusting pH by adding 0.1 M hydrochloric acid or 0.1 M sodium hydroxide to attain the target pH. A 0.1 g sample of sorbent was then added, and the pH was re-measured after 24 hrs for each replicate with each experimental pH evaluated in triplicate. The pH_{pzc} was calculated by plotting the difference in pH (y-axis) against the initial pH (x-axis). The point where the line intersects the x-axis is identified as the pH_{pzc}.

2.6. Phosphorus adsorption experiments

Adsorption experiments were carried out to determine the phosphorus adsorption capacity of Fe−WC and Fe−PyOM as a function of pH between 4 and 8, the typical pH range of agricultural drainage water. A 50 mg l^{-1}, $P-PO_4$ stock solution was prepared by dissolving potassium dihydrogen phosphate, KH_2PO_4 (AnalaR, ACS grade) and pH−adjusted with either 0.1 M HCl or 0.1 M NaOH.

An aliquot of 0.05 g of each media was then added to 25 mL P solution in triplicate across a concentration series between 5 and 2000 mg l^{-1} P. All experiments were conducted in triplicate and at a pre−defined ratio of P to solid of 25 mg g^{-1}. At the end of the experiment, the suspension was filtered through a 0.45 μm membrane syringe filter (Sartorius) and the filtrate was analysed for P by UV−Vis spectrometry (Dynamica, Halo VIS−20) at 880 nm using the ascorbic acid method. The P adsorption per unit of adsorbent was then calculated by the following equation:

$$q_e = \frac{(C_i - C_f)V}{M} \quad (1)$$

Where C_i and C_f (mg $P-PO_4$ l^{-1}) are the initial and final equilibrium concentrations of $P-PO_4$; V (L) is the volume of the $P-PO_4$ solution, and M (g) is the adsorbent weight.

Adsorption isotherm models of Langmuir and Freundlich were applied to explain the adsorption behaviours. Eq. (2) represents the Langmuir isotherm.

$$q_e = \frac{q_{max} K_L C_e}{1 + K_L C_e} \quad (2)$$

where, q_e (mg g^{-1}) denotes the adsorption capacity per unit mass at the adsorption equilibrium; C_e (mg l^{-1}) represents the concentration of

solution at the adsorption equilibrium; q_{max} (mg g^{-1}) represents the maximum adsorption capacity per unit mass; K_L denotes the Langmuir equilibrium constant. The linear form of Langmuir isotherm is as follows (eq. 3);

$$\frac{1}{q_e} = \frac{1}{K_L q_{max}} \frac{1}{C_e} + \frac{1}{q_{max}} \quad (3)$$

Eq. (4) represents the Freundlich isotherm where q_e represents the adsorption capacity per unit mass at the adsorption equilibrium; C_e denotes the solution concentration at equilibrium; K_f and n represent Freundlich temperature constants.

$$q_e = K_f C_e^{\frac{1}{n}} \quad (4)$$

The linear form of Freundlich isotherm is as follows Eq. (5)

$$Log\ q_e = LogK_f + \frac{1}{n}\ Log\ C_e \quad (5)$$

2.7. Phosphate adsorption column experiments

Column experiments were conducted to evaluate the long-term P removal performance of the functionalized media (Fig. 1). All treatments including the control (WC) were carried out in triplicate. Glass columns (diameter 1.4 cm) were filled with 1 g of glass wool fitted overlain by stainless steel mesh (500 μm), with 6 g of adsorbent and 48 g of wood above. The upper section of the columns was then filled with 1 g of glass wool, 30 g of glass beads and finally fitted with stainless steel mesh (500 μm). Glass beads and wool were used to prevent the floatation of the materials with the mesh serving as a screen for the packed materials. A 2 mg $P{-}PO_4$ l^{-1} concentration was fed upwards into the columns at the flow rate of 2 ml min^{-1} for 7.5 hrs (pH 5.5–6). The packed columns were initially rinsed with 0.001 M NaCl solution during adjustment of the flow rate before the experiment. This also served to ensure the conditions enabling electrostatic interactions could operate between the media surfaces and ions present in the influent. Finally, the effluent was collected every 30 min and analysed for the remaining P concentration using the ascorbic acid method (Standard Method Phosphorus 4500-P) by UV–Vis spectrophotometry (Dynamica HALO VIS−20, UK).

The performance of the column reactors was evaluated by relative concentration (breakthrough) curves and% P removal using the following equations.

$$RC = \frac{C_f}{C_i} \quad (6)$$

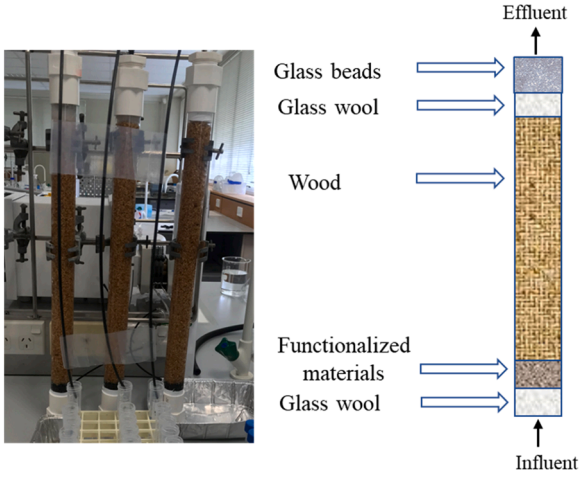

Fig. 1. Setup of the column reactors used in flowing P-adsorption experiments.

$$RC\% = \frac{(C_i - C_f)}{C_i} \times 100 \quad (7)$$

2.8. Characterization of media before and after P-exposure

Raw materials and the functionalized composites were characterised before and after P adsorption for changes in the surface morphology and mineralogy. *X*−ray diffraction (XRD, Panalytical Empyrean Series 2) was run over the 5 to 80 (2θ) range to identify the iron oxide crystallographic structures (Table 2). An aliquot of 200 mg of sample was digested by using 10 mL of conc. nitric acid, HNO_3 (Sigma Aldrich, USA) using microwave-assisted digestion (Multiwave 3000 microwave sample preparation system, Anton Paar, Graz, Austria). Inductively coupled plasma mass spectrometry (ICP−MS) (Agilent 8900, United States) was then used to analyse the metal content present in the digested samples. Additionally, *X*−ray fluorescence (Bruker WD XRF S8 Tiger) was used to quantify the% iron oxide. For XRF, powdered samples were ignited at 1100 °C for 1 hour to make fusion discs in a Neo Claisse Fusion Furnace (Malvern Panalytical, United Kingdom) composed of 0.8 g of sample, 8 g of flux (57.0 % Lithium Tetraborate: 43.0 % Lithium Metaborate), and 0.1 − 0.2 g ammonium iodide (releasing agent). All samples were coated in a 5 nm platinum layer using Quorum 150 V ES plus and imaged for morphology and surface texture by scanning electron microscopy (Hitachi Regulus SU8230 FE-SEM, Japan) at 5 kV. The particle size of the powdered sample was determined by a particle size analyzer MASTERSIZER 3000 (Malvern Panalytical Ltd, United Kingdom). Functional groups present in the composites were further characterised by Fourier-transform infrared spectroscopy (Perlin−Elmer, USA). X-ray photoelectron spectroscopy (Kratos Analytical, Manchester, U.K) measurements were obtained on a Kratos Axis UltraDLD instrument equipped with a hemispherical electron energy analyzer at the University of Auckland. For experimental details see [26].

3. Results

3.1. Effect of solution pH on the adsorption of phosphate to functionalized media

The effect of solution pH on phosphate adsorption was determined for the functionalized and unaltered materials across the pH range of 4 to 8, at a solution P concentration of 40 mg l^{-1}. Fig. 2a shows the amount of P adsorbed onto akaganeite, WC, Fe-WC, PyOM, and Fe-PyOM as a function of pH. As shown in Fig. 2a, the adsorption capacity of akaganeite powder (21.5 mg g^{-1}) was much higher than the non-powdered functionalized media due to large differences in their respective surface areas. Among the functionalized materials, Fe−WC had the highest adsorption capacity at pH 4 (8.17 mg g^{-1}) and pH 5 (5.55 mg g^{-1}) whereas Fe−PyOM had the highest adsorption capacity at pH 6 (4.77 mg g^{-1}), pH 7 (4.17 mg g^{-1}), and pH 8 (3.45 mg g^{-1}) (Fig. 2a). pH, therefore, had a pronounced effect, with the percentage of phosphate adsorbed onto functionalized wood and functionalized biochar decreasing from 37% to 11.4% and 30% to 17%, respectively as the pH rose from 4 to 8. Hence, low pH values had a positive impact on P removal (Fig. 3), consistent a with electrostatic binding mechanism.

The measured point of zero charge (pH_{pzc}) values for akaganeite, PyOM, Fe−PyOM, WC, and Fe-WC were 7.4, 7.5, 9, 4.5, 4.5 respectively (Fig. 2b). Above these pH values, functionalized materials are predominantly negatively charged, favouring cationic adsorption. Hence, pH values lower than the pzc promote positively charged surfaces which favor anionic adsorption. Hence, P adsorption on iron hydr(oxide) is favoured under more acidic conditions below pH 7. The pH_{pzc} value of PyOM indicates an increase in surface functional groups (e.g. phenols) with pKa values > 4.5, following pyrolysis. The pH_{pzc} value of Fe−PyOM (ca. 9) was around 1.5 pH units higher (> an order−of−magnitude shift), as a result of the addition of the iron hydr(oxide) surface coating.

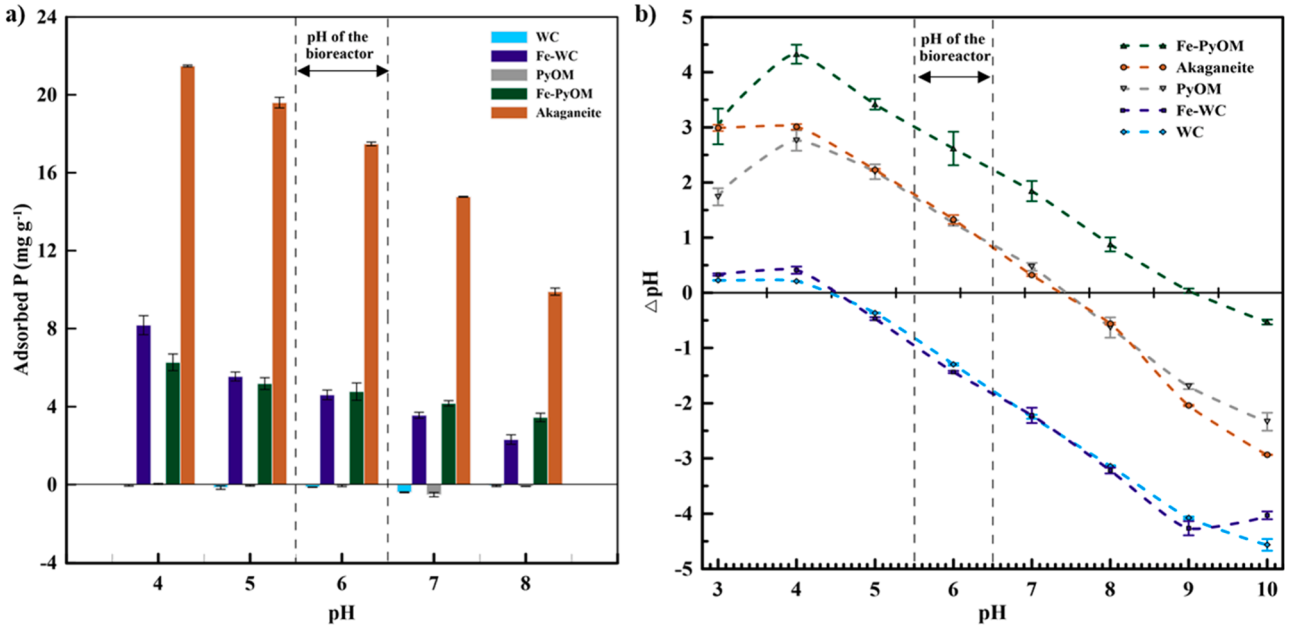

Fig. 2. a) Phosphorus adsorption by different iron−oxide−functionalized materials across an environmentally−relevant range of pH b) pH−drift titration experiments for determination of the point of zero charge (pzc) of functionalized and non−functionalized materials.

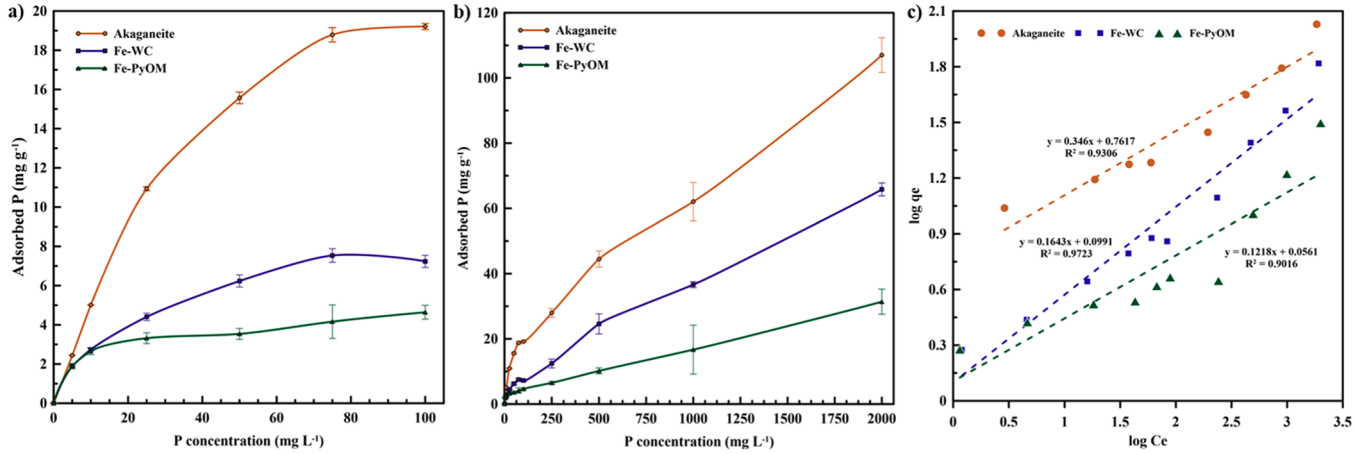

Fig. 3. P adsorption isotherms of akaganeite, functionalized wood, and functionalized PyOM showing a narrow (a) and large (b) range of concentrations; panel (c) shows the linear fit of the Freundlich isotherms.

The small variation observed between WC and Fe−WC therefore demonstrates that the native functional groups at the wood surface dominate, and the charge shift contributed by the iron hydroxides was minimal.

3.2. P adsorption isotherms

Fig. 3 shows the P adsorption isotherms of powdered akaganeite, Fe−WC and Fe−PyOM chips (2 − 2.8 mm). Phosphorus adsorption in the batch experiments increased with P concentration, approaching an apparent plateau at a solution concentration of 100 mg l^{-1}. However, the proportion of adsorbed P increased when the solution concentration was further increased from 250 to 2000 mg l^{-1}, suggesting an abundance of unsaturated P adsorption sites. Akaganeite exhibited the highest P removal of 107 mg g^{-1} whereas functionalized wood and functionalized biochar had adsorption capacities corresponding to 65.8 mg g^{-1} and 31.4 mg g^{-1}, respectively. Clearly, the low particle size of the akaganeite (69 μm) was the main factor in driving its higher adsorption capacity compared to the functionalized bio media (2–3 mm), which had functionally equivalent Fe mineralogy.

To evaluate the characteristics of P adsorption on the functionalized materials, Freundlich and Langmuir models were used to fit the P adsorption isotherms. Freundlich isotherms implicitly describe a multilayer adsorption process on heterogeneous surfaces, whereas Langmuir isotherms are intended to explicitly model monolayer adsorption [27]. As illustrated in Fig. 3c, the adsorption isotherms were best described by the Freundlich model, indicating that the P adsorption was multilayer in nature, likely attributed to electrostatic interactions with the iron hydr(oxide) surfaces. The isotherm parameters are presented in Table 1.

3.3. P adsorption to experimental media under flowing conditions

To better understand the ability of the experimental media to remove P under flowing conditions, P adsorption was examined in a series of column experiments. Fig. 4(a) shows the breakthrough curves for the functionalized and raw materials. The wood treatment effectively served as the control, because natural pine woodchips inhibit adsorbtion of

Table 1
Isotherm parameters for the removal of P on Fe-functionalised media.

Type of isotherm	Parameters	Akaganeite	Fe-WC	Fe-PyOM
Langmuir	q_{max} (mg g^{-1})	107	65.8	31.4
	KL (L mg^{-1})	0.18	0.19	0.43
	R^2	0.63	0.79	0.61
Freundlich	K_f	5.77	0.79	0.88
	1/n	2.89	6.09	8.21
	R^2	0.93	0.96	0.90

Table 2
Metal analysis of the unaltered and the functionalized materials (mg/g of material).

Sample Name	P (mg)	Mn (mg)	Fe (mg)	Mg (mg)	Al (mg)	Ca (mg)	Zn (mg)
WC	0.09	0.04	0.64	0.21	0.32	0.69	0.07
Fe-WC	0.03	0.08	24.0	0.04	0.05	0.37	0.02
PyOM	0.38	0.19	1.87	1.17	2.42	3.22	0.05
Fe-PyOM	0.06	0.04	86.2	0.33	0.08	0.83	0.01

phosphorus due to electrostatic repulsion at pH values greater than 4.5. Data from prior to 2.5 hrs were truncated because during this interval P leached from the fresh woodchips, as previously reported in field bioreactor studies following commissioning [28] (the detailed figure is included in the supplementary information).

In the wood-only control, the ratio of P concentration in the effluent to that in the influent (C/C_i) remained at ~1 throughout the experiment, whereas C/C_i remained below 0.56 throughout the Fe-WC and the Fe-PyOM experiments. P adsorption in the Fe-WC treatment slowed after 7 h, approaching C/C_i of 0.55 for functionalized biochar and 0.32 for functionalized wood, consistent with the hierarchy of adsorption capacities of these media (Fig. 4a. Notably, the functionalized materials did not reach the point of breakthrough (i.e., where $C = C_i$), suggesting continuous adsorption as expected for the proposed multi-layer adsorption mechanism (see the adsorption isotherm data (Fig. 3). Between the suite of investigated media, functionalized biochar achieved the best P removal under flowing conditions, with a maximum of 88 % P removal, compared to 73.4 % P removal by functionalised wood. Accordingly, the results indicate favourable DRP retention is possible under conditions of continuous flow needed for use in field-scale bioreactors.

3.4. Characterization of the functionalised media

Various types of iron oxides and hydroxides can form during chemical precipitation or hydrolysis processes depending on the pH, temperature, reagent concentrations, and other physical parameters. Hence, it was necessary to characterise the mineralogy of the Fe (hydr)oxides synthesised in these experiments. Unaltered and functionalized materials were first characterised by XRD (Fig. 5). The broad peak at 20−25° in the wood and functionalized materials corresponds to cellulose and deformed cellulose crystal structures. The major peak at 35° corresponds akaganeite with Miller indices of (211), other peaks were observed at 11.84° (110), 16.71° (200), 26.9° (310), 26.63° (301), 46.26° (411), 56.22° (521), 61.12° (002), 64.63° (514), 67.94° (321) for the iron hydr (oxide). The common signature peak patterns at 43.08° (400), 53.45° (422), and 73.99° (533) were identified as magnetite for both functionalized wood and biochar. Other peaks correspond to magnetite at 33.56° (114), 34.98° (212), 42.05° (220), 61.83° (440) in functionalized biochar, and 18.29° (111), 30.08° (220), 35.43° (311), 65.76° (531) in functionalized wood. The peak patterns were identified using the High score Plus database (Malvern Panalytical Ltd, United Kingdom), confirming that the precipitated iron (hydr)oxide was mainly akaganeite, with smaller contributions from iron oxide (WC) and magnetite (PyOM).

FTIR spectra were also used to identify the functional groups on the functionalized materials. Fig. 6 shows the peak patterns of akaganeite, WC, PyOM, Fe-WC, and Fe-PyOM. Overall, FTIR spectra were dominated by the primary substrates, although surface hydroxyl groups, which play an important role in the development of surface charge, can be discerned (Fig. 5) [29–31]. The adsorption peaks of O—H (3400 cm^{-1}) [32] indicate the hydroxyl and deformed hydroxyl groups on the surfaces of Fe-PyOM and Fe−WC. Peaks at 1627−1639 cm^{-1} and 1385 cm^{-1} can also be assigned to the O—H deformation and O—H bending vibrations of WC, Fe−WC and akaganeite [33]. The band at 697 cm^{-1} of akaganeite is denoted the vibrational mode due to the O—H- - -Cl hydrogen bonds [34].

The SEM images (Fig. 7) depict the changes of surface morphology

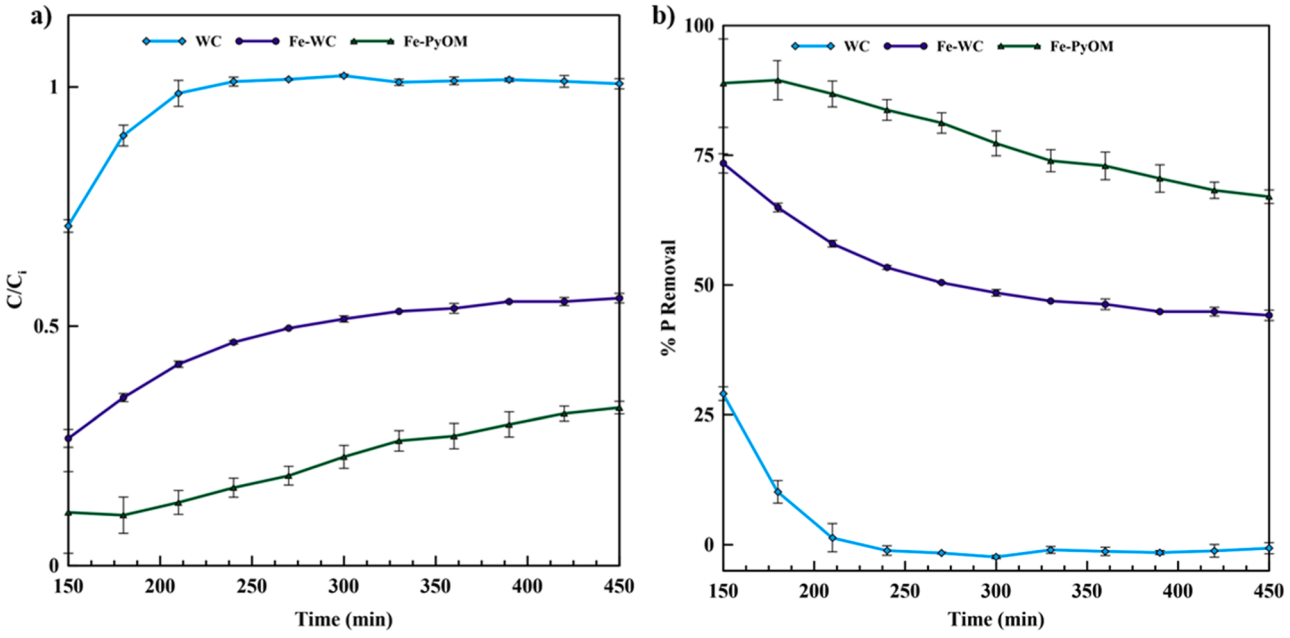

Fig. 4. Results of continuous−flow P adsorption experiments using columns packed with wood only (control), and wood plus functionalized wood and biochar. (a) P breakthrough curves (b) P removal (%) as a function of time.

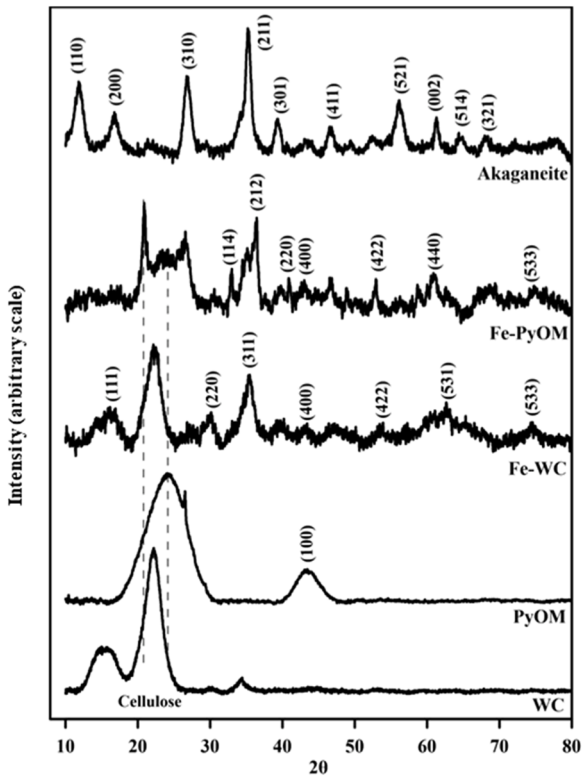

Fig. 5. XRD spectra of raw and functionalized materials.

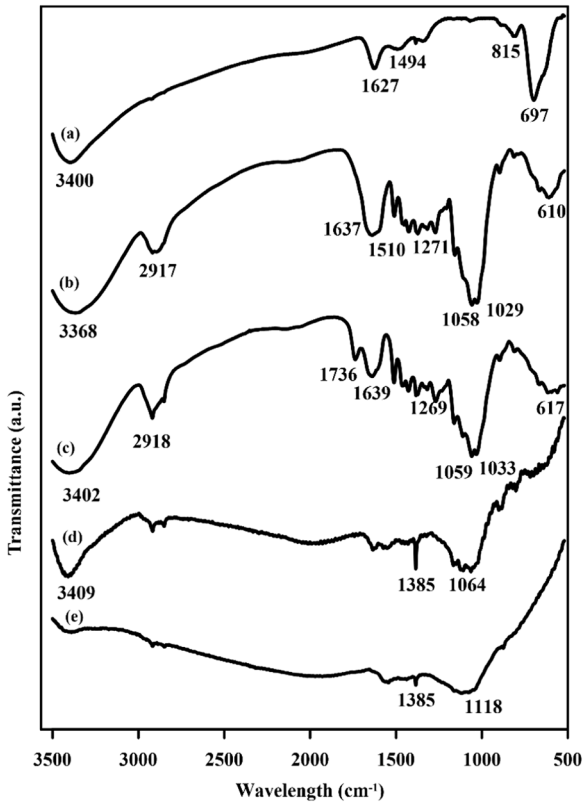

Fig. 6. FTIR spectra of (a) akaganeite (b) Fe-WC (c) WC (d) Fe-PyOM (e) PyOM.

and texture that occurred with the deposition of iron hydr(oxide). Akaganeite (Fig. 7g) has a relatively rough surface with a tunnel-shaped morphology (not resolved at magnifications used here), whereas functionalized materials have rough surfaces with surface clusters of FeOx crystals, demonstrating that the surface of the functionalized media was caked in iron hydroxide structures.

SEM images obtained after P adsorption indicate a change in the iron hydr(oxide) surface morphology. The surfaces of akaganeite and functionalized wood after P adsorption appear to be rougher and with greater image contrast, whereas the functionalized biochar following exposure to P, was smoother with less contrast. SEM images are highly sensitive to conductivity which could lead to observed morphological changes that may not be due to iron hydr(oxide) changes [35].

To understand the mechanisms responsible for phosphate adsorption by iron oxide functionalized media, we obtained XPS data for modified wood (Fe-WC) and functionalized biochar (Fe-PyOM) before, and after exposure to phosphate, at pH values between 4 and 8 (Fig. 7). High-resolution XPS spectral data were obtained and deconvoluted for P2p, C1s, O1s, and Fe2p (see SI).

Consistent with the P adsorption experiments, we observed a prominent P 2p peak (~133.3 eV) in the functionalised media, which indicates ejected 2p electrons from P, following P adsorption at lower pH (pH 4 and 6). This spectral feature, which represents surface adsorbed Fe-O-P (Fig. 8 and Table S1), disappeared entirely at pH 8, indicating negligible P binding, likely due to electrostatic repulsion as hypothesised based on adsorption isotherm results [36].

To further elucidate the mechanisms responsible for P adsorption, the O 1 s spectrum was used to interrogate the surface binding environment (see the SI for further information on the spectral features). The O 1 s peaks revealed an increase in the atomic percentage of the P-OH, $P = O$, and Fe-O-P at pH 4 and 6, with these species decreasing dramatically at pH 8, consistent with negligible phosphate adsorption.

The O1s spectral peaks also revealed a difference in bonding between phosphate and iron oxide between Fe-WC and Fe-PyOM. The intensity of the $P = O$ and Fe-O-P peaks increased significantly after phosphate adsorption, with peak intensity of Fe-PyOM >> Fe-WC. Conversely, the peak representing electrostatic interactions between P and Fe-OH (531–532 eV) increased by 26 % for Fe-WC after P adsorption, but decreased for Fe-PyOM. The peaks around 533–533.4 eV correspond to carbonates and carboxylate groups [37] on the Fe-WC and Fe-PyOM surfaces, which shift upon phosphorus adsorption.The high-resolution Fe 2p spectra were also deconvoluted, with peak assignments presented in Fig. 8 and Table S1. The satellite peak position for Fe $2p_{3/2}$ and Fe $2p_{1/2}$ are sensitive to oxidation state and were used to characterise the Fe species involved in P adsorption. The spectra for pure akageneite (β-FOOH) revealed several Fe2p peaks at 711.2 eV and 724.85 eV, representing the Fe^{3+} species [38,39]. Following P adsorption, the Fe 2p spectra changed indicating the formation of Fe-O-P complexes. For the pH 4 and 6 treatments, the peaks representing Fe^{3+} in Fe-WC shifted 0.3 – 0.7 eV after P adsorption, and were accompanied by a reduction in atomic percent for Fe^{3+} and a corresponding increase in the atomic percent of the satellite peak (~720 eV). The deconvolution of the Fe 2p spectra is complicated and requires careful consideration of the experimental conditions. Additional peaks in the Fe 2p spectra between 709 – 710 eV would suggest that there was possibly some Fe^{2+} present on the surface of the sorbents, which could also participate in the adsorption of P.

4. Discussion

4.1. Mechanisms of P removal on functionalised media

This study introduced the concept of Fe-functionalisation of woodchips and PyOM at particle sizes relevant to edge-of-field mitigations, such as denitrifying woodchip bioreactors, denitrification walls and saturated buffers. Our results show that Fe-functionalisation modifies wood and PyOM surfaces enabling strong binding of P under solution conditions and pH values typical of these systems.

Clearly, pH strongly affected the sorbents' surface charge and adsorption capacities. The mechanisms responsible for P adsorption by

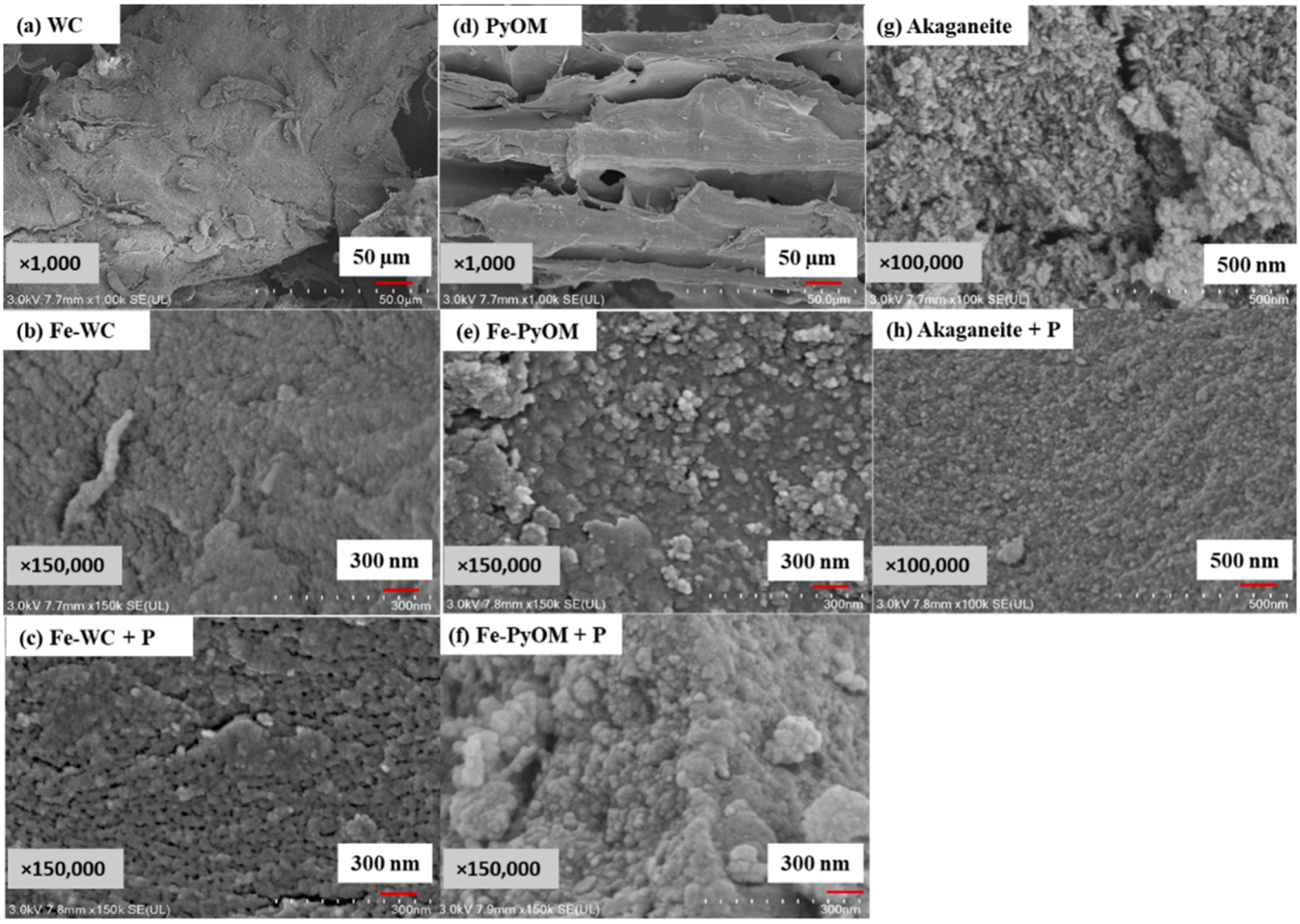

Fig. 7. SEM images of the unaltered and functionalized materials at magnifications between 1000 and 150,000x.

the synthesised iron (hydr)oxides include non-specific adsorption, electrostatic interaction, and specific adsorption (or 'chemisorption') [40,41]. Below the PZC, phosphate adsorption is expected to be driven by electrostatic attraction between the positively charged surface and negatively charged phosphate species (PZC was 4.5 and 9 for Fe-WC and Fe-PyOM, respectively). Modifying wood and biochar materials with iron oxide increases the hydroxyl groups available on the surface and at edges, and thus leads to an increase in the adsorption capacity of these media. This was particularly obvious at pH 4, where Fe-WC and Fe-PyOM had the highest P adsorption capacity (8.17 mg g^{-1} and 6.27 mg g^{-1}).

The higher P adsorption capacity and therefore P 2p XPS signal seen here at lower pH is consistent with the effects of pH on the surface charge of the materials. At lower pH, a high positive surface charge for the iron oxides allows the adsorption of dihydrogen phosphate ($H_2PO_4^-$), which dominates between pH 4–6. As the pH increases, the dominant P species shifts to hydrogen phosphate (HPO_4^{2-}) increasing the anionic charge. However, the simultaneously decreasing surface charge at this pH ensures an overall lowering of the P adsorption capacity, counteracting the effect of increased charge on the HPO_4^{2-} ion.

Above the PZC, the batch experiments indicate some additional degree of P adsorption, suggesting that ligand exchange may be responsible for P adsorption under alkaline pH conditions. Several studies [42, 36] have reported chemisorption of phosphate to iron oxides between pH 3–6 through ligand exchange, whereby deprotonation of the iron hydroxyl group creates a reactive Fe site compatible with the oxygen in phosphate, creating different types of Fe-O coordination bonds, such as monodentate or bidentate complexes. When the pH was above the PZC, the surface chemisorbed Fe-O-P atomic percentage decreased and disappeared at pH 8. This can be attributed to the strong electrostatic surface repulsion of HPO_4^{2-} ions.

The XPS O1s peaks revealed the adsorption of P across the pH range, leading to an increase in the atomic percentage of the P-OH, $P = O$, and Fe-O-P at pH 4 and 6. However, at pH 8, the intensity of these peaks decreased dramatically, confirming that the adsorption of phosphate at this pH is very low or negligible. Our findings from the O1s and Fe 2p spectra agree with other studies [43,36,44] and the heretofor discussed mechanisms, reporting an increase in P-containing functional groups at high pH, attributed to ligand exchange with surface hydroxyl groups and formation of Fe-O-P bonds. This suggests that the adsorption of P by electrostatic interactions is not the only mechanism responsible for P retention by Fe impregnated biomedia, and in fact, chemisorption also plays a role albeit numerically less significant than electrostatic binding at lower pH values.

Overall, our findings suggest that electrostatic P binding is an important process for both Fe-WC and Fe-PyOM and chemisorption plays a more critical role in the binding of P by Fe-PyOM than it does for Fe-WC. The contribution of these mechanisms to the adsorption process for each sorbent was different and could impact the capacity for P retention under different environmental conditions encountered in field studies.

4.2. *Performance characteristics of Fe-based media for P removal*

In our study, Fe-PyOM exhibited the highest P removal capacity, capturing 88 % P from 2 mg l^{-1} P under flowing conditions, without

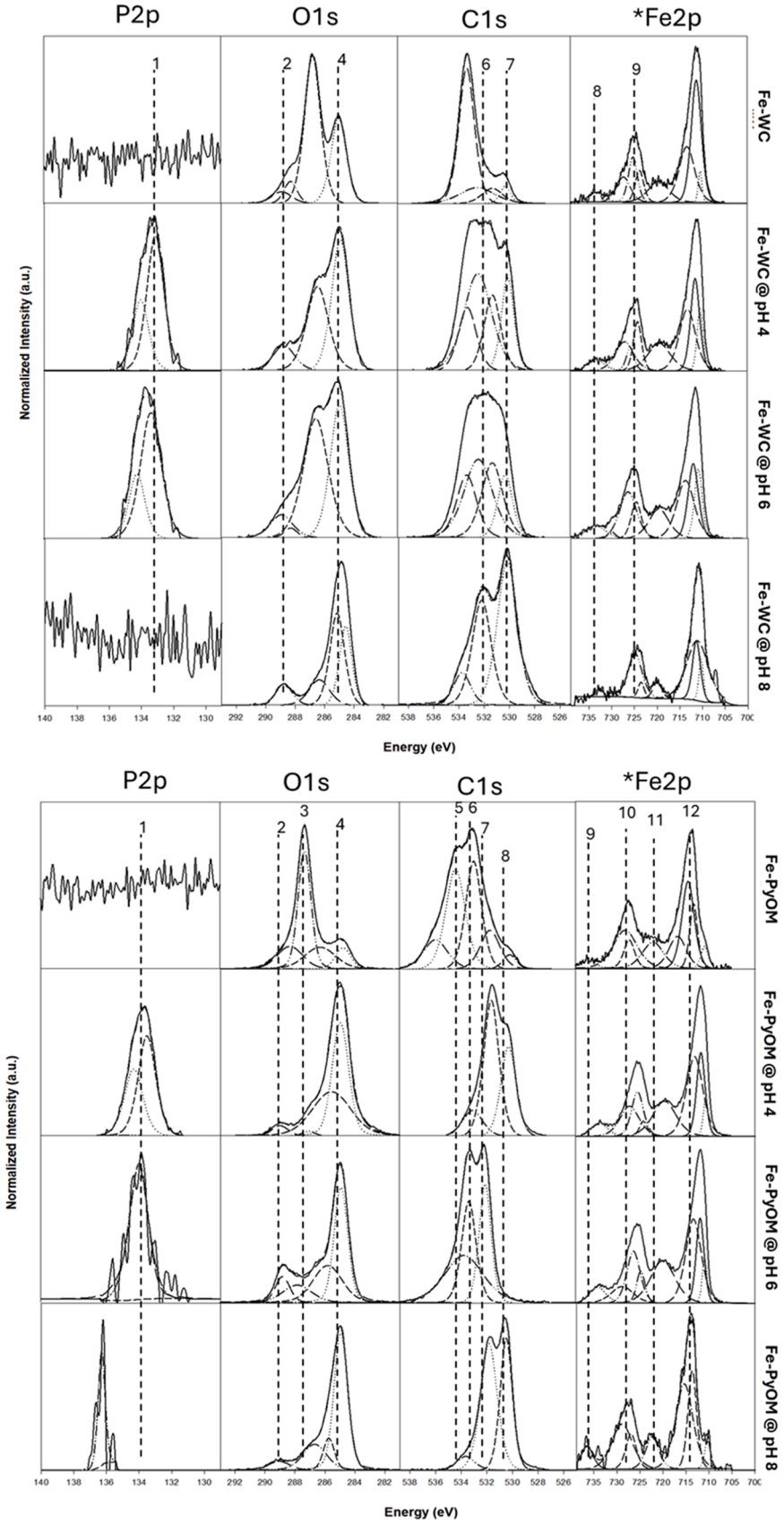

Fig. 8. XPS spectra of Fe-WC and Fe-PyOM before and after P adsorption at different solution pH values of pH 4, 6 and 8.

reaching breakthrough ($C/C_i = 0.55$), thereby indicating an abundance of unsaturated P sorption sites. The Fe_2O_3 content of Fe-PyOM was notably high, (Table 3) which suggested that the substantial coverage of iron oxide particles on the Fe-PyOM surface contributed toward its high adsorption capacity.

Our results suggest a multilayer adsorption mechanism operates between P and the Fe-biomedia surfaces at favourable pH, leading the adsorption capacity to scale with P concentration (Fig. 2). For instance, akaganeite exhibited lower adsorption at low concentrations (2.44 mg g^{-1} at 5 mg l^{-1} P) and higher adsorption at higher P concentrations (107 mg g^{-1} at 2000 mg l^{-1} P). At high initial P, the concentration gradient between phosphate and adsorption sites increases, leading to higher utilization of binding sites, boosting the removal capacity, but also leading to progressively weaker interaction [10]. At lower pH, protonated surface hydroxyl groups tend to attract negatively charged phosphate ions, resulting stronger phosphate binding. At higher pH, deprotonated hydroxyl groups instead electrostatically repulse phosphate ions, leading to fewer complexes between phosphate and surface adsorption sites and a decrease in P adsorption capacity [9]. Consequently, the adsorption capacity and binding strength of the Fe-based media is expected to covary with influent pH and the degree of PO_4^{3-} loading. This however does not preculde the use of surface modified media in denitrifying bioreactors, because to be effective, introduced media only need to attenuate P, thereby allowing longer hydraulic residence times and correspondingly higher rates of biological P uptake [45].

Table 4 compares the P adsorption capacities of akaganeite, Fe-WC and Fe-PyOM versus other iron coated composite materials from the literature. The high P adsorption capacities of the media from this study compare well with other adsorbents, despite the larger particle sizes employed in our study. Thus, the low-cost preparation method and high P adsorption capacity of these media suggest potential for field-scale applications, particularly Fe-PyOM due to its likely greater longevity and adsorption capacity.

Generally, agricultural drainage water is slightly acidic (pH 5.5 − 6.5), which enables a positive surface charge to develop of introduced iron hydro(oxide) surfaces and favouring P adsorption via electrostatic attraction [43]. The pH_{pzc} of Fe-PyOM (ca. pH 9) would thus ensure a consistently favourable condition for electrostatic attraction of phosphate anions. Whereas, the lower pH_{pzc} of Fe-WC (ca. pH 4.5) would appear to be incompatible with P adsorption under typical field conditions. Nevertheless, Fe−WC exhibited consistent P removal at pH > pH_{pzc}, indicating P adsorption via a non-electrostatic mechanism.

Removal of P was in fact observed for akaganeite, Fe−PyOM, and Fe−WC even at solution pH exceeding pH_{pzc} values, which we attribute to ligand−exchange, whereby the formation of inner−sphere complexes of bidentate and binuclear nature, occurs with protonated iron hydro (oxide) groups, with P replacing the hydroxyl groups present on the iron hydro(oxide) surface [36]. Conversely, when pH exceeds the pH_{pzc}, the formation of outer−sphere complexes is hindered, lowering overall adsorption capacity as observed here.

4.3. Bridging laboratory and field: further considerations for practical use

While Fe−PyOM media can remove P under flowing conditions via multi−layer adsorption, it remains to be determined whether Fe−PyOM can be feasibly used under low-DO (Dissolved Oxygen) conditions encountered in denitrifying bioreactors and under oscillating redox conditions. In bioreactors, oscillating redox conditions would be expected to lead to the release of P via dissolution of Fe oxides [45,56]. The challenge would therefore be to stabilise Fe-media, ensuring their longevity. As a solution, we concluded that positioning the Fe−impregnated materials closer to bioreactor inlets where higher DO conditions generally prevail, would minimize the dissolution of iron hydro(oxide)s, consistent with our recent work characterising these processes in a pilot-scale denitrifying bioreactor [45].

Considering the stability of iron oxides in aqueous environments, both low pH and low pe values are counterproductive to the addition Fe-biomedia in bioreactors, since these conditions favour Fe^{3+} reduction to soluble Fe^{2+}. Therefore, another viable strategy would be to buffer either pH or pe via the addition of basic (e.g. $CaCO_3$) or oxidising (e.g. MnO_2) minerals. For example, recent studies have used manganese oxide (MnO_2) as a substrate in constructed wetlands for the purpose of effective nitrogen removal [57], enabled by its relatively high redox potential (1.23 V) [58].

Another challenge is the presence of coexisting anions in agricultural drainage, mainly SO_4^{2-}, Cl^- and NO_3^- [59], which could compete with phosphorus for adsorption onto iron hydroxide surfaces [48]. However, slightly acidic conditions in agricultural drainage enable the surface of iron hydroxide particles to preferentially adsorb $H_2PO_4^-$ due to its higher surface surface reactivity over more hydrophilic ions, like SO_4^{2-}.

The issue of filter clogging has also been raised in studies investigating the use of FeOx-based sorbents for phosphorus removal. Clogging could be minimized by employing coarse particle fractions as demonstrated here and elsewhere [60], or by combining FeOx with another substrate [61], such as woodchips combined with Fe-PyOM.

Numerous factors must be taken into account when establishing filtration and treatment systems on farms, especially within bioreactors due to the varying solution properties and high turbidity [59]. These considerations include the P load expected in agricultural drainage, the adsorption capacity of the materials, the average hydraulic retention time, as well as handling procedures, and the maintenance of filter media. In the context of this study, the Fe-WC and Fe-PyOM composites demonstrate an adsorption capacity of 4.60 and 4.77 mg P g^{-1}, respectively, at the typical pH (pH 6) of agricultural drainage. If 50 kg of Fe-PyOM were to be incorporated into a 60 m^3 bioreactor, it is anticipated that the system could passively adsorb around 239 g P per flush, assuming an ambient P concentration of ~4 mg l^{-1}. As shown by our previous studies, P released by desorption would ultimately be expected to be biologically accumulated assuming a sufficiently long hydraulic retention. Thus, relatively small amounts of Fe-modified biomedia could potentially be employed in these systems with the aim of attenuating P relative to flow, thereby allowing enhanced retention and time for bioaccumulation.

Table 3
XRF analysis of the functionalized materials.

Sample Name	SiO_2 (%)	Al_2O_3 (%)	MnO (%)	Fe_2O_3 (%)	MgO (%)	CaO (%)	CO_2 (%)
Fe-WC	0.06	0.04	0.02	17.14	0.02	0.09	83.90
Fe-PyOM	0.08	0.04	0.01	20.27	0.09	0.23	81.11

5. Conclusions

Fe-functionalized bio-media were synthesized using readily available pine woodchips and a commercial byproduct of pyrolyzed woodchips. Iron coated woodchips and pyrolyzed woodchips demonstrated high P adsorption despite the use of larger particle sizes (2–3 mm) than typically employed in adsorption media, including adsorptive removal under flowing conditions. Adsorption was most favored under slightly acidic conditions, demonstrating a pronounced effect at pH 4 compared with pH 8, with adsorption increasing from 11 % to 37 % for Fe-WC and from 17 % to 30 % for Fe-PyOM, respectively. Ligand exchange with surface hydroxyl groups, the formation of Fe-O-P bonds, and pH-dependent surface chemisorption were systematically described, aided by the use of XPS. We suggest there is potential for Fe-based composites to be integrated within denitrifying bioreactors and other edge-of-field mitigations to increase P removal from drainage water. Future studies are required to evaluate their practical use in field trials.

Table 4
A comparison of the phosphate adsorption capacity of different Fe-based composite materials.

Description	Surface area (m^2 g^{-1})	Particle size (nm)	pH	pH_{pzc}	P adsorption capacity (mg g^{-1})	Reference
Magnetite/pyrite nanocomposite	–	–	3	6.7	24.8	[46]
Magnetite bio-activated carbon	520.2	0.6–5	7	–	21.2	[47]
Polyaminated Fe_3O_4 @ chitosan core-shell magnetic nanoparticles	74.7	11.1	4	10	50.8	[48]
Hydrous zirconia coated magnetite	–	10–50	6.2	–	32.3	[49]
			6.7–6.9		29.7	
Humic acid coated magnetite	–	–	6.6	–	28.9	[50]
Biochar coated magnetite	99.9	–	6.5	–	3.38	[51]
Ferrihydrite-coated lanthanum-decorated magnetite	85.8	–	6.7	–	44.8	[52]
Citric acid-coated magnetite	97.5	39.7	–	–	2.5	[53]
Magnetite modified tuff grains	49	13.5	4	–	1.9	[54]
Goethite coated kaolinite	39.6	-	5	6.1	75.1	[55]
Goethite kaolinite mixture	34.2	-	5	7.0	64.6	
Akaganeite	-	**69 μm**	**6.5**	**7.4**	**107**	**This study**
Fe-WC	-	**2–3 mm**	**6.5**	**4.5**	**65.8**	
Fe-PyOM	-	**2–3 mm**	**6.5**	**9.0**	**31.4**	

Author statement

The authors declare no competing interests or other factors that preclude publication according to the publishers standard conditions.

CRediT authorship contribution statement

Gimhani N. Perera: Writing – review & editing, Writing – original draft, Methodology, Formal analysis, Data curation, Conceptualization. **Dorisel Torres Rojas:** Writing – review & editing, Writing – original draft, Supervision, Formal analysis, Conceptualization. **Sebastian N Höpker:** Formal analysis. **Greg Olsen:** Supervision, Formal analysis. **Rupert Craggs:** Supervision, Funding acquisition. **Adam Hartland:** Writing – review & editing, Writing – original draft, Supervision, Project administration, Methodology, Funding acquisition, Conceptualization.

Declaration of competing interest

The authors declare the following financial interests/personal relationships which may be considered as potential competing interests:

Adam Hartland reports financial support was provided by Ministry of Business Innovation and Employment. If there are other authors, they declare that they have no known competing financial interests or personal relationships that could have appeared to influence the work reported in this paper.

Data availability

Data is provided in tables and supplement

Acknowledgements

Primary funding for this research was provided by the Ministry for Business Innovation and Employment (MBIE) under Contract No. C01 × 1818, wthrough the program "Te Waiora Joint Institute for Freshwater Management," a collaboration between the University of Waikato and NIWA. We would like to thank Ben Woodward (NIWA), Chris Tanner (NIWA) and Louis Schipper (University of Waikato) for assistance in project development, Annie Barker (University of Waikato) for help with laboratory analysis and Amir Mohammadi (University of Waikato) for guidance with laboratory work.

Supplementary materials

Supplementary material associated with this article can be found, in the online version, at doi:10.1016/j.surfin.2024.104566.

References

[1] L. Gosch, H. Liu, B. Lennartz, Performance of a woodchip bioreactor for the treatment of nitrate-laden agricultural drainage water in northeastern Germany, Environments. 7 (9) (2020).
[2] U. Thapa, L. Ahiablame, J. Kjaersgaard, C. Hay, Field evaluation of four denitrifying woodchip bioreactors for nitrogen removal in eastern South Dakota, United States, Sci. Total Environ 855 (2023) 158740, https://doi.org/10.1016/j.scitotenv.2022.158740.
[3] H.L Golterman, Natural phosphate sources in relation to phosphate budgets: a contribution to the understanding of eutrophication, in: S.H. Jenkins, K.J. Ives (Eds.), Phosphorus in Fresh Water and the Marine Environment, Pergamon, 1973, pp. 3–17, https://doi.org/10.1016/B978-0-08-017697-0.50006-7.
[4] L.E. Christianson, A. Bhandari, M.J. Helmers, Pilot-scale evaluation of denitrification drainage bioreactors: reactor geometry and performance, J. Environ. Eng 137 (4) (2011) 213–220, https://doi.org/10.1061/(ASCE)EE.1943-7870.0000316.
[5] C.M. Greenan, T.B. Moorman, T.B. Parkin, T.C. Kaspar, D.B. Jaynes, Denitrification in wood chip bioreactors at different water flows, J. Environ. Qual. 38 (4) (2009) 1664–1671, https://doi.org/10.2134/jeq2008.0413.
[6] W.D. Robertson, Nitrate removal rates in woodchip media of varying age, Ecol. Eng 36 (11) (2010) 1581–1587, https://doi.org/10.1016/j.ecoleng.2010.01.008.
[7] D.B. Jaynes, T.C. Kaspar, T.B. Moorman, T.B. Parkin, In situ bioreactors and deep drain-pipe installation to reduce nitrate losses in artificially drained fields, J. Environ. Qual. 37 (2) (2008) 429–436, https://doi.org/10.2134/jeq2007.0279.
[8] A.P. Sanchez Bustamante-Bailon, A. Margenot, R.A.C. Cooke, L.E Christianson, Phosphorus removal in denitrifying woodchip bioreactors varies by wood type and water chemistry, Environ. Sci. Pollut. Res. Int. 29 (5) (2022) 6733–6743, https://doi.org/10.1007/s11356-021-15835-w.
[9] M. Li, J. Liu, Y. Xu, G. Qian, Phosphate adsorption on metal oxides and metal hydroxides: a comparative review, Environ. Rev 24 (3) (2016) 319–332, https://doi.org/10.1139/er-2015-0080.
[10] R. Liu, L. Chi, X. Wang, Y. Sui, Y. Wang, H. Arandiyan, Review of metal (hydr)oxide and other adsorptive materials for phosphate removal from water, J. Environ. Chem. Eng. 6 (4) (2018) 5269–5286, https://doi.org/10.1016/j.jece.2018.08.008.
[11] A. Ashraf, G. Liu, M. Arif, M.M. Mian, A. Rashid, B. Yousaf, M.I. Khawar, L. Riaz, R. Safeer, Insights into the synthesis and application of biochar assisted graphene-based materials in antibiotic remediation, J. Clean Prod. 361 (2022) 132211.
[12] J. Fito, K.K. Kefeni, T.T. Nkambule, The potential of biochar-photocatalytic nanocomposites for removal of organic micropollutants from wastewater, Sci. Total Environ 829 (2022) 154648.
[13] N. Wang, J. Feng, J. Chen, J. Wang, W. Yan, Adsorption mechanism of phosphate by polyaniline/TiO2 composite from wastewater, Chem. Eng. J. 316 (2017) 33–40, https://doi.org/10.1016/j.cej.2017.01.066.
[14] M.K. Shahid, Y. Kim, Y.-G. Choi, Magnetite synthesis using iron oxide waste and its application for phosphate adsorption with column and batch reactors, Chem. Eng. Res. Des 148 (2019) 169–179, https://doi.org/10.1016/j.cherd.2019.06.001.
[15] S.-Y. Yoon, C.-G. Lee, J.-A. Park, J.-H. Kim, S.-B. Kim, S.-H. Lee, J.-W. Choi, Kinetic, equilibrium and thermodynamic studies for phosphate adsorption to magnetic iron oxide nanoparticles, Chem. Eng. J 236 (2014) 341–347, https://doi.org/10.1016/j.cej.2013.09.053.
[16] L. Zeng, X. Li, J. Liu, Adsorptive removal of phosphate from aqueous solutions using iron oxide tailings, Water Res. 38 (5) (2004) 1318–1326, https://doi.org/10.1016/j.watres.2003.12.009.
[17] R. Li, C. Kelly, R. Keegan, L. Xiao, L. Morrison, X. Zhan, Phosphorus removal from wastewater using natural pyrrhotite, Colloids Surf. A: Physicochem. Eng. Asp 427 (2013) 13–18, https://doi.org/10.1016/j.colsurfa.2013.02.066.

[18] S.J. Montalvo, L.E. Guerrero, Z. Milán, R. Borja, Nitrogen and phosphorus removal using a novel integrated system of natural zeolite and lime, J. Environ. Sci. Heal, Part A 46 (12) (2011) 1385–1391, https://doi.org/10.1080/10934529.2011.606709.
[19] N. Xie, L. Yi, J. Li, W. Wang, T. Gu, M.-G. Ma, S. Wang, S. Liu, A green synthesis strategy toward calcined calcium-aluminum layered double hydroxide with sludge as aluminum source for efficient removal of phosphate from water, Surf. Interf. 46 (2024) 104075, https://doi.org/10.1016/j.surfin.2024.104075.
[20] B. Sulzberger, D. Suter, C. Siffert, S. Banwart, W. Stumm, Dissolution of Fe(III) (Hydr)oxides in natural waters; laboratory assessment on the kinetics controlled by surface coordination, Mar. Chem. 28 (1) (1989) 127–144, https://doi.org/10.1016/0304-4203(89)90191-6.
[21] A. Rivas, R. Singh, D.J. Horne, J. Roygard, A. Matthews, M.J. Hedley, Contrasting subsurface denitrification characteristics under temperate pasture lands and its implications for nutrient management in agricultural catchments, J. Environ. Manage. 272 (2020) 111067, https://doi.org/10.1016/j.jenvman.2020.111067.
[22] M.R. Pelaez-Samaniego, V. Yadama, E. Lowell, R. Espinoza-Herrera, A review of wood thermal pretreatments to improve wood composite properties, Wood Sci. Technol. 47 (2013) 1285–1319.
[23] S.K. Ramasahayam, G. Gunawan, C. Finlay, T. Viswanathan, Renewable resource-based magnetic nanocomposites for removal and recovery of phosphorous from contaminated waters, Water, Air, Soil Pollut 223 (8) (2012) 4853–4863, https://doi.org/10.1007/s11270-012-1241-2.
[24] H. Dai, Y. Sun, D. Wan, H.N. Abbasi, Z. Guo, H. Geng, X. Wang, Y. Chen, Simultaneous denitrification and phosphorus removal: a review on the functional strains and activated sludge processes, Sci. Total Environ 835 (2022) 155409, https://doi.org/10.1016/j.scitotenv.2022.155409.
[25] E.N. Bakatula, D. Richard, C.M. Neculita, G.J. Zagury, Determination of point of zero charge of natural organic materials, Environ. Sci. Poll. Res 25 (8) (2018) 7823–7833, https://doi.org/10.1007/s11356-017-1115-7.
[26] J. Leveneur, G.I.N. Waterhouse, J. Kennedy, J.B. Metson, D.R.G. Mitchell, Nucleation and growth of Fe nanoparticles in SiO2: a TEM, XPS, and Fe ʟ-Edge XANES Investigation, J. Phys. Chem. C 115 (43) (2011) 20978–20985, https://doi.org/10.1021/jp206357c.
[27] S. Kalam, S.A. Abu-Khamsin, M.S. Kamal, S. Patil, Surfactant adsorption isotherms: a review, ACS. Omega 6 (48) (2021) 32342–32348, https://doi.org/10.1021/acsomega.1c04661.
[28] K.L. Sharrer, L.E. Christianson, C. Lepine, S.T. Summerfelt, Modeling and mitigation of denitrification 'woodchip' bioreactor phosphorus releases during treatment of aquaculture wastewater, Ecol. Eng 93 (2016) 135–143, https://doi.org/10.1016/j.ecoleng.2016.05.019.
[29] C. Chizallet, G. Costentin, M. Che, F. Delbecq, P. Sautet, Infrared characterization of hydroxyl groups on MgO: a periodic and cluster density functional theory study, J. Am. Chem. Soc. 129 (20) (2007) 6442–6452.
[30] K. Hadjiivanov, Identification and characterization of surface hydroxyl groups by infrared spectroscopy, in: Advances in Catalysis, 57, Elsevier, 2014, pp. 99–318.
[31] G. Richmond, Molecular bonding and interactions at aqueous surfaces as probed by vibrational sum frequency spectroscopy, Chem. Rev. 102 (8) (2002) 2693–2724.
[32] M.G.N. Perera, Y.R. Galagedara, Y. Ren, M. Jayaweera, Y. Zhao, R. Weerasooriya, Fabrication of fullerenol-incorporated thin-film nanocomposite forward osmosis membranes for improved desalination performances, J. Poly. Res. 25 (9) (2018) 199, https://doi.org/10.1007/s10965-018-1593-4.
[33] H. Fu, X. Quan, Complexes of fulvic acid on the surface of hematite, goethite, and akaganeite: FTIR observation, Chemosphere 63 (3) (2006) 403–410, https://doi.org/10.1016/j.chemosphere.2005.08.054.
[34] E.A. Deliyanni, E.N. Peleka, N.K. Lazaridis, Comparative study of phosphates removal from aqueous solutions by nanocrystalline akaganéite and hybrid surfactant-akaganéite, Sep. Purif. Technol. 52 (3) (2007) 478–486, https://doi.org/10.1016/j.seppur.2006.05.028.
[35] K.-H. Kim, K.-Y. Lee, H.-J. Kim, E. Cho, S.-Y. Lee, T.-H. Lim, S.P. Yoon, I.C. Hwang, J.H. Jang, The effects of Nafion® ionomer content in PEMFC MEAs prepared by a catalyst-coated membrane (CCM) spraying method, Int. J. Hydro. Ener 35 (5) (2010) 2119–2126, https://doi.org/10.1016/j.ijhydene.2009.11.058.
[36] A.G. Karunanayake, C.M. Navarathna, S.R. Gunatilake, M. Crowley, R. Anderson, D. Mohan, F. Perez, C.U. Pittman Jr., T Mlsna, Fe3O4 Nanoparticles dispersed on douglas fir biochar for phosphate sorption, ACS. Appl. Nano Mater. 2 (6) (2019) 3467–3479, https://doi.org/10.1021/acsanm.9b00430.
[37] X. Xu, A. Schierz, N. Xu, X. Cao, Comparison of the characteristics and mechanisms of Hg(II) sorption by biochars and activated carbon, J. Colloid Interf. Sci. 463 (2016) 55–60, https://doi.org/10.1016/j.jcis.2015.10.003.
[38] W. Ma, Y. Zhang, Y. Li, Y. Wang, R. Sun, Y. Wu, C. Han, The formation of uniform straw-like β-FeOOH nanostructures with superior catalytic performance for the degradation of Rhodamine B, J. Nanopar. Res 23 (1) (2021) 19, https://doi.org/10.1007/s11051-020-05116-x.
[39] Y.-X. Zhang, Y. Jia, A facile solution approach for the synthesis of akaganéite (β-FeOOH) nanorods and their ion-exchange mechanism toward As(V) ions, Appl. Surf. Sci. 290 (2014) 102–106, https://doi.org/10.1016/j.apsusc.2013.11.007.
[40] A.M. Pintor, B.R. Vieira, C.C. Brandao, R.A. Boaventura, C.M. Botelho, Complexation mechanisms in arsenic and phosphorus adsorption onto iron-coated cork granulates, J. Environ. Chem. Eng. 8 (5) (2020) 104184.
[41] Q. Wang, Z. Liao, D. Yao, Z. Yang, Y. Wu, C. Tang, Phosphorus immobilization in water and sediment using iron-based materials: a review, Sci. Total Environ 767 (2021) 144246.
[42] D.A. Almasri, N.B. Saleh, M.A. Atieh, G. McKay, S. Ahzi, Adsorption of phosphate on iron oxide doped halloysite nanotubes, Sci. Rep. 9 (1) (2019) 3232, https://doi.org/10.1038/s41598-019-39035-2.
[43] T. Daou, S. Begin-Colin, J.-M. Greneche, F. Thomas, A. Derory, P. Bernhardt, P. Legaré, G. Pourroy, Phosphate adsorption properties of magnetite-based nanoparticles, Chem. Mater 19 (18) (2007) 4494–4505.
[44] Z. Zhang, H. Yu, R. Zhu, X. Zhang, L. Yan, Phosphate adsorption performance and mechanisms by nanoporous biochar–iron oxides from aqueous solutions, Environ. Sci. Pollut. Res 27 (22) (2020) 28132–28145.
[45] G.N. Perera, D.T. Rojas, A. Rivas, G. Barkle, B. Moorhead, L.A. Schipper, R. Craggs, A. Hartland, Elucidating phosphorus removal dynamics in a denitrifying woodchip bioreactor, Sci. Total Environ 917 (2024) 170478, https://doi.org/10.1016/j.scitotenv.2024.170478.
[46] W. Cai, F. Fu, L. Zhu, B. Tang, Simultaneous removal of chromium(VI) and phosphate from water using easily separable magnetite/pyrite nanocomposite, J. Alloys Compd. 803 (2019) 118–125, https://doi.org/10.1016/j.jallcom.2019.06.285.
[47] T. Han, X. Lu, Y. Sun, J. Jiang, W. Yang, P.G. Jönsson, Magnetic bio-activated carbon production from lignin via a streamlined process and its use in phosphate removal from aqueous solutions, Sci. Total Environ 708 (2020) 135069, https://doi.org/10.1016/j.scitotenv.2019.135069.
[48] C.-C. Fu, H.N. Tran, X.-H. Chen, R.-S. Juang, Preparation of polyaminated Fe3O4@chitosan core-shell magnetic nanoparticles for efficient adsorption of phosphate in aqueous solutions, J. Indus. Eng. Chem. 83 (2020) 235–246, https://doi.org/10.1016/j.jiec.2019.11.033.
[49] W. Fang, Z. Wang, Q. Xie, Y. Liu, D. Wu, Formation of Fe3O4@ZrO2 nanocomposite and its performance as a magnetic adsorbent for phosphate uptake: influences of end-point pH and stirring rate during synthesis process, Chem. Eng. Res. Des 145 (2019) 194–202, https://doi.org/10.1016/j.cherd.2019.03.013.
[50] M. Rashid, N.T. Price, M.Á. Gracia Pinilla, K.E O'Shea, Effective removal of phosphate from aqueous solution using humic acid coated magnetite nanoparticles, Water Res. 123 (2017) 353–360, https://doi.org/10.1016/j.watres.2017.06.085.
[51] M. Riddle, H. Cederlund, F. Schmieder, L. Bergström, Magnetite-coated biochar as a soil phosphate filter: from laboratory to field lysimeter, Geoderma 327 (2018) 45–54, https://doi.org/10.1016/j.geoderma.2018.04.025.
[52] H. Fu, Y. Yang, R. Zhu, J. Liu, M. Usman, Q. Chen, H. He, Superior adsorption of phosphate by ferrihydrite-coated and lanthanum-decorated magnetite, J. Colloid Interf. Sci. 530 (2018) 704–713, https://doi.org/10.1016/j.jcis.2018.07.025.
[53] Z. Yu, C. Zhang, Z. Zheng, L. Hu, X. Li, Z. Yang, C. Ma, G. Zeng, Enhancing phosphate adsorption capacity of SDS-based magnetite by surface modification of citric acid, Appl. Surf. Sci. 403 (2017) 413–425, https://doi.org/10.1016/j.apsusc.2017.01.163.
[54] A.B. Savić, D. Čokeša, M. Savić Biserčić, I. Častvan-Janković, R. Petrović, L. S. Živković, Multifunctional use of magnetite-coated tuff grains in water treatment: removal of arsenates and phosphates, Adv. Pow. Technol. 30 (8) (2019) 1687–1695, https://doi.org/10.1016/j.apt.2019.05.020.
[55] S. Wei, W. Tan, F. Liu, W. Zhao, L. Weng, Surface properties and phosphate adsorption of binary systems containing goethite and kaolinite, Geoderma 213 (2014) 478–484, https://doi.org/10.1016/j.geoderma.2013.09.001.
[56] G. Ross, F. Haghseresht, T.E. Cloete, The effect of pH and anoxia on the performance of Phoslock®, a phosphorus binding clay, Harmf. Algae 7 (4) (2008) 545–550, https://doi.org/10.1016/j.hal.2007.12.007.
[57] C. Cheng, Q. He, J. Zhang, H. Chai, Y. Yang, S.G. Pavlostathis, H. Wu, New insight into ammonium oxidation processes and mechanisms mediated by manganese oxide in constructed wetlands, Water Res. 215 (2022) 118251, https://doi.org/10.1016/j.watres.2022.118251.
[58] W. Liu, N.B. Sutton, H.H.M. Rijnaarts, A.A.M. Langenhoff, Pharmaceutical removal from water with iron- or manganese-based technologies: a review, Crit. Rev. Environ. Sci. Technol. 46 (19–20) (2016) 1584–1621, https://doi.org/10.1080/10643389.2016.1251236.
[59] A. Rivas, G. Barkle, R. Stenger, B. Moorhead, J. Clague, Nitrate removal and secondary effects of a woodchip bioreactor for the treatment of subsurface drainage with dynamic flows under pastoral agriculture, Ecol. Eng 148 (2020) 105786, https://doi.org/10.1016/j.ecoleng.2020.105786.
[60] C.S. Dunets, Y. Zheng, M. Dixon, Use of phosphorus-sorbing materials to remove phosphate from greenhouse wastewater, Environ. Technol. 36 (14) (2015) 1759–1770, https://doi.org/10.1080/09593330.2015.1009497.
[61] S.A. White, W.H.J. Strosnider, M.E.M. Chase, M.A. Schlautman, Removal and reuse of phosphorus from plant nursery irrigation return water with reclaimed iron oxides, Ecol. Eng 160 (2021) 106153, https://doi.org/10.1016/j.ecoleng.2021.106153.

Chapter 5. Phosphorus removal by iron oxides in lab-scale denitrifying woodchip bioreactors with and without manganese dioxide

Gimhani N Perera [a], Dorisel Torres Rojas [a], Adam Hartland [a,b*]

[a]Environmental Research Institute, School of Science, Faculty of Science and Engineering, University of Waikato, Kirikirioa Hamilton, New Zealand.

[b]Lincoln Agritech Ltd, Ruakura, Kirikirioa Hamilton 3214.

[*] Corresponding author. Email: adam.hartland@waikato.ac.nz

Abstract

In freshwater systems, sedimentary iron oxides facilitate phosphorus (P) removal via surface adsorption reactions, but also release P under anaerobic conditions, due to reductive dissolution of Fe(III) to Fe(II) coupled to microbial biomass oxidation. Denitrifying bioreactors (DBRs) are predominantly anaerobic systems, but redox gradients from oxic to sulfidic are common. Dynamic oscillations in redox potential in DBRs occur in response to varying flow and nutrient loads, leading to consumption of a range of electron acceptors including O_2, N(V), Mn(IV), Fe(III) and S(VI), in order of reactivity. This study investigates whether iron-facilitated phosphorus removal can be harnessed within DBRs, and whether the prevailing oxidation and reduction conditions can be buffered by MnO_x thereby allowing the preservation of FeO_x adsorbents. Three treatments were tested in duplicated bench-scale experiments (wood only, wood+FeO_x, and wood+FeO_x+MnO_2) to establish the potential for redox buffering and simultaneous P removal under reducing conditions. Average nitrate and phosphate removal efficiencies were 16.1 ± 13.2%, 71.4 ± 26.7%, and 85.9 ± 5.27 % for NO_3^-, and 0%, 95.5 ± 1.92% and 96.3 ± 0.8%, respectively for wood only, wood+FeO_x, and wood+FeO_x+MnO_2 treatments. In addition to removing the majority of dissolved P, the FeO_x treatments also had

significantly lower dissolved organic matter although this did not noticeably inhibit nitrate removal. Overall, MnO_2 appeared to partially enhance FeO_x stability while substantially enhancing denitrification. Hence, FeO_x and MnO_2 are potentially effective amendments for enhancing DBR efficiency and function.

KEYWORDS; denitrifying woodchip bioreactors, Iron oxides, Manganese oxides, Phosphorus removal, nitrification

Graphical Abstract

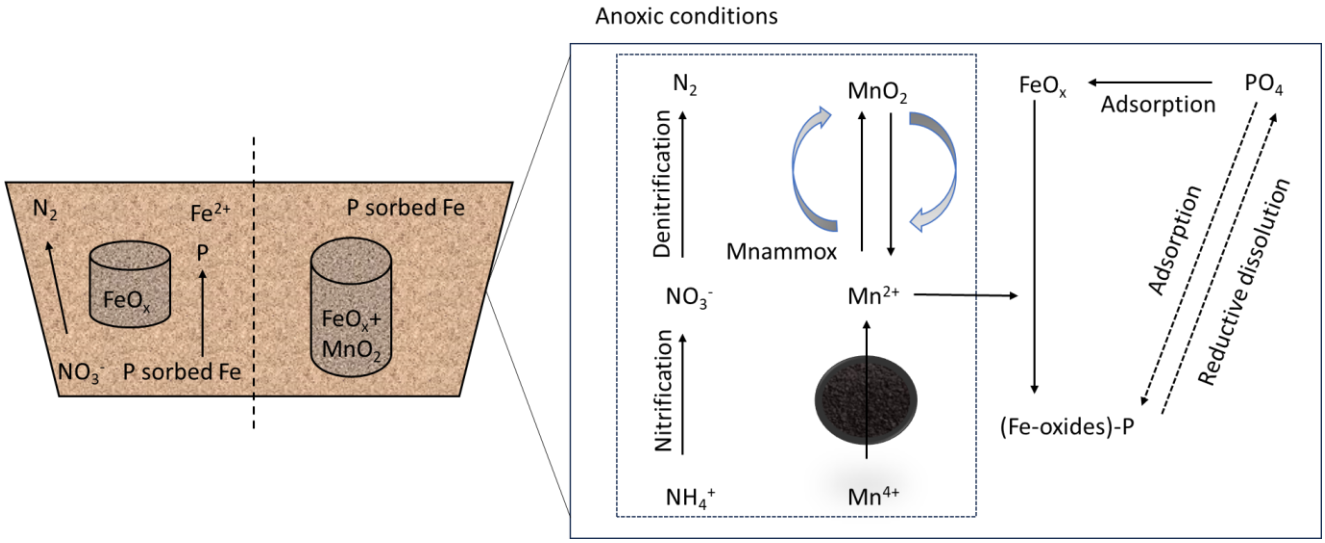

5.1 Introduction

Denitrifying woodchip bioreactors (DBRs) have gained widespread recognition as an emerging technology for the removal of nitrate from agricultural drainage water, primarily due to their cost-effective operation, practicality, and environmentally friendly approach (Dougherty et al., 2020; Greenan et al., 2009; Lepine et al., 2018; Schipper et al., 2010). Pollutants within bioreactors can be eliminated through a combination of physical and biochemical processes,

primarily driven by microbes under varying oxic and anoxic conditions (Christianson et al., 2011; Rivas et al., 2020; Sanchez Bustamante-Bailon et al., 2022).

In DBRs, a series of redox reactions take place when oxygen is limited. Primarily, microorganisms gain energy through respiration by mediating redox reactions between an electron donor and an electron acceptor. Once oxygen is depleted, nitrate becomes the preferable electron acceptor, subsequently followed by dissimilatory reduction of manganese, iron, and sulfate in the anaerobic, carbon-rich DBR environment (McMahon & Chapelle, 2008). In addition to nitrate removal, it is worth emphasizing that DBRs can also demonstrate a certain degree of phosphorus removal. As described in Chapter 3 of this thesis, this capability is likely affected by a combination of chemical and biological factors and is probably limited by a low bioavailable P supply in contrast to NO_3^-.

The use of iron (hydr)oxides to capture P from water has been widely studied (Li et al., 2016; Weng et al., 2012; Zeng et al., 2004), with methods of P capture largely mimicking the natural processes of adsorption and chemical precipitation, owing to their environmental compatibility, cost efficiency, and flexibility (Liu et al., 2018). Nevertheless, the stability of these materials under real-world conditions has not been thoroughly examined (Hua et al., 2016) and studies are typically do not consider the effects of oscillating redox conditions. In this regard, the reductive dissolution of P-sorbing Fe hydr(oxides) is a key factor controlling the release of phosphorus in aqueous environments (Colombo et al., 2014; Smith et al., 2023), with substantial P releases coincident with iron-reducing conditions in saturated soils and sediments (Smith et al. 2021; Hartland et al., 2015; Saeed et al., 2018).

In principle, iron reduction can be inhibited by an excess of oxidants with higher redox potentials. The concept of redox buffering, first observed and characterized in marine sediment studies (Berner, 1971), has only recently been explored in ecological engineering applications.

Recent studies have explored the introduction of manganese oxides in constructed wetlands (CWs), and reported significant enhancement of water quality and reductions in greenhouse gas emissions, through participation of Mn in nitrification and redox buffering (Cheng et al., 2022; Cheng et al., 2021; Yang et al., 2019). Hence, iron and manganese oxides may be highly compatible in DBRs due to their similar redox phases and potentials: MnO_2 (s) is a strong oxidizing agent with a high redox potential of 1.23 V, whereas $Fe(OH)_3$ (s) has a lower redox potential of 0.67 V (Ding et al., 2015). Because Mn is less abundant in earth materials compared to Fe, it is rarely the superior electron acceptor under natural conditions in terms of mass (Schippers & Jørgensen, 2002). Therefore, its ratio to Fe needs to be artificially increased in engineered contexts to achieve a redox buffering affect (Cheng et al., 2022).

In previous chapters, the characterization of iron hydr(oxide) impregnated woodchips and pyrolyzed wood for the purpose of P removal in DBRs was introduced. Because prevalent reducing conditions in DBRs will inevitably affect iron hydr(oxide) solubility, this study was designed to investigate whether MnO_2 could buffer redox potential and suppress the reductive dissolution of iron oxide, thereby enhancing DRP retention on introduced Fe oxide surfaces.

5.2 Materials and methods

5.2.1 Mesocosm experimental design

A mesocosm bioreactor study was conducted to investigate the potential of manganese oxides to stabilize iron oxide under conditions comparable to denitrifying bioreactors experiencing variable NO_3^- supply. Three treatment reactors were established in duplicate: Wood-only, Wood+FeOx, and Wood+FeO_x+MnO_2 (Fig. 5.1). The wood treatment formed the control, while the Wood+FeOx, and Wood+FeO_x+MnO_2 treatments assessed the dissolution of iron and, consequently, the removal of phosphorus, with and without the presence of MnO_2.

The wood only treatment consisted of 400 g of wood, while the Wood+FeO_x treatment consisted of 400 g of wood and 40 g of FeO_x-impregnated PyOM (synthesis procedure was in chapter 4). The Wood+FeO_x+MnO_2 treatment included 400 g of wood, 40 g of FeO_x-impregnated PyOM, and 10 g of MnO_2-impregnated PyOM (hereafter referred to as FeOx and MnO_2). The MnO_x was synthesized for the bioreactor project and was confirmed by various characterization techniques. The FeO_x and MnO_2 materials used were functionalized in the laboratory using pyrolyzed PyOM as the substrate. The methodology for FeO_x synthesis is described in Chapter 4. All the reactors were filled with 1.5 L of nutrient solution to saturate the materials and incubated and inoculated with 1 mL of outlet effluent from the Tatuanui bioreactor for 5 days to facilitate the growth of microbes. The composition of nutrient-enriched bioreactor water was as follows: Na 145 mg L^{-1}, Mg 28.2 mg L^{-1}, K 50 mg L^{-1}, Ca 58.4 mg L^{-1}, Fe 4.28 mg L^{-1}, P 84.5 mg L^{-1}, SO_4 21.2 mg L^{-1}. The experiment was conducted in hermetically-sealed, oxygen-free 2000 mL PFA (perfluoroalkoxy) jars equipped with screw lids with two 1/4" ports for reactor spiking and aliquot removal (Savillex, USA). The reactors were designed to replicate as close as possible, the actual conditions within DBRs, and PFA was specifically selected to inhibit losses of solutes to the reactor walls, thereby providing assurance that changes in solution composition related mainly to biogeochemical processes in question, rather than adsorptive loss of dissolved ions.

5.2.2 Water sampling and analysis

This experiment was conducted over a period of approximately two months, running from December 2021 to mid-January 2022. Following pre-conditioning, the experiment was divided into five stages. Each stage involved the introduction of a nitrate spike into the system every five days (120 hours). Nitrate was added to each spike in the reactor based on a daily nitrate

requirement of 155 mg, determined in a pre-experimental trial which characterized the average nitrate removal rate. Consequently, 776 mg of nitrate was added to every reactor in each spike. After each spike, samples were collected at 0.5, 1, 2, 4, 8, 12, 24, 48, and 96-hour intervals. To further minimise the potential for oxidation, the reactors were placed in an oxygen-free environment under a nitrogen (N_2) atmosphere, and samples were collected using a three-way valve to prevent exposure to oxygen (Fig. 5.1). After collection, the samples were filtered using 0.45 μm syringe filters (Sartorius Stedim, Germany) and stored in sealed tubes at -5°C until analysis. Total organic carbon (TOC) was measured using an OI Analytical Aurora 1030W TOC analyzer (Washington, USA). Nitrate (NO_3^-), sulfate (SO_4^{2-}), Phosphate (PO_4^{3-}) and chloride (Cl^-) were analyzed using an ICS-2000 Ion Chromatograph from Thermo Fisher (Brdjanovic et al.) employing an isocratic method (5 mM KOH, 40 minutes). Metals (total iron [Fe], manganese [Mn^{2+}]) were determined through inductively coupled plasma mass spectrometry (ICP-MS), using an Agilent 8900 ICP-MS (United States) controlled by MassHunter Workstation Version 4.5 and connected to an SPS4 autosampler (Mohammadi et al., 2022). Instrumental limits of quantification (LOQs) were 0.1 μg L^{-1} (Fe and Mn) and 0.1 mg L^{-1} (NO_3^-, SO_4^{2-}, PO_4^{3-} and SO_4^{2-}). Each data point was accompanied by a calibration curve consisting of five data points for both metals and anions.

5.2.3 Data analysis

Statistical analysis was performed using SPSS 25.0 software, consisting of the analysis of variance (ANOVA) post-hoc tests (Tukey's Honestly Significant Difference) to determine whether there was a significant difference between treatments. Correlation matrices were used to evaluate significant differences ($P < 0.05$) between treatments. Pearson correlation was conducted to assess whether there is a linear relationship between samples and to determine

the nature of the relationship, whether it is positive or negative, between the variables. The average of the duplicate treatments was used for the statistical analysis.

Figure 5. 1. Illustration of the experimental set up

5.3 Results

5.3.1 Variations in redox sensitive analytes

In Fig. 5.2, the concentrations of nitrate (NO_3^-), Mn and Fe over the course of the experiments are shown. Nitrate oscillations reflect the introduction of the NO_3^- spike followed by its removal by denitrification. Mn and Fe concentrations on the other hand reflect the generation of Mn^{2+} and Fe^{2+} ions by reductive dissolution, and hence increases in Fe and Mn concentration are interpreted to reflect the progression of dissimilatory MnO_2 and FeO_x dissolution, respectively. Whereas, lowering of NO_3^- concentration is interpreted as reflective of denitrification of NO_3^- to $N_2(g)$. Consequently, the concentration dynamics of these components differ markedly: NO_3^- generally showed rapid increases in concentration following each spike, followed by (more or less) exponential declines in concentration during the phase of denitrification.

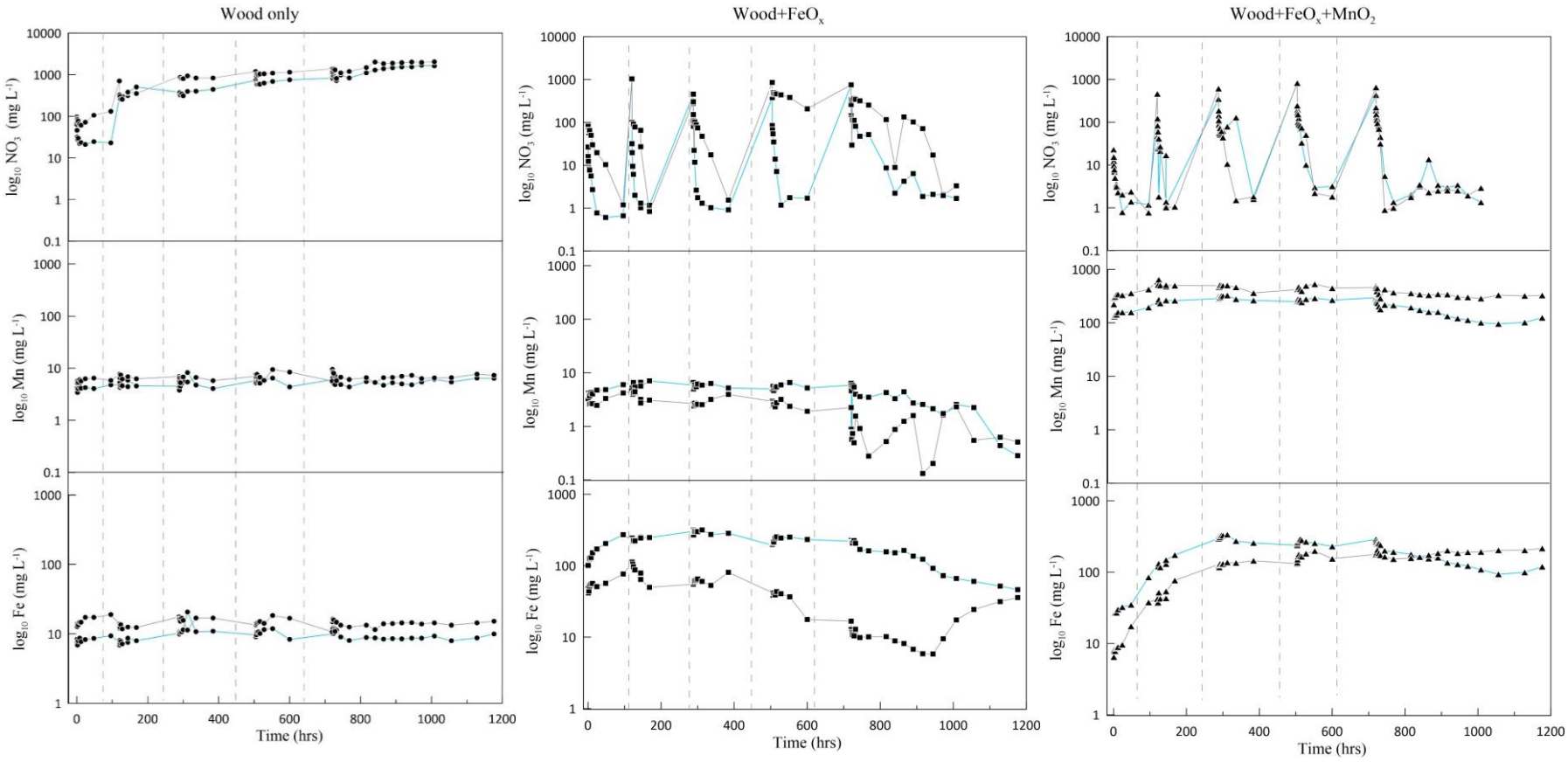

Figure 5. 2. Variations in the major electron acceptors NO_3^-, Fe and Mn concentrations in the Wood only (control), Wood+FeO_x and Wood+FeO_x+MnO_2 treatments (duplicate treatments). Note that Fe and Mn concentrations mainly reflect generation of Fe^{2+} and Mn^{2+} (products of reduction) whereas NO_3^- is the reactant in the corresponding carbon oxidation reaction.

In the wood-only treatment, NO_3^- concentrations varied within each spike, but exhibited an overall rising trend, starting from concentrations around 20 mg L^{-1} and reaching 2000 mg L^{-1}. In contrast, NO_3^- concentrations in the wood+FeO_x treatment exhibited dynamic oscillations following the introduction of each NO_3^- spike, rapidly declining to baseline concentrations between 0.6 to 0.8 mg L^{-1}. Similarly, NO_3^- concentrations in the wood+FeO_x+MnO_2 treatment also showed rapid and nearly complete NO_3^- losses, with concentrations declining rapidly to approximately 0 to 0.8 mg L^{-1}.

For each spike the % NO_3^- removal was calculated based on the initial NO_3^- solution concentration of each reactor following spike addition. Average removal efficiencies for the wood-only, wood+FeO_x and, wood+FeO_x+MnO_2 treatments were 16.1 ± 13.2 %, 71.4 ± 26.7 % and 85.9 ± 5.27 % respectively. In the wood treatment, nitrate was initially removed by up to 70%, but showed declining efficiency over time, resulting in the accumulation of nitrate over the course of the experiment. Higher nitrate removal efficiencies were observed in both wood+FeO_x and wood+FeO_x+MnO_2 treatments, in which up to 100% of the NO_3^- spike was removed. However, NO_3^- removal was less consistent in the wood+FeOx treatments, with NO_3^- removal efficiency being less than 50% in spikes 1 to 4, suggesting a less chemically reducing environment, compared to the wood+FeO_x+MnO_2 treatments.

In the wood+FeO_x+MnO_2 treatments, the Mn concentration ranged from 96 to 640 mg L^{-1}, showing an overall increasing trend prior to each NO_3 spike, but decreasing in the final stage, with variations in magnitude between the two replicates. For example, in one of the wood+FeO_x+MnO_2 treatments, Mn concentration continuously increased from 126 to 325 mg L^{-1} in a typical cycle, while in another case, it initially declined from 276 to 96 mg L^{-1}, only to then rise to 124 mg L^{-1}. This suggests that Mn played a role in maintaining the redox state in these treatments to some extent by dissolving Mn and preventing Fe dissolution. In contrast, Mn and Fe concentrations remained relatively constant in the wood-only treatment, with minor

fluctuations. The differences in magnitude within the treatments may be attributed to variations in the surface functionalization of biochar with manganese. The biochar used in our experiment had a particle size of 2-3 mm and was morphologically heterogeneous, resulting in differing surface areas, even though we used the same quantities for both wood+FeO_x+MnO_2 treatments.

Concentrations of iron provide indicative evidence for the progression of less energetic redox reactions in which Fe is cycled between insoluble (Fe^{3+}) and soluble (Fe^{2+}) oxidation states within the bioreactors (Fig. 5.2). In the wood+FeO_x treatment, apparent dissolution of Fe was observed following peak nitrate removal, showing consistent declines in concentration at each NO_3^- spike. Dissolved Fe concentrations reached up to 120 mg L^{-1} between NO_3^- spike 1 and 2, after which the Fe concentration declined and remained fairly constant at around 40 mg L^{-1}. Unsurprisingly, dissolved iron concentrations were lowest in the wood-only treatment, consistent with the lower background Fe concentration of the nutrient solution (6.90 – 20.7 mg L^{-1}). But nevertheless, Fe still showed a pattern of oscillation in the wood-only treatments from lower-to-higher concentrations following each spike, indicative of biogeochemical Fe cycling associated with NO_3^- additions.

Contrastingly, in the wood+FeO_x+MnO_2 treatment, Fe dissolution (concentration increases) were observed following spikes 1, 2, and 3, then steadily declining in spikes 4 and 5, while exhibiting temporary increases superimposed on the overall lowering trend. In the wood+FeO_x+MnO_2 treatment, Fe dissolution occurred following spikes 1 and 2, with an overall lowering of concentration in spikes 3, 4, and 5, again with excursions to higher concentrations that were subordinate to the overall lowering trend.

5.3.2 Variations in components with an affinity for adsorption to Fe oxides

As previously introduced, phosphorus has a high affinity for adsorption to iron oxides at the circumneutral to slightly acidic pH values typical of bioreactors. The polyanionic nature of dissolved organic carbon (DOC) also confers an affinity for adsorption and sequestration in Fe oxides (Wen et al., 2023). In Fig. 5.3, the concentrations of Fe, P and TOC are displayed for the duplicate reactors over the time span of this study.

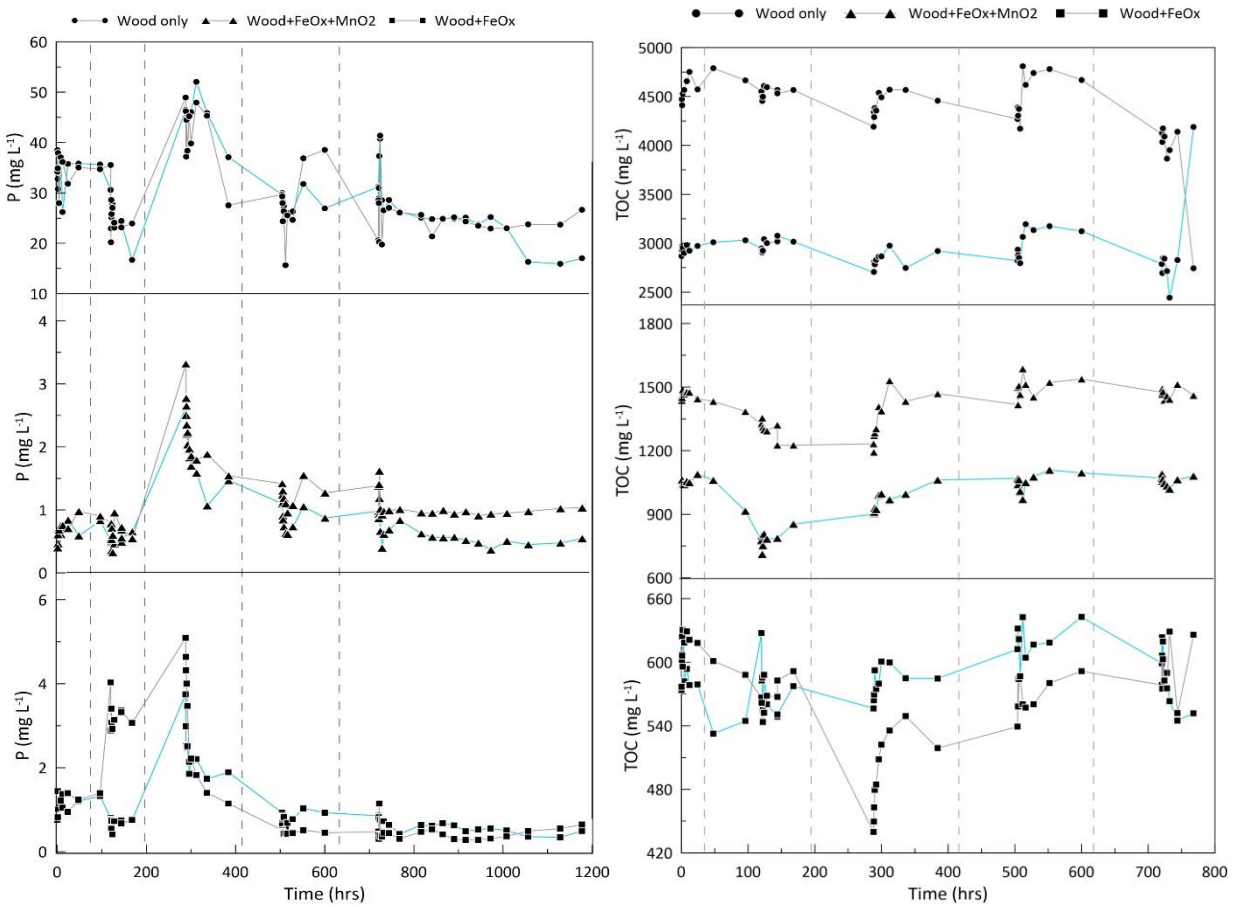

Figure 5. 3. Phosphorus(P) and TOC concentrations over time in the wood only, wood+FeO_x only and, wood+FeO_x+MnO_2 reactor treatments.

As shown in Fig. 5.3, Fe concentrations were an order of magnitude higher in the Fe-containing treatments than the wood-only treatment. But overall, Fe concentrations were comparable in both wood+FeO_x and wood+FeO_x+MnO_2 treatments, reaching a concentration maximum around 350 mg L^{-1}. While the total degree of Fe dissolution appears comparable between treatments with and without MnO_2, the latter exhibited more gradual Fe increases compared to the wood+FeO_x treatment.

Evidence for the continued presence and survival of Fe oxides is seen in the P and TOC data, which showed marked differences in concentration between the wood-only control and the mineral-amended treatments (Fig. 5.3). Both P and TOC concentrations were highest in the wood-only controls. In the controls, P and TOC were an order-of-magnitude higher than the FeO_x containing treatments. P concentrations were similar in the wood+FeO_x+MnO_2 and wood+FeO_x treatments (declining to < 1 mg L^{-1} in the later stages of spike 5), but TOC concentrations differed significantly, being lowest in the wood+FeO_x reactors.

Organic matter produced within the denitrifying bioreactors is typically removed through chemical, physical and biological processes depending on the denitrification rate. But the introduction of metal oxides in these experiments drastically reduced the concentration of TOC in solution. The average TOC generated in the wood only treatment ranged from 2900 to 4400 mg L^{-1}. TOC dynamics within the wood-only reactors showed the effect of NO_3^- additions, showing corresponding declines in TOC following NO_3^- addition and subsequent partial or complete recovery in TOC concentration as NO_3^- was consumed. Compared with the wood only treatment, TOC was significantly lower in the wood+FeO_x+MnO_2 treatments (710 – 1585 mg L^{-1}), and lower still in the wood+FeO_x treatments (440 – 640 mg L^{-1}) ($p < 0.05$).

Table 5. 1 Average pH and solute concentrations of the experimental bioreactors. All the data are given as average ± standard deviation.

Parameter	Wood only	Wood+FeO_x only	Wood+FeO_x+MnO_2
pH	3.72 ± 0.21	5.23 ± 0.14	6.56 ± 0.28
Fe (mg L^{-1})	12.0 ± 3.16	123 ± 95.8	156 ± 89.4
Mn (mg L^{-1})	5.93 ± 1.23	3.50 ± 1.91	319 ± 124
TP (mg L^{-1})	30.4 ± 2.5	1.25 ± 0.53	1.03 ± 0.22
TP Removal efficiency (%)	–	95.5 ± 1.92	96.3 ± 0.78
TOC (mg L^{-1})	3660 ± 1054	577 ± 32.3	1196 ± 306
NO_3-N (mg L^{-1})	730 ± 214	139 ± 97.9	82.7 ± 22.0
NO_3-N Removal efficiency (%)	16.1 ± 13.2	71.4 ± 26.7	85.9 ± 5.27

In the wood-only treatments, P fluctuated within the range of 10–50 mg L^{-1}. Despite the dissolution of Fe and the leaching of P, significantly higher degrees of P removal were evident in both the wood+FeO_x-only (0.28 – 5.09 mg L^{-1}, $p < 0.05$) and wood+FeO_x+MnO_2 (0.32 – 3.32 mg L^{-1}, $p < 0.05$) treatments. The average P concentrations in the wood-only, wood+FeO_x-only, and wood+FeO_x+MnO_2 treatments were 30.4 ± 2.5 mg L^{-1}, 1.25 ± 0.53 mg L^{-1} and 1.03 ± 0.22 mg L^{-1}, respectively (Table 1). The assembled data in totality suggest that the addition of iron and manganese oxides could potentially improve DBR performance overall, both through higher rates of denitrification and P removal efficiency (Table 5.1).

5.4 Discussion

5.4.1 Nitrate removal in pre-conditioned mesocosm reactors

Denitrifying woodchip bioreactors are engineered for the purpose of accelerating the microbiological denitrification process. This process involves transforming dissolved nitrate in water into gaseous nitrogen, as it flows through the bioreactors. When dissolved oxygen is limited, a diverse range of anaerobic denitrifying bacteria can effectively use NO_3^- as a terminal electron acceptor during the decomposition of organic substances (Aalto et al., 2020). The primary material in bioreactors is wood chips, which serve as both a growth surface and a carbon source, promoting denitrification by facilitating biofilm formation (Abusallout & Hua,

2017). However, many factors have the potential to influence the denitrification performance of woodchip bioreactors including dissolved oxygen concentrations, nitrate loading, hydraulic retention time, and carbon availability. In this study, although the wood-only treatment is not limited by either nitrogen (range 20 – 2000 mg L^{-1}) or carbon (TOC is around 2400 – 4800 mg L^{-1}), in-situ microbes were unable to remove nitrate effectively from the nitrate spikes.

The introduction of nitrate led to the accumulation of nitrate in the wood-only treatments. This suggests that the denitrifying bacteria present in the wood-only treatment did not efficiently remove nitrate, while FeO_x and MnO_2 additions evidently enhanced microbial activity, leading to increased nitrate removal. Hence, the addition of either/both manganese oxide and iron oxide significantly improved the efficiency of NO_3^- removal ($p < 0.05$), with manganese oxide showing a slightly better performance than iron oxide in experimental stages. These findings align well with previously reported studies that have investigated the impact of MnO_2 and FeO_x on NO_3^- removal (Cheng et al., 2022; Cheng et al., 2021). Interestingly, the reduction in DOC in both the wood+FeO_x and wood+FeO_x+MnO_2 treatments did not seem to impact the nitrate removal efficiency. This suggests that the introduction of FeO_x and MnO_2 could serve as a viable option to enhance nutrient removal in bioreactors.

The NO_3^- removal rate in wood+FeO_x+MnO_2 treatments followed the general pattern of Fe and Mn dissolution following peak NO_3^- removal, indicating that secondary dissimilatory redox reactions between Mn(IV) and Fe(III) oxides contributed to organic carbon metabolism. In the mineral-amended reactors, NO_3^- removal through denitrification may have been the primary pathway for N loss. Apparent denitrification rates were highest in the wood+FeO_x+MnO_2 treatments, indicating a role for MnO_2 in denitrification, or potentially more efficient denitrification at higher pH (Table 5.1). It has been reported that denitrification becomes more efficient as pH increases from 5 to 9 (Qian et al., 2019). This is because, at higher pH ranges, partial denitrification supplies nitrite for anaerobic ammonium oxidation (anammox). If MnO_2

was actively involved in denitrification reactions as a direct electron acceptor, it may have been less effective in buffering the redox potential above the level of Fe(III) reduction (Table 5.1). Alternatively, these results could also reflect the adsorption of NO_3^- onto the mineral oxide surfaces (Cheng et al. 2021).

Under anoxic conditions, MnO_2-mediated ammonia oxidation (Mnammox) is primarily governed by Mn-reducing bacteria. Yang et al. (2019) found that addition of MnO_2 resulted in an improvement in denitrification, which was attributed to an increase in the abundance of denitrifying bacteria. Indeed, there is substantial evidence supporting the active involvement of manganese oxides in the nitrogen cycle within marine ecosystems (Bartlett et al., 2008; Hulth et al., 2005). Consequently, the processes of nitrification and denitrification are interconnected with the reduction of manganese oxides and the oxidation of Mn^{2+} in anaerobic conditions. This process oxidizes NH_4-N to N_2 by involving MnO_2 as a direct electron acceptor (Jia et al., 2023; Swathi et al., 2017). The reduced manganese (Mn^{2+}) reacts with nitrate in this redox cycle, allowing nitrate to be reduced to N_2 (eq. 3), thereby facilitating denitrification (Equations 1-3). While this reaction pathway plausibly explains the higher rate of denitrification in the MnO_2-amended reactors, we currently lack corroborating NH_4^+ data.

$$2NH_3 + 3MnO_2 + 6H^+ \rightarrow 3Mn^{2+} + N_2 + 6H_2O \quad (1)$$

$$8MnO_2 + 2NH_4^+ + 12H^+ \rightarrow 8Mn^{2+} + 2NO_3^- + 10H_2O \quad (2)$$

$$5Mn^{2+} + 2NO_3^- + 4H_2O \rightarrow 5MnO_2 + N_2 + 8H^+ \quad (3)$$

Under anaerobic conditions, MnO_2 can undergo reductive dissolution to form soluble Mn^{2+} through microbial and chemical reduction pathways (Myers & Nealson, 1988; Villinski et al., 2003; Yao & Millero, 1993). Mn^{2+} can be reoxidised by the addition of a strong oxidant like

NO_3^-, leading to the formation of either Mn^{3+} or the creation of insoluble Mn(IV) oxides. Subsequently, Mn^{2+} can be oxidized to reprecipitate MnO_2 through microbially-mediated oxidation, involving heterotrophs and manganese-oxidizing microorganisms (Hansel, 2017; Yu & Leadbetter, 2020). Zhang et al., (2022) inferred that Mn-reducing bacteria invariably coexist with Mn-oxidizing bacteria within the same environment, facilitating continuous Mn redox cycling. Under anaerobic conditions, heterotrophic Mn-reducing bacteria can utilize organic matter as an electron donor, while employing MnO_x as a terminal electron acceptor, resulting in the production of Mn^{2+} and dissolved inorganic carbon. Concurrently, Mn^{2+} is oxidized, leading to the formation of specific oxidized minerals alongside the oxidation of other metal ions. We further note that the Mn-amended reactors had consistently higher pH values, possibly indicative of greater DIC generation as shown by Zhang et al., (2022).

5.4.2 Organic carbon removal in the presence of mineral oxides

Soluble organic compounds sourced from woodchips usually contain a significant amount of lignin, tannins, and various phenolic compounds (Svensson et al., 2014). These compounds often contain an abundance of carboxyl and hydroxyl functional groups, making them prone to strong adsorption onto iron oxide surfaces through ligand exchange, hydrophobic and electrostatic interactions (Arnarson & Keil, 2000; Gu et al., 1994; Weng et al., 2012). In low–pH conditions such as is typical in agricultural drainage, the primary interaction between organic matter and iron oxide surfaces is through ligand exchange. But, once the iron oxide surfaces become saturated with organic matter, the sorption mechanism is more likely to involve hydrophobic effects (Chi & Amy, 2004). In this experiment, the measured pH of all the reactors were between 3.72 – 6.56, conditions which are favorable for the adsorption of organic matter onto iron oxide surfaces via these mechanisms. This observation is in line with

the findings of Lai and Chen (2001), who concluded that adsorption of organic matter to metal oxide surfaces increases significantly under slightly acidic conditions (pH around 4 – 5). Interestingly, although the wood+FeO_x and the wood+FeO_x+MnO_2 treatments effectively removed organic matter, this did not appear to influence the removal dynamics of nitrate and phosphorus.

Yan et al. (2017) concluded that P can be adsorbed onto iron oxide, even after the formation of iron oxide–organic matter complexes. This finding provides insight into the mechanisms governing denitrifying bioreactors, particularly in relation to the behavior of iron oxide–organic matter complexes to attenuate P, and indicate that the formation of organic complexes on mineral surfaces as well as microbial biofilms, do not inhibit the adsorptive removal of P, despite other researchers reporting inhibition of P adsorption onto iron oxides due to competitive interactions with organic matter at the Fe oxide surface (Hunt et al., 2007; Weng et al., 2008).

5.4.3 Phosphorus removal in the presence of mineral oxides

The mechanisms for phosphorus removal in denitrifying bioreactors include adsorption, precipitation, and biological uptake. Our results indicate that there was effective P removal in both the wood+FeO_x–only and the wood+FeO_x+MnO_2 treatments, even following the incomplete dissolution of Fe. Dissolved P concentrations in wood+FeO_x and wood+FeO_x+MnO_2 treatments were always significantly lower than the wood only treatment, demonstrating that the addition of both manganese oxides and iron oxides can facilitate P removal in DBRs. However, Pearson correlation analysis (Table 5.2) demonstrated that P had a positive correlation with dissolved iron concentration in the period following peak NO_3 removal. Interestingly, similar trends can be observed between Fe dissolution and the P release

in the intervals between NO_3^- removal and the subsequent NO_3^- spike, indicative of reductive FeOx dissolution and simultaneous release of adsorbed P during these intervals.

Table 5. 2. Pearson correlation coefficients between P and N with Fe and Mn (S1 to S5 refer to the period between minimum NO_3^- concentrations and the subsequent NO_3^-spike).

		Fe (mg L^{-1})					Mn (mg L^{-1})				
		S1	S2	S3	S4	S5	S1	S2	S3	S4	S5
Wood+FeO_x	P (mg L^{-1})	0.887	0.210	0.054	-0.217	0.690	0.883	-0.015	-0.366	0.285	0.300
Wood+FeO_x+MnO_2		0.644	-0.018	0.092	-0.510	0.643	0.940	-0.420	0.353	0.366	0.683
Wood+FeO_x	N (mg L^{-1})	-0.898	0.750	0.093	-0.488	0.657	-0.824	0.619	-0.077	-0.010	0.703
Wood+FeO_x+MnO_2		-0.454	-0.302	-0.134	-0.639	0.721	-0.867	0.383	0.164	-0.419	0.718

Phosphorus–iron geochemical processes in sediments and aquatic systems have been studied for many decades. Under oxic conditions, iron oxide demonstrates a robust capacity to bind with P. Conversely, in anoxic conditions, iron minerals serve as significant electron acceptors, facilitating the reductive dissolution of iron oxide and consequent phosphorus release (Hartland et al., 2015; Saeed et al., 2018). Reduced Fe^{2+} ions can precipitate with P and form the Fe-P phase vivianite ($Fe_3(PO_4)_2$) (Heinrich et al., 2021; Wu et al., 2023). Thus, Fe and P can form insoluble minerals under both reduced and oxic conditions depending on their stoichiometric relationships.

5.4.4 Effects of pyrolyzed biochar on denitrification

In this experiment, FeO_x and MnO_2 were synthesized onto biochar. However, a control treatment with biochar alone was not incorporated into the experimental design due to logistical constraints. However, it has been shown previously that biochar can enhance nitrate removal (Chen et al., 2020; Guo et al., 2023). Biochar is a carbon-rich substance formed through the pyrolysis of biomass under anoxic conditions, with a porous structure, higher surface area, and the ability to serve as a substrate for biofilm attachment (Deng et al., 2021). Furthermore, the

presence of surface functional groups like quinone and phenolic compounds can also conceivably enhance denitrification rates (Li et al., 2018; Wang et al., 2022). The high cation exchange capacity of biochar, as well as the presence abundant of negatively charged functional groups (hydroxyl, carboxyl and phenolic groups) can favour N adsorption, with NH_4^+ and NO_3^- being adsorbed to biochar depending on its properties and the solution chemical conditions (Deng et al., 2021). Ji et al. (2020) reported that the use of biochar can enhance the diversity of microbes, especially nitrifying bacterial groups. In the experiment reported here, biochar was a common denominator in both mineral amendments and may therefore have impacted denitrification efficiencies to some extent.

5.4.5 Environmental significance

DBRs are effective systems that continue to be widely used to remove nutrients in agricultural drainage. However, these systems frequently operate under variable redox conditions. During drainage seasons, organic matter is oxidized by molecular oxygen, followed energetically by denitrification, reduction of manganese and iron, sulfate reduction, and methane production. Iron oxides have been shown to be a useful substrate for P removal in DBRs due to their cost-effectiveness and environmental compatibility. Manganese oxides have also been used in constructed wetlands to mitigate greenhouse gas emissions, but not previously in a DBR context. We show that this same principle can be applied in DBRs to potentially minimise the progression of the redox transformations by providing an adequate amount of MnO_2 to inhibit iron reduction allowing for continued P adsorption. We further show that MnO_2 can additionally enhance denitrification and P removal, with significantly higher removal efficiencies in the presence of FeO_x and MnO_2 than wood and FeO_x only.

5.5 Conclusions

This study investigated the impact of manganese dioxide and iron oxides, on the ability of DBRs to buffer reducing conditions and facilitate phosphorus removal. The study revealed that both manganese dioxide and iron oxides had a similar effect on phosphorus (P) and nitrogen (N) removal, with slightly better performance observed in the treatment involving manganese dioxide (MnO_2). Therefore, manganese and iron oxides appear to be a beneficial amendment to the usual woodchip substrate of DBRs, and further comprehensive research should be conducted to confirm this.

References

Aalto, S. L., Suurnäkki, S., von Ahnen, M., Siljanen, H. M. P., Pedersen, P. B., & Tiirola, M. (2020). Nitrate removal microbiology in woodchip bioreactors: A case-study with full-scale bioreactors treating aquaculture effluents. *Science of The Total Environment*, *723*, 138093. https://doi.org/https://doi.org/10.1016/j.scitotenv.2020.138093

Abusallout, I., & Hua, G. (2017). Characterization of dissolved organic carbon leached from a woodchip bioreactor. *Chemosphere*, *183*, 36-43. https://doi.org/https://doi.org/10.1016/j.chemosphere.2017.05.066

Arnarson, T. S., & Keil, R. G. (2000). Mechanisms of pore water organic matter adsorption to montmorillonite. *Marine chemistry*, *71*(3-4), 309-320.

Bartlett, R., Mortimer, R. J., & Morris, K. (2008). Anoxic nitrification: evidence from Humber Estuary sediments (UK). *Chemical Geology*, *250*(1-4), 29-39.

Berner, R. A. (1971). *Principles of chemical sedimentology*. McGraw-Hill.

Brdjanovic, D., Logemann, S., M. van Loosdrecht, M. C., Hooijmans, C. M., J. Alaerts, G., & Heijnen, J. J. (1998). Influence of temperature on biological phosphorus removal: process and molecular ecological studies. *Water Research*, *32*(4), 1035-1048. https://doi.org/https://doi.org/10.1016/S0043-1354(97)00322-9

Chen, X., Zhu, H., Banuelos, G., Shutes, B., Yan, B., & Cheng, R. (2020). Biochar reduces nitrous oxide but increases methane emissions in batch wetland mesocosms. *Chemical Engineering Journal*, *392*, 124842.

Cheng, C., He, Q., Zhang, J., Chai, H., Yang, Y., Pavlostathis, S. G., & Wu, H. (2022). New insight into ammonium oxidation processes and mechanisms mediated by manganese oxide in constructed wetlands. *Water Research*, *215*, 118251. https://doi.org/https://doi.org/10.1016/j.watres.2022.118251

Cheng, S., Qin, C., Xie, H., Wang, W., Zhang, J., Hu, Z., & Liang, S. (2021). Comprehensive evaluation of manganese oxides and iron oxides as metal substrate materials for constructed wetlands from the perspective of water quality and greenhouse effect.

Ecotoxicology and Environmental Safety, *221*, 112451. https://doi.org/https://doi.org/10.1016/j.ecoenv.2021.112451

Chi, F.-H., & Amy, G. L. (2004). Kinetic study on the sorption of dissolved natural organic matter onto different aquifer materials: the effects of hydrophobicity and functional groups. *Journal of Colloid and Interface Science*, *274*(2), 380-391. https://doi.org/https://doi.org/10.1016/j.jcis.2003.12.049

Christianson, L. E., Bhandari, A., & Helmers, M. J. (2011). Pilot-Scale Evaluation of Denitrification Drainage Bioreactors: Reactor Geometry and Performance. *Journal of Environmental Engineering*, *137*(4), 213-220. https://doi.org/doi:10.1061/(ASCE)EE.1943-7870.0000316

Colombo, C., Palumbo, G., He, J.-Z., Pinton, R., & Cesco, S. (2014). Review on iron availability in soil: interaction of Fe minerals, plants, and microbes. *Journal of soils and sediments*, *14*, 538-548.

Deng, S., Chen, J., & Chang, J. (2021). Application of biochar as an innovative substrate in constructed wetlands/biofilters for wastewater treatment: Performance and ecological benefits. *Journal of Cleaner Production*, *293*, 126156. https://doi.org/https://doi.org/10.1016/j.jclepro.2021.126156

Ding, J., Su, M., Wu, C., & Lin, K. (2015). Transformation of triclosan to 2,8-dichlorodibenzo-p-dioxin by iron and manganese oxides under near dry conditions. *Chemosphere*, *133*, 41-46. https://doi.org/https://doi.org/10.1016/j.chemosphere.2015.03.055

Dougherty, H., Cooke, R. A. C., Bhattarai, R., & Christianson, L. (2020). Design flow and nitrate removal evaluation of a wide denitrifying bioreactor with baffles. *Ecological Engineering*, *158*, 106068. https://doi.org/https://doi.org/10.1016/j.ecoleng.2020.106068

Greenan, C. M., Moorman, T. B., Parkin, T. B., Kaspar, T. C., & Jaynes, D. B. (2009). Denitrification in Wood Chip Bioreactors at Different Water Flows [https://doi.org/10.2134/jeq2008.0413]. *Journal of Environmental Quality*, *38*(4), 1664-1671. https://doi.org/https://doi.org/10.2134/jeq2008.0413

Gu, B., Schmitt, J., Chen, Z., Liang, L., & McCarthy, J. F. (1994). Adsorption and desorption of natural organic matter on iron oxide: mechanisms and models. *Environmental Science & Technology*, *28*(1), 38-46.

Guo, F., Luo, Y., Nie, W., Xiong, Z., Yang, X., Yan, J., Liu, T., Chen, M., & Chen, Y. (2023). Biochar boosts nitrate removal in constructed wetlands for secondary effluent treatment: Linking nitrate removal to the metabolic pathway of denitrification and biochar properties. *Bioresource Technology*, *379*, 129000. https://doi.org/https://doi.org/10.1016/j.biortech.2023.129000

Hansel, C. M. (2017). Manganese in marine microbiology. *Advances in microbial physiology*, *70*, 37-83.

Hartland, A., Andersen, M. S., & Hamilton, D. P. (2015). Phosphorus and arsenic distributions in a seasonally stratified, iron- and manganese-rich lake: microbiological and geochemical controls. *Environmental Chemistry*, *12*(6), 708-722. https://doi.org/https://doi.org/10.1071/EN14094

Heinrich, L., Rothe, M., Braun, B., & Hupfer, M. (2021). Transformation of redox-sensitive to redox-stable iron-bound phosphorus in anoxic lake sediments under laboratory conditions. *Water Research*, *189*, 116609. https://doi.org/https://doi.org/10.1016/j.watres.2020.116609

Hua, G., Salo, M. W., Schmit, C. G., & Hay, C. H. (2016). Nitrate and phosphate removal from agricultural subsurface drainage using laboratory woodchip bioreactors and recycled steel byproduct filters. *Water Research*, *102*, 180-189. https://doi.org/https://doi.org/10.1016/j.watres.2016.06.022

Hulth, S., Aller, R. C., Canfield, D. E., Dalsgaard, T., Engström, P., Gilbert, F., Sundbäck, K., & Thamdrup, B. (2005). Nitrogen removal in marine environments: recent findings and future research challenges. *Marine chemistry*, *94*(1-4), 125-145.

Hunt, J. F., Ohno, T., He, Z., Honeycutt, C. W., & Dail, D. B. (2007). Inhibition of phosphorus sorption to goethite, gibbsite, and kaolin by fresh and decomposed organic matter. *Biology and fertility of soils*, *44*, 277-288.

Ji, B., Chen, J., Mei, J., Chang, J., Li, X., Jia, W., & Qu, Y. (2020). Roles of biochar media and oxygen supply strategies in treatment performance, greenhouse gas emissions, and bacterial community features of subsurface-flow constructed wetlands. *Bioresource Technology*, *302*, 122890. https://doi.org/https://doi.org/10.1016/j.biortech.2020.122890

Jia, L., Zhou, Q., Li, Y., & Wu, W. (2023). Application of manganese oxides in wastewater treatment: Biogeochemical Mn cycling driven by bacteria. *Chemosphere*, *336*, 139219. https://doi.org/https://doi.org/10.1016/j.chemosphere.2023.139219

Lai, C. H., & Chen, C. Y. (2001). Removal of metal ions and humic acid from water by iron-coated filter media. *Chemosphere*, *44*(5), 1177-1184. https://doi.org/https://doi.org/10.1016/S0045-6535(00)00307-6

Lepine, C., Christianson, L., Davidson, J., & Summerfelt, S. (2018). Woodchip bioreactors as treatment for recirculating aquaculture systems' wastewater: A cost assessment of nitrogen removal. *Aquacultural Engineering*, *83*, 85-92. https://doi.org/https://doi.org/10.1016/j.aquaeng.2018.09.001

Li, J., Fan, J., Zhang, J., Hu, Z., & Liang, S. (2018). Preparation and evaluation of wetland plant-based biochar for nitrogen removal enhancement in surface flow constructed wetlands. *Environmental Science and Pollution Research*, *25*(14), 13929-13937. https://doi.org/10.1007/s11356-018-1597-y

Li, M., Liu, J., Xu, Y., & Qian, G. (2016). Phosphate adsorption on metal oxides and metal hydroxides: A comparative review. *Environmental Reviews*, *24*(3), 319-332. https://doi.org/10.1139/er-2015-0080

Liu, R., Chi, L., Wang, X., Sui, Y., Wang, Y., & Arandiyan, H. (2018). Review of metal (hydr)oxide and other adsorptive materials for phosphate removal from water. *Journal of Environmental Chemical Engineering*, *6*(4), 5269-5286. https://doi.org/https://doi.org/10.1016/j.jece.2018.08.008

McMahon, P. B., & Chapelle, F. H. (2008). Redox Processes and Water Quality of Selected Principal Aquifer Systems. *Groundwater*, *46*(2), 259-271. https://doi.org/https://doi.org/10.1111/j.1745-6584.2007.00385.x

Myers, C. R., & Nealson, K. H. (1988). Bacterial manganese reduction and growth with manganese oxide as the sole electron acceptor. *Science*, *240*(4857), 1319-1321.

Qian, W., Ma, B., Li, X., Zhang, Q., & Peng, Y. (2019). Long-term effect of pH on denitrification: High pH benefits achieving partial-denitrification. *Bioresource Technology*, *278*, 444-449. https://doi.org/https://doi.org/10.1016/j.biortech.2019.01.105

Rivas, A., Barkle, G., Stenger, R., Moorhead, B., & Clague, J. (2020). Nitrate removal and secondary effects of a woodchip bioreactor for the treatment of subsurface drainage with dynamic flows under pastoral agriculture. *Ecological Engineering*, *148*, 105786. https://doi.org/https://doi.org/10.1016/j.ecoleng.2020.105786

Saeed, H., Hartland, A., Lehto, N. J., Baalousha, M., Sikder, M., Sandwell, D., Mucalo, M., & Hamilton, D. P. (2018). Regulation of phosphorus bioavailability by iron nanoparticles in a monomictic lake. *Scientific Reports*, *8*(1), 17736. https://doi.org/10.1038/s41598-018-36103-x

Sanchez Bustamante-Bailon, A. P., Margenot, A., Cooke, R. A. C., & Christianson, L. E. (2022). Phosphorus removal in denitrifying woodchip bioreactors varies by wood type and water chemistry. *Environ Sci Pollut Res Int*, *29*(5), 6733-6743. https://doi.org/10.1007/s11356-021-15835-w

Schipper, L. A., Robertson, W. D., Gold, A. J., Jaynes, D. B., & Cameron, S. C. (2010). Denitrifying bioreactors—An approach for reducing nitrate loads to receiving waters. *Ecological Engineering*, *36*(11), 1532-1543. https://doi.org/https://doi.org/10.1016/j.ecoleng.2010.04.008

Schippers, A., & Jørgensen, B. B. (2002). Biogeochemistry of pyrite and iron sulfide oxidation in marine sediments. *Geochimica et Cosmochimica Acta*, *66*(1), 85-92. https://doi.org/https://doi.org/10.1016/S0016-7037(01)00745-1

Smith, G. J., McDowell, R. W., Condron, L. M., Daly, K., Ó hUallacháin, D., & Fenton, O. (2021). Reductive dissolution of phosphorus associated with iron-oxides during saturation in agricultural soil profiles. *Journal of Environmental Quality*, *50*(5), 1207-1219. https://doi.org/https://doi.org/10.1002/jeq2.20256

Smith, G. J., McDowell, R. W., Condron, L. M., Daly, K., Ó hUallacháin, D., & Fenton, O. (2023). Phosphorus and iron-oxide transport from a hydrologically isolated grassland hillslope. *Journal of Environmental Management*, *329*, 117008. https://doi.org/https://doi.org/10.1016/j.jenvman.2022.117008

Svensson, H., Marques, M., Kaczala, F., & Hogland, W. (2014). Leaching patterns from wood of different tree species and environmental implications related to wood storage areas. *Water and Environment Journal*, *28*(2), 277-284.

Swathi, D., Sabumon, P., & Maliyekkal, S. M. (2017). Microbial mediated anoxic nitrification-denitrification in the presence of nanoscale oxides of manganese. *International Biodeterioration & Biodegradation*, *119*, 499-510.

Villinski, J. E., Saiers, J. E., & Conklin, M. H. (2003). The effects of reaction-product formation on the reductive dissolution of MnO2 by Fe (II). *Environmental Science & Technology*, *37*(24), 5589-5596.

Wang, H., Xu, J., Sheng, L., & Teng, H. (2022). Study on treatment of city tail water by constructed wetland with corn straw biochar substrate. *Environmental Technology & Innovation*, *28*, 102855. https://doi.org/https://doi.org/10.1016/j.eti.2022.102855

Wen, S., Liu, J., Lu, Y., Dai, J., Huang, X., An, S., Jeppesen, E., Liu, Z., & Du, Y. (2023). Composition regulates organic matter adsorption onto iron (oxy)hydroxides and competition with phosphate: Implications for organic carbon, phosphorus immobilization in lakes. *Journal of Environmental Sciences*. https://doi.org/https://doi.org/10.1016/j.jes.2023.07.038

Weng, L., Van Riemsdijk, W. H., & Hiemstra, T. (2008). Humic nanoparticles at the oxide−water interface: interactions with phosphate ion adsorption. *Environmental Science & Technology*, *42*(23), 8747-8752.

Weng, L., Van Riemsdijk, W. H., & Hiemstra, T. (2012). Factors controlling phosphate interaction with iron oxides. *Journal of Environmental Quality*, *41*(3), 628-635.

Wu, X., Jiang, Q., & Ma, T. (2023). Geochemical processes of phosphorus-iron on sediment-water interface during discharge of groundwater to freshwater lakes: Kinetic and mechanistic insights. *Science of The Total Environment*, *901*, 165962. https://doi.org/https://doi.org/10.1016/j.scitotenv.2023.165962

Yan, J., Jiang, T., Yao, Y., Wang, J., Cai, Y., Green, N. W., & Wei, S. (2017). Underestimation of phosphorus fraction change in the supernatant after phosphorus adsorption onto iron oxides and iron oxide–natural organic matter complexes. *Journal of Environmental Sciences*, *55*, 197-205. https://doi.org/https://doi.org/10.1016/j.jes.2016.08.005

Yang, Y., Liu, J., Zhang, N., Xie, H., Zhang, J., Hu, Z., & Wang, Q. (2019). Influence of application of manganese ore in constructed wetlands on the mechanisms and improvement of nitrogen and phosphorus removal. *Ecotoxicology and Environmental Safety*, *170*, 446-452. https://doi.org/https://doi.org/10.1016/j.ecoenv.2018.12.024

Yao, W., & Millero, F. J. (1993). The rate of sulfide oxidation by δMnO2 in seawater. *Geochimica et Cosmochimica Acta*, *57*(14), 3359-3365.

Yu, H., & Leadbetter, J. R. (2020). Bacterial chemolithoautotrophy via manganese oxidation. *Nature*, *583*(7816), 453-458.

Zeng, L., Li, X., & Liu, J. (2004). Adsorptive removal of phosphate from aqueous solutions using iron oxide tailings. *Water Research*, *38*(5), 1318-1326. https://doi.org/https://doi.org/10.1016/j.watres.2003.12.009

Chapter 6 Summary, Conclusions and Recommendations

6.1. Summary and Conclusions

Elevated levels of phosphorus (P) in agricultural drainage contribute significantly to the widespread degradation of water quality in both freshwater and marine receiving environments globally. This thesis presents research investigating the P biogeochemistry of denitrifying bioreactors, with a primary focus on the dynamics of phosphorus removal and the potential for augmentation with reactive minerals for enhancement of P and N removal. The investigation involved studies of iron-P redox cycling in an established bioreactor system, the use of novel composite materials for P removal, and the assessment of the stability of these composite materials under oscillating redox conditions. Additionally, the study evaluated the fate of these materials when positioned in the bioreactor environment under prevailing reduced conditions.

This section summarises the main findings of the study.

1. In **Chapter 3**, the bioreactor monitoring results obtained over two consecutive drainage seasons (2017 & 2018) and additional measurements made in 2021 provide crucial insights. Strong correlations between Fe and P at both the inlet and outlet during season 1 suggested the importance of Fe in P cycling. Attenuation of P relative to Fe was used as evidence of biological phosphorus retention within the bioreactor following the gradual reduction of soil-derived Mn and Fe oxides. This suggests that, over time, Fe (and Mn) oxides were removed by reductive dissolution, generating P as a by-product, but this was mainly biologically retained. This suggests that P removal rates can scale with P supply, potentially reaching a similar order to nitrate-N removal rates. The conclusion drawn is that when positioned near the reactor inlet, Fe−oxides should be

preserved by oxic conditions and may even grow in size and mass, effectively replenishing their P adsorption capacity over time.

2. **Chapter 4** outlines the synthesis of iron composite materials designed for P adsorption, demonstrating their efficient removal of P from aqueous solutions. The study establishes that adsorption is particularly favoured at low pH values (pH 4-6). The mechanisms governing P adsorption by the synthesized iron (hydr)oxides involved non-specific adsorption, electrostatic interaction, and specific adsorption. In the column experiment, the absence of P breakthrough indicates an abundance of unsaturated P sorption sites, ensuring consistently favorable conditions for the electrostatic attraction of phosphate anions from agricultural drainage, which typically has a pH slightly below neutral. XPS analysis suggests a multilayer adsorption mechanism operating between P and the Fe-bio media surfaces at favourable pH, resulting in the adsorption capacity scaling with P concentration. Based on conservative estimates, even small amounts of Fe-modified bio media may prove effective in these systems, leading to a reduction in P levels relative to flow. This approach enhances retention and allows more time for bioaccumulation, addressing a critical issue in the performance of these passive treatment systems. Overall, the findings contribute valuable insights to the field of P removal and offer practical solutions for environmental and industrial applications.
3. The findings from **Chapter 5** suggest a significant improvement in nitrate and phosphorus removal when incorporating both Fe and Mn functionalized media. The removal of NO_3^- was enhanced in treatments amended with these materials. Dissimilatory redox reactions between Mn(IV) and Fe(III) oxides contributed to organic carbon metabolism. Reduced manganese (Mn^{2+}) appeared to react with nitrate, facilitating denitrification, but potentially limiting its effectiveness in buffering the redox potential above the level of Fe(III) reduction. While the adsorption of organic

matter onto metal oxide surfaces did not seem to influence the removal dynamics of nitrate and phosphorus, reactors with FeO_x and MnO_2 displayed higher removal efficiency for TOC, nitrogen and phosphorus. It was confirmed that the formation of organic complexes on mineral surfaces and microbial biofilms did not inhibit the adsorptive removal of P, contradicting other reports of inhibition of P adsorption onto iron oxides due to competitive interactions with organic matter at the Fe oxide surface. The results indicated effective P removal in both the wood+FeOx–only and the wood+FeOx+MnO_2 treatments, even following the incomplete dissolution of FeOx minerals. Dissolved P concentrations in wood+FeOx and wood+FeOx+MnO_2 treatments were consistently lower than in the wood-only treatment, demonstrating that the addition of both manganese dioxide and iron oxides can enhance P removal in denitrifying woodchip bioreactors (DBRs).

6.2 Recommendations and future research

Denitrifying woodchip bioreactors have proven to be a promising technology for mitigating phosphorus in agricultural runoff, which can be enhanced by utilization of biological and chemical processes. Despite the potential of this approach, this study was limited to lab-scale. Long-term field studies must overcome the challenges of synthesizing large quantities of Fe-functionalized media and MnO_2 inorder to achieve practical scale in real-world applications.

To advance this field, future research and development efforts could focus on improving the efficiency and scalability of Fe-PyOM synthesis. Specifically, long-term field studies would be valuable to assess the sustained performance of Fe-based biomedia in woodchip bioreactors over extended periods, complemented by in-situ field measurements and laboratory analysis.

This comprehensive approach would allow for the investigation of phosphorus adsorption, redox conditions, and the measurement of redox species, including dissolved oxygen (DO), Fe^{2+}, HS^-, NH_4^+, and other analyses as outlined in Chapter 3.

Appendices

Chapter 3. Elucidating phosphorus removal dynamics in a denitrifying woodchip bioreactor

M Gimhani N Perera [a,b], Dorisel Torres Rojas [a], Aldrin Rivas[c], Greg Barkle[d], Brian Moorhead[c], Louis A. Schipper[a], Rupert Craggs[b], Adam Hartland [a,c*]

[a]Environmental Research Institute, School of Science, Faculty of Science and Engineering, University of Waikato, Kirikirioa Hamilton, New Zealand.

[b]National Institute of Water and Atmospheric Research Ltd (NIWA), PO Box 11115, Kirikirioa Hamilton 3251, New Zealand.

[c]Lincoln Agritech Ltd, Ruakura, Kirikirioa Hamilton 3214.

[d]Land and Water Research Ltd, Kirikirioa Hamilton 3217.

[*] Corresponding author. Email: adam.hartland@waikato.ac.nz

Measurements from the field have been entered into the PHREEQC input datasheet in the following sequence.

1 "SELECTED_OUTPUT" has been entered at the beginning of the input file. The intended output results have been defined as subtopics of the output file. The subtopics are file, reset, totals, saturation_indices, pH, pe, Alkalinity, ionic_strength, and percent_error.

2 The "Solution 1" has to be entered directly beneath the percent_error command, the unit is defined as mg/L under the solution command

3 The corresponding parameters for the solution 1 have been entered as "Temp, pH, Fe (+2), Fe (+3), Mn, Na, K, Ca, Mg, S (6), S (-2), Cl, Alkalinity". The pe stands for oxidation-reduction

potential is based on the calculation of the redox couple of S (6) and S (-2) which was entered after the pH and re-runs the model.

4 The next keywords of "SAVE solution 1" and "Use solution 1" have been entered. "EQUILIBRIUM_PHASES 1" is important to enter to obtain output data when the system is at its equilibrium of $Fe(OH)_3(a)$ 0 $1e^{-3}$.

Table 3 S3.1 PHREEQC input of the bioreactor data for the drainage season 2021

Sample	Date	Temp	pH	Fe(+2)	Fe(+3)	Mn	Na	K	Ca	Mg	S(6)	S(-2)	Cl	Alk	N(+5)
Inlet	27/7	12.7	6.10	0.01	0.02	0.15	21.2	8.41	62.6	22.1	96.4	0.02	91.9	39.8	52.2
C1		13.4	6.56	0.38	0.27	0.16	22.1	8.81	53.7	21.7	103	0.01	67.1	59.8	40.6
C2		14.7	6.20	0.10	0.08	0.19	22.1	8.33	53.8	21.8	108	0.19	59.5	74.3	31.3
C3		15.7	6.30	0.33	0.30	0.15	28.0	7.63	52.7	19.9	77.5	0.32	15.7	216	7.08
Outlet		16.6	6.16	0.37	0.37	0.15	47.0	7.66	48.6	19.2	88.4	0.60	21.5	223	11.0
Inlet	17/8	12.7	6.03	0.04	0.01	0.11	59.8	3.62	44.3	16.3	149	0.00	42.4	43.7	76.8
C1		13.6	6.55	0.13	0.05	0.15	87.6	5.07	49.9	19.0	133	0.49	38.3	226	26.9
C2		14.1	6.51	0.10	0.04	0.15	65.3	5.18	47.5	19.3	124	0.05	27.0	205	14.5
C3		14.1	6.39	0.32	0.15	0.14	91.1	5.05	40.9	16.4	102	0.00	21.9	282	9.37
Outlet		14.6	6.26	0.23	0.11	0.15	72.7	4.78	40.4	15.5	131	0.05	35.2	155	21.0
Inlet	27/9	13.9	5.79	0.02	0.01	0.15	17.9	6.38	48.3	19.0	114	0.00	43.5	40.5	41.6
C1		14.0	5.90	0.07	0.03	0.15	20.0	6.65	46.6	17.1	121	0.00	29.9	53.5	34.5
C2		14.0	6.04	0.15	0.09	0.15	15.8	7.44	49.2	16.3	119	0.00	28.5	58.4	28.7
C3		14.0	6.09	0.26	0.16	0.16	19.4	8.24	49.3	16.8	106	0.00	19.2	107	26.3
Outlet		14.3	6.10	0.25	0.17	0.16	40.1	8.51	47.0	17.1	108	0.00	26.3	133	35.3

Example of a PHREEQC input file

```
SELECTED_OUTPUT
-file C:\Users\perer\Desktop\ModelOut corrected\PHREEQCout_Exp2.1.prn
-reset false
-totals C(4) Fe Fe(+2) Fe(+3) Mn Mn(+2) S S(6) S(-2)
-saturation_indices Calcite Fe(OH)3(a) Goethite Hematite Pyrite FeS(ppt)
-pH
-pe
-alkalinity
-ionic_strength
-percent_error
Solution 1 # equal to inlet of Tatanui
-units mg/L #
Temp   12.7
pH       6.10
pe -1.91
```

Fe(+2) 0.01
Fe(+3) 0.02
Mn 0.15
Na 21.2
K 8.41
Ca 62.6
Mg 22.1
S(6) 96.4
S(-2) 0.02
Cl 91.9
Alkalinity 39.8
SAVE solution 1
Use Solution 1
EQUILIBRIUM_PHASES 1
$Fe(OH)_3(a)$ 0 0 precipitate # name (must be defined in PHASES), Saturation Index (Default: 0), initial amount (moles, default: 10 moles)

Table 3 S3.2 Measurements of N, P, Fe, S, and Mn (outlet−inlet) for the drainage seasons of 2017 and 2018

	Inlet (mg L^{-1})					Outlet (mg L^{-1})					Net change (mg L^{-1})				
Date	**N**	**P**	**Fe**	**S**	**Mn**	**N**	**P**	**Fe**	**S**	**Mn**	**ΔN**	**ΔP**	**ΔFe**	**ΔS**	**ΔMn**
17/8/2017	7.46	0.02	0.01	135	0.14	0.00	0.32	1.63	120	1.72	-7.46	0.30	1.61	-14.4	1.58
22/8/2017	6.90	0.02	0.02	134	0.15	0.00	0.36	1.96	113	1.94	-6.90	0.33	1.94	-21.8	1.79
29/8/2017	8.52	0.05	0.02	113	0.12	0.00	0.15	1.16	108	1.55	-8.52	0.11	1.14	-4.70	1.43
1/9/2017	6.88	0.04	0.01	123	0.13	0.00	0.05	0.65	105	1.04	-6.88	0.01	0.63	-17.6	0.90
4/9/2017	6.42	0.03	0.01	118	0.13	0.00	0.11	0.69	84	0.77	-6.42	0.08	0.68	-34.3	0.64
7/9/2017	6.44	0.04	0.01	110	0.12	0.00	0.06	0.39	91	0.65	-6.44	0.02	0.38	-19.0	0.52
8/9/2017	6.53	0.04	0.01	109	0.12	0.01	0.05	0.31	101	0.64	-6.53	0.01	0.30	-8.43	0.52
12/9/2017	6.15	0.06	0.02	96.4	0.11	0.01	0.07	0.24	89.2	0.01	-6.14	0.01	0.22	-7.19	-0.10
15/9/2017	5.96	0.03	0.01	91.4	0.12	0.01	0.00	0.40	27.3	0.00	-5.95	-0.03	0.39	-64.2	-0.12
26/9/2017	3.52	0.14	0.10	66.9	0.17	0.01	0.07	0.36	59.1	0.42	-3.51	-0.07	0.27	-7.74	0.26
6/10/2017	3.20	0.00	0.00	0.0	0.00	0.01	0.00	0.00	0.00	0.00	-3.19	0.00	0.00	0.00	0.00
16/10/2017	3.07	0.02	0.04	141	0.28	0.01	0.17	1.11	36.3	0.46	-3.06	0.16	1.07	-105	0.18
30/10/2017	7.87	0.29	0.34	26.6	0.07	0.00	0.29	1.18	28.2	0.37	-7.87	0.00	0.84	1.63	0.30
6/11/2017	3.38	0.09	0.11	78.1	0.19	0.01	0.08	0.07	93.8	0.27	-3.37	-0.01	-0.04	15.6	0.08
1/6/2018	0.00	0.06	0.04	143	0.16	0.00	0.01	0.97	126	0.27	0.00	-0.05	0.94	-17.0	0.10
8/6/2018	0.00	0.07	0.03	128	0.17	14.2	0.01	0.52	107	0.27	14.2	-0.06	0.49	-21.0	0.11
20/6/2018	0.00	0.04	0.06	131	0.18	0.00	0.00	0.22	124	0.23	0.00	-0.04	0.16	-6.77	0.05
5/7/2018	0.00	0.02	0.04	135	0.21	0.00	0.00	0.11	133	0.19	0.00	-0.02	0.07	-2.23	-0.01
20/7/2018	12.8	0.14	0.01	539	0.12	8.43	0.04	0.02	512	0.14	-4.37	-0.10	0.01	-27.3	0.01
2/8/2018	0.00	0.12	0.01	527	0.19	0.00	0.05	0.04	525	0.11	0.00	-0.07	0.03	-2.10	-0.07
16/8/2018	9.45	0.02	0.01	341	0.13	0.88	0.01	0.01	337	0.12	-8.57	-0.01	0.01	-3.49	-0.01
4/9/2018	8.23	0.04	0.01	256	0.08	3.13	0.01	0.01	310	0.12	-5.10	-0.03	0.00	54.1	0.04
19/9/2018	0.00	0.04	0.00	269	0.26	0.00	0.03	0.07	254	0.11	0.00	-0.01	0.06	-15.6	-0.15

Table 3 S3.3 Measurements of temperature, ORP, pH, DO, EC, TDS and flow rate for the drainage season of 2021

Date	Sampling well	Flow rate (m^3 day^{-1})	Temperature (°C)	ORP (mv)	pH	DO (mg L^{-1})	EC (µS cm^{-1})	TDS (mg L^{-1})
27/7/2021	Inlet	7.52	12.7	98.8	6.10	8.45	758	492
	C1	7.52	13.4	-122	6.56	0.10	668	435
	C2	7.52	14.7	-185	6.20	0.31	689	447
	C3	6.91	15.7	-227	6.30	0.85	625	406
	Outlet	6.91	16.6	-244	6.16	1.28	611	395
17/8/2021	Inlet	0.69	12.7	176	6.03	6.95	694	451
	C1	0.69	13.6	-188	6.55	0.13	671	435
	C2	0.69	14.1	-66.0	6.51	0.26	676	439
	C3	0.69	14.1	-179	6.39	0.24	608	395
	Outlet	0.69	14.6	-144	6.26	0.90	628	407
27/9/2021	Inlet	4.75	13.9	140	5.79	6.12	615	399
	C1	4.75	14.0	111	5.90	0.17	595	387
	C2	4.75	14.0	94.7	6.04	0.30	604	394
	C3	4.75	14.0	75.0	6.09	0.31	602	390
	Outlet	4.75	14.3	58.7	6.10	0.39	586	382

Derivation of the removal rate equation (Hassanpour et al., 2017)

$$RR_A = \frac{[\Delta C_A]}{HRT} \quad (1)$$

$$[\Delta C_A] = C_{A_{inlet}} - C_{A_{outlet}} \quad (2)$$

$$HRT = \frac{\emptyset V_s}{Q} \quad (3)$$

$$V_s = A.d \quad (4)$$

Substituting eq. (4) to (1)

$$HRT = \frac{\emptyset A.d}{Q} \quad (5)$$

Substituting HRT in eq. 1

$$RR_A = \frac{[\Delta C_A]Q}{\emptyset V_S} \quad (6)$$

$$RR_A = \frac{[\Delta C_A]Q}{\emptyset A.d} \quad (7)$$

Where;

RR_A is removal rate analyte

$[\Delta C_A]$ is concentration analyte difference between inlet and outlet

Pinlet is the P concentration in the inlet

Poutlet is the P concentration in the outlet

HRT is hydraulic retention time

Vs is the saturated volume of the bioreactor (m^3) which is 56.3 m3 (Rivas et al., 2020)

∅ is the effective or drainable porosity

Q is the flow through the bioreactor ($m^3\ d^{-1}$)

A is surface area of bioreactor

d is active height to water in bioreactor

Assumptions to this equation are 1) defining a specific time for the P concentration difference and 2) flow through the reactor needs to be match with the P concentration difference.

Calculations for the Fe:P correlation

The coefficient of determination, or R^2

$$R^2 = 1 - \frac{sum\ squared\ regression\ (SSR)}{total\ sum\ of\ squares\ (SST)} \quad (8)$$

Saturation Index (SI)

The saturation index (SI) is calculated by comparing the chemical activities of the dissolved ions of the mineral (ion activity product, IAP) with their solubility product (Ksp). In equation form, SI = log(IAP/Ksp).

$$SI = log\left(\frac{IAP}{Ksp}\right)$$

References

Hassanpour, B., Giri, S., Pluer, W. T., Steenhuis, T. S., & Geohring, L. D. (2017). Seasonal performance of denitrifying bioreactors in the Northeastern United States: Field trials. *Journal of Environmental Management, 202*, 242-253. doi:https://doi.org/10.1016/j.jenvman.2017.06.054

Rivas, A., Barkle, G., Stenger, R., Moorhead, B., & Clague, J. (2020). Nitrate removal and secondary effects of a woodchip bioreactor for the treatment of subsurface drainage with dynamic flows under pastoral agriculture. *Ecological Engineering, 148*, 105786. doi:https://doi.org/10.1016/j.ecoleng.2020.105786

Chapter 4. Iron–based composites for in–field phosphorus removal from agricultural drainage

M Gimhani N Perera[a,b], Dorisel Torres Rojas[a], Sebastian N. Hoepker[a], Greg Olsen[b], Rupert Craggs[b], Adam Hartland[a,c*]

[a]Environmental Research Institute, School of Science, Faculty of Science and Engineering, University of Waikato, Kirikirioa Hamilton, New Zealand.

[b]National Institute of Water and Atmospheric Research Ltd (NIWA), PO Box 11115, Kirikirioa Hamilton 3251, New Zealand.

[c]Lincoln Agritech Ltd, Ruakura, Kirikirioa Hamilton 3214.

[*] Corresponding author. Email: adam.hartland@waikato.ac.nz

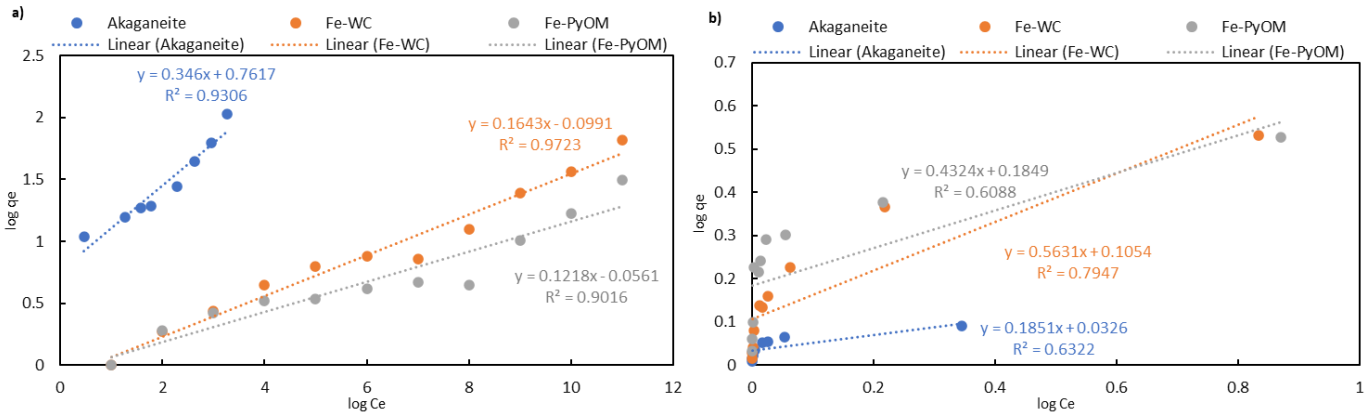

Figure 4 S4.1 Linear fit of a) Freundlich b) Langmuir isotherms

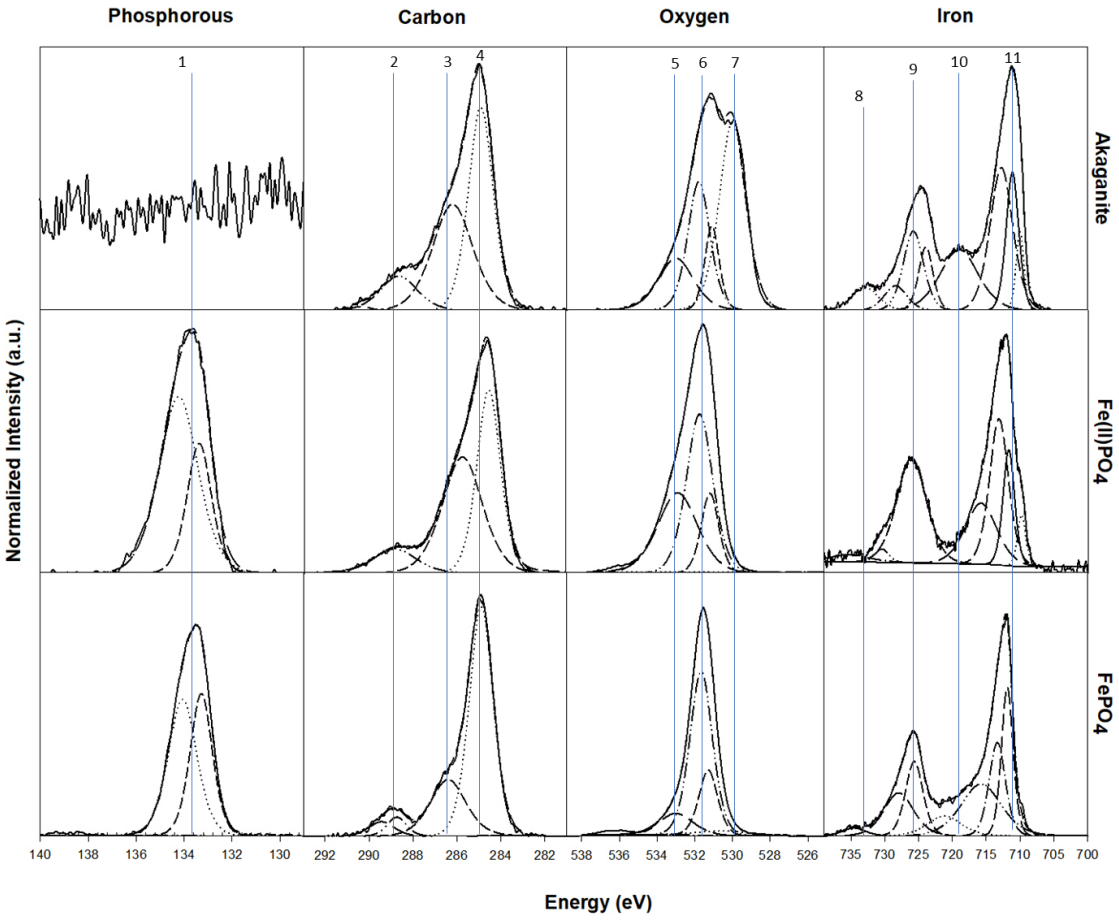

Figure 4 S4.2 Binding energies in XPS spectrum.

Figure S2 illustrates the typical O1s spectrum and the contribution of the different bonds to the total spectrum in Table S1. The O1s spectrum for the sorbents before and after phosphate adsorption were deconvoluted with four spectral features between 529 – 536 eV. The lowest

spectral band between 529.5 – 530.5 eV represents the oxygen from iron oxides (Daou et al., 2007). The 530.5 – 531.8 eV spectral band is attributed to P=O, C=O, and Fe-O-P functional groups. The spectral feature between 531.8 – 532.8 eV represents P or Fe hydroxy and ether groups (Karunanayake et al., 2019).

Table 4 S4.1 P2P, C1S, O1S, and Fe2P XPS peak assignments for akaganeite, Fe-WC, and Fe-PyOM before and after P adsorption

Core level	Bond		Akaganite	Ferrous phosphate	Ferric phosphate	Fe-WC	Fe-WC pH 4	Fe-WC pH 6	Fe-WC pH 8	Fe-PyOM	Fe-PyOM pH 4	Fe-PyOM pH 6	Fe-PyOM pH 8
P2p	Fe-O-P	Binding energy (eV)	-	133.4	133.3	-	133.1	133.4	-	-	133.5	-	-
		Atomic percentage %	-	31.8	44.9	-	67.2	71.7	-	-	59.1	-	-
P2p	H_3PO_4	Binding energy (eV)	-	134.2	134.1	-	134.0	134.2	-	-	134.3	134.01	-
		Atomic percentage %	-	68.2	55.1	-	32.8	28.3	-	-	41.0	87.1	-
C1s	C-C/C=C	Binding energy (eV)	284.9	284.5	284.9	285.0	284.9	284.9	284.8	284.8	285.0	284.9	284.9
		Atomic percentage %	52.4	47.6	63.5	31.7	44.3	38.8	64.9	10.6	49.1	45.0	61.8
C1s	C-O-C/C-OH	Binding energy (eV)	286.3	285.5	-	286.8	286.3	286.5	285.9	286.3	285.5	285.8	285.7
		Atomic percentage %	35.7	31.7	-	55.3	45.2	49.9	25.4	21.7	44.7	30.5	11.8
C1s	C=O	Binding energy (eV)	288.4	286.6	286.2	288.3	288.4	288.6	288.8	287.4	287.1	287.8	286.7
		Binding energy (eV)	7.64	8.93	27.8	11.9	6.6	11.3	9.7	49.2	1.6	14.2	20.3
C1s	O=C-OH(R)	Atomic percentage %	289.4	288.6	289.0	289.4	289.2	-	-	288.3	289.0	288.8	289.1
		Binding energy (eV)	4.25	11.8	8.6	1.1	3.9	-	-	18.5	4.5	10.4	6.1
O1s	Fe-O-Fe	Atomic percentage %	530.0	530.5	530.5	530.3	530.1	530.3	530.1	530.2	530.29	530.5	530.5
		Binding energy (eV)	45.8	4.05	4.3	5.7	18.6	16.0	52.9	3.7	33.69	40.6	2.5
O1s	P=O/Fe-O-P/Fe-OH	Atomic percentage %	531.1	531.3	531.3	531.3	531.3	531.3	530.5	531.7	531.63	531.8	532.1
		Binding energy (eV)	11.2	15.3	20.8	10.1	20.1	24.9	-	14.2	53.19	53.2	34.7
O1s	O-C/P-OH/Fe-OH	Binding energy (eV)	531.8	531.8	531.7	532.5	532.5	532.5	532.3	533.0	533.09	533.6	533.4
		Atomic percentage %	26.3	45.7	62.6	17.5	43.0	42.6	36.9	32.3	13.12	6.3	46.3
O1s	O-C=O	Binding energy (eV)	533.0	533.0	533.0	533.3	533.3	533.4	533.9	534.4	-	-	534.9
		Atomic percentage %	16.7	34.9	12.4	66.7	18.3	16.5	10.2	36.6	-	-	16.5
Fe2p	Fe 2p 3/2	Binding energy (eV)	710.0	709.8	-	710.4	710.4	710.7	710.3	710.95	710.7	710.9	710.3
		Atomic percentage %	5.23	4.21	-	3.0	8.8	12.0	6.6	3.9	4.2	4.5	3.5
Fe2p	Fe 2p 3/2	Binding energy (eV)	711.1	711.7	711.9	711.2	711.5	711.9	711.1	711.7	711.7	711.9	-
		Binding energy (eV)	14.9	13.4	19.6	32.6	20.2	17.5	44.6	-	15.9	13.8	-
Fe2p	Fe 2p 3/2	Atomic percentage %	712.8	713.1	713.4	713.3	713.2	713.6	711.3	713.3	713.1	713.4	713.6
		Binding energy (eV)	27.9	27.7	17.3	22.9	24.5	23.2	16.3	12.2	29.3	27.3	19.0
Fe2p		Atomic percentage %	-	715.8	715.8	-	-	-	-	714.5	-	-	715.3

Core level	Bond		Akaganite	Ferrous phosphate	Ferric phosphate	Fe-WC	Fe-WC pH 4	Fe-WC pH 6	Fe-WC pH 8	Fe-PyOM	Fe-PyOM pH 4	Fe-PyOM pH 6	Fe-PyOM pH 8
		Binding energy (eV)	-	19.2	23.8	-	-	-	-	26.0	-	-	32.8
Fe2p	Fe 2p 3/2 satellite	Atomic percentage %	719.0	-	-	719.6	719.4	719.4	720.0	716.8	719.7	720.0	-
		Binding energy (eV)	20.1	-	-	11.0	15.1	13.5	4.9	13.3	18.5	21.5	-
Fe2p	Fe 2p 1/2	Binding energy (eV)	723.9	-	721.2	723.7	724.2	724.4	723.5	722.2	724.2	724.8	722.3
		Atomic percentage %	7.83	-	7.6	6.9	9.8	8.5	3.2	13.1	2.6	5.5	9.5
Fe2p	Fe 2p 1/2	Binding energy (eV)	725.8	726.1	725.6	725.2	725.8	726.2	724.9	727.3	725.5	726.4	726.9
		Atomic percentage %	13.7	30.9	14.9	10.6	4.3	18.1	21.3	7.3	11.9	14.4	8.4
Fe2p	Fe 2p 1/2	Binding energy (eV)	728.4	730.5	727.9	727.3	727.0	729.8	729.8	728.2	727.2	728.8	728.9
		Atomic percentage %	4.89	1.77	14.6	9.1	12.8	1.2	1.1	21.6	13.0	7.6	20.6
Fe2p	Fe 2p 1/2 satellite	Binding energy (eV)	732.9	735.4	734.6	733.2	733.3	733.4	732.8	736.4	733.7	734.1	736.5
		Atomic percentage %	5.40	2.94	2.1	3.9	4.4	6.1	2.1	2.6	4.7	5.3	6.3

Chapter 5 Phosphorus removal by iron oxides in lab-scale denitrifying woodchip bioreactors with and without manganese dioxide

Gimhani N Perera [a], Dorisel Torres Rojas [a], Adam Hartland [a,b*]

[a]Environmental Research Institute, School of Science, Faculty of Science and Engineering, University of Waikato, Kirikirioa Hamilton, New Zealand.

[b]Lincoln Agritech Ltd, Ruakura, Kirikirioa Hamilton 3214.

[*] Corresponding author. Email: adam.hartland@waikato.ac.nz

Statistical Analysis

Table 5 S5.1 Average concentrations ± standard deviation, minimum and maximum of the variables of TN, TP, Fe, Mn and TOC

		Wood only	Wood+FeO_x only	Wood+FeO_x+MnO_2
S1	TN mg L^{-1}	58.7 ± 32.8	26.2 ± 26.9	6.95 ± 6.48
S2		341 ± 112	150 ± 329	59.6 ± 108
S3		612 ± 252	93.0 ± 123	110 ± 143
S4		846 ± 222	271 ± 252	166 ± 239
S5		1331 ± 418	147 ± 193	74.7 ± 137
S1-S5		730 ± 543	139 ± 217	82.7 ± 198
	max	2040	1059	834
	min	21.3	0.6	0.0
S1	Fe mg L^{-1}	11.6 ± 3.91	105 ± 64.6	23.7 ± 18.7
S2		10.2 ± 2.66	162 ± 76	90.2 ± 47.1
S3		13.8 ± 3.34	179 ± 121	219 ± 93.2
S4		12.5 ± 2.74	131 ± 97.3	213 ± 55.8
S5		11.7 ± 2.67	80.7 ± 81.4	184 ± 45.7
S1-S5		12.0 ± 3.16	123 ± 95.8	156 ± 89.4
	max	20.7	317	336
	min	6.90	5.78	6.44
S1	Mn mg L^{-1}	4.93 ± 0.94	3.58 ± 1.02	236 ± 98.5
S2		5.85 ± 1.18	5.10 ± 1.43	391 ± 144
S3		5.68 ± 1.16	4.28 ± 1.64	387 ± 94.8
S4		6.46 ± 1.18	4.01 ± 1.53	358 ± 99.0
S5		6.28 ± 1.17	2.11 ± 1.83	269 ± 109
S1-S5		5.93 ± 1.23	3.50 ± 1.91	319 ± 124

	max	9.57	7.06	639.14
	min	3.43	0.03	96.01
S1	TP mg L^{-1}	34.4 ± 3.35	1.19 ± 0.20	0.68 ± 0.15
S2		25.1 ± 4.04	1.96 ± 1.34	0.71 ± 0.16
S3		43.5 ± 5.57	2.72 ± 1.12	0.72 ± 0.53
S4		28.0 ± 4.66	0.63 ± 0.20	0.70 ± 0.26
S5		25.7 ± 5.37	1.59 ± 1.02	0.69 ± 0.29
S1-S5		30.4 ± 8.24	1.25 ± 1.10	0.67 ± 0.59
	max	52.1	5.09	3.32
	min	15.7	0.28	0.32
S1	TOC mg L^{-1}	3770 ± 843	595 ± 26.5	1247 ± 231
S2		3762 ± 804	570 ± 21.2	1041 ± 267
S3		3619 ± 827	538 ± 51.9	1154 ± 219
S4		3755 ± 802	813 ± 30.5	1273 ± 229
S5		3405 ± 700	589 ± 26.4	1264 ± 213
S1-S5		1412 ± 794	2495 ± 39.6	731 ± 240
	max	4809	643	1586
	min	2442	440	711

1.1 Univariate Analysis of Variance

Between-Subjects Factors

		Value Label	N
Spike	1.00	Spike_1	141
	2.00	Spike_2	135
	3.00	Spike_3	150
	4.00	Spike_4	150
	5.00	Spike_5	264
Treatment	1.00	Wood Only	280
	2.00	Wood + Fe	280
	3.00	Wood + Fe + Mn	280
Factor	1.00	Fe	174
	2.00	Mn	174
	3.00	NO3	168
	4.00	PO4	174
	5.00	TOC	150

Descriptive Statistics

Dependent Variable: Score

Spike	Treatment	Factor	Mean	Std. Deviation	N
Spike_1	Wood Only	Fe	11.6333	1.39344	9
		Mn	4.9256	.34370	9
		NO3	58.7200	13.61688	10
		PO4	34.4222	1.75555	9
		TOC	3770.4100	77.74905	10
		Total	824.4709	1548.59163	47
	Wood + Fe	Fe	104.6400	31.24382	9
		Mn	3.5811	.65539	9
		NO3	26.1700	17.21537	10
		PO4	1.1889	.09280	9
		TOC	595.1100	18.73330	10
		Total	153.1381	235.83849	47
	Wood + Fe + Mn	Fe	23.7278	14.37778	9
		Mn	235.4444	37.28308	9
		NO3	6.9500	6.54612	10
		PO4	.6889	.15366	9
		TOC	1247.1200	34.91176	10
		Total	316.5840	497.18943	47
	Total	Fe	46.6670	46.20549	27
		Mn	81.3170	112.97187	27
		NO3	30.6133	25.20165	30
		PO4	12.1000	16.11597	27
		TOC	1870.8800	1393.54832	30
		Total	431.3977	984.75649	141
Spike_2	Wood Only	Fe	10.2267	.52245	9
		Mn	5.8456	.45211	9
		NO3	340.7667	81.67126	9
		PO4	25.1556	3.79576	9
		TOC	3761.9778	51.30338	9
		Total	828.7944	1489.26735	45
	Wood + Fe	Fe	162.1211	8.85527	9

		Mn	5.0967	.43139	9
		NO3	150.2333	337.54730	9
		PO4	1.9667	.20000	9
		TOC	569.5889	14.14164	9
		Total	177.8013	254.54805	45
		Fe	90.1711	14.96173	9
		Mn	391.3333	29.20188	9
		NO3	59.5667	91.02368	9
	Wood + Fe + Mn	PO4	.5889	.09280	9
		TOC	1040.7111	16.92413	9
		Total	316.4742	393.15960	45
		Fe	87.5063	63.95306	27
		Mn	134.0919	186.06922	27
		NO3	183.5222	232.20846	27
	Total	PO4	9.2370	11.67687	27
		TOC	1790.7593	1434.20754	27
		Total	441.0233	937.69731	135
		Fe	13.7980	.87333	10
		Mn	5.6790	.67270	10
		NO3	611.6200	33.52793	10
	Wood Only	PO4	43.4800	5.20402	10
		TOC	3618.9900	97.13107	10
		Total	858.7134	1413.91521	50
		Fe	179.0990	8.36429	10
		Mn	4.2810	.29853	10
		NO3	93.0500	117.83128	10
	Wood + Fe	PO4	2.7100	.98933	10
		TOC	537.8300	24.97572	10
		Total	163.3940	206.84938	50
Spike_3		Fe	218.9930	11.20334	10
		Mn	387.2000	29.09295	10
		NO3	109.6600	137.41513	10
	Wood + Fe + Mn	PO4	2.0900	.50211	10
		TOC	1154.3500	78.39755	10
		Total	374.4586	420.09239	50
		Fe	137.2967	90.68753	30
		Mn	132.3867	183.97711	30
		NO3	271.4433	265.36918	30
	Total	PO4	16.0933	19.91982	30
		TOC	1770.3900	1355.78141	30
		Total	465.5220	902.68530	150

		Fe	12.4880	1.07868	10
		Mn	6.4580	.58585	10
		NO3	846.3600	65.43044	10
	Wood Only	PO4	28.0000	3.84708	10
		TOC	3754.7600	192.14241	10
		Total	929.6132	1466.05959	50
		Fe	131.4950	10.92478	10
		Mn	4.0080	.34724	10
		NO3	271.2300	133.23190	10
	Wood + Fe	PO4	.6400	.08433	10
		TOC	595.0400	12.85580	10
		Total	200.4826	230.44380	50
Spike_4		Fe	213.3240	17.23257	10
		Mn	357.6000	26.28561	10
		NO3	165.9700	245.58191	10
	Wood + Fe + Mn	PO4	1.0500	.16499	10
		TOC	1273.3000	30.15596	10
		Total	402.2488	467.12133	50
		Fe	119.1023	84.63643	30
		Mn	122.6887	169.58393	30
		NO3	427.8533	343.59645	30
	Total	PO4	9.8967	13.19654	30
		TOC	1874.3667	1385.64450	30
		Total	510.7815	944.02206	150
		Fe	11.6990	1.07262	20
		Mn	6.2755	.73585	20
		NO3	1330.5176	366.00781	17
	Wood Only	PO4	25.7100	4.49396	20
		TOC	3430.4818	439.84822	11
		Total	695.7703	1179.51727	88
Spike_5		Fe	80.7005	29.93934	20
		Mn	2.1345	1.01313	20
		NO3	147.2000	178.84509	17
	Wood + Fe	PO4	.5300	.11743	20
		TOC	584.2091	39.28339	11
		Total	120.4091	201.18617	88
		Fe	184.0515	30.62427	20
	Wood + Fe + Mn	Mn	269.3500	57.82576	20
		NO3	74.7235	136.05144	17
		PO4	.8500	.19331	20

		TOC	1242.9727	101.31822	11
		Total	273.0458	388.59650	88
		Fe	92.1503	75.44879	60
		Mn	92.5867	130.25998	60
		NO3	517.4804	630.11459	51
	Total	PO4	9.0300	12.16579	60
		TOC	1752.5545	1261.12972	33
		Total	363.0751	763.55786	264
		Fe	11.9583	1.46806	58
		Mn	5.9279	.78337	58
		NO3	729.5125	513.85960	56
	Wood Only	PO4	30.4345	7.83831	58
		TOC	3660.6940	260.64502	50
		Total	809.6071	1383.75904	280
		Fe	122.7724	44.31823	58
		Mn	3.5117	1.29291	58
		NO3	138.5536	192.41016	56
	Wood + Fe	PO4	1.2500	.93269	58
		TOC	576.6480	32.01674	50
		Total	157.1014	222.91738	280
Total		Fe	155.6774	73.72349	58
		Mn	318.5517	74.44960	58
		NO3	82.7179	148.65791	56
	Wood + Fe + Mn	PO4	1.0328	.56456	58
		TOC	1195.7360	103.40592	50
		Total	328.5150	428.84629	280
		Fe	96.8027	78.99499	174
		Mn	109.3305	154.40607	174
		NO3	316.9280	438.83874	168
	Total	PO4	10.9057	14.57500	174
		TOC	1811.0260	1346.33521	150
		Total	431.7412	889.27072	840

Levene's Test of Equality of Error Variances[a]

Dependent Variable: Score

F	df1	df2	Sig.

10.114	74	765	.000

Tests the null hypothesis that the error variance of the dependent variable is equal across groups.

a. Design: Intercept + Spike + Treatment + Factor + Spike * Treatment + Spike * Factor + Treatment * Factor + Spike * Treatment * Factor

Tests of Between-Subjects Effects

Dependent Variable: Score

Source	Type III Sum of Squares	df	Mean Square	F	Sig.
Corrected Model	655667354.818[a]	74	8860369.660	867.234	.000
Intercept	168768614.786	1	168768614.786	16518.708	.000
Spike	1027999.688	4	256999.922	25.155	.000
Treatment	69293118.344	2	34646559.172	3391.130	.000
Factor	349820278.391	4	87455069.598	8559.913	.000
Spike * Treatment	689700.510	8	86212.564	8.438	.000
Spike * Factor	4924172.725	16	307760.795	30.123	.000
Treatment * Factor	217216604.426	8	27152075.553	2657.587	.000
Spike * Treatment * Factor	7660026.373	32	239375.824	23.430	.000
Error	7815865.065	765	10216.817		
Total	820059576.644	840			
Corrected Total	663483219.883	839			

a. R Squared = .988 (Adjusted R Squared = .987)

Estimated Marginal Means

Spike * Treatment * Factor

Dependent Variable: Score

Spike	Treatment	Factor	Mean	Std. Error	95% Confidence Interval	
					Lower Bound	Upper Bound
	Wood Only	Fe	11.633	33.693	-54.508	77.775

		Mn	4.926	33.693	-61.216	71.067
		NO3	58.720	31.964	-4.027	121.467
		PO4	34.422	33.693	-31.719	100.563
		TOC	3770.410	31.964	3707.663	3833.157
		Fe	104.640	33.693	38.499	170.781
		Mn	3.581	33.693	-62.560	69.722
Spike_1	Wood + Fe	NO3	26.170	31.964	-36.577	88.917
		PO4	1.189	33.693	-64.952	67.330
		TOC	595.110	31.964	532.363	657.857
		Fe	23.728	33.693	-42.413	89.869
		Mn	235.444	33.693	169.303	301.586
	Wood + Fe + Mn	NO3	6.950	31.964	-55.797	69.697
		PO4	.689	33.693	-65.452	66.830
		TOC	1247.120	31.964	1184.373	1309.867
		Fe	10.227	33.693	-55.915	76.368
		Mn	5.846	33.693	-60.296	71.987
	Wood Only	NO3	340.767	33.693	274.625	406.908
		PO4	25.156	33.693	-40.986	91.297
		TOC	3761.978	33.693	3695.837	3828.119
		Fe	162.121	33.693	95.980	228.262
		Mn	5.097	33.693	-61.045	71.238
Spike_2	Wood + Fe	NO3	150.233	33.693	84.092	216.375
		PO4	1.967	33.693	-64.175	68.108
		TOC	569.589	33.693	503.448	635.730
		Fe	90.171	33.693	24.030	156.312
		Mn	391.333	33.693	325.192	457.475
	Wood + Fe + Mn	NO3	59.567	33.693	-6.575	125.708
		PO4	.589	33.693	-65.552	66.730
		TOC	1040.711	33.693	974.570	1106.852
		Fe	13.798	31.964	-48.949	76.545
		Mn	5.679	31.964	-57.068	68.426
	Wood Only	NO3	611.620	31.964	548.873	674.367
		PO4	43.480	31.964	-19.267	106.227
		TOC	3618.990	31.964	3556.243	3681.737
Spike_3		Fe	179.099	31.964	116.352	241.846
		Mn	4.281	31.964	-58.466	67.028
	Wood + Fe	NO3	93.050	31.964	30.303	155.797
		PO4	2.710	31.964	-60.037	65.457
		TOC	537.830	31.964	475.083	600.577

		Fe	218.993	31.964	156.246	281.740
		Mn	387.200	31.964	324.453	449.947
	Wood + Fe + Mn	NO3	109.660	31.964	46.913	172.407
		PO4	2.090	31.964	-60.657	64.837
		TOC	1154.350	31.964	1091.603	1217.097
		Fe	12.488	31.964	-50.259	75.235
		Mn	6.458	31.964	-56.289	69.205
	Wood Only	NO3	846.360	31.964	783.613	909.107
		PO4	28.000	31.964	-34.747	90.747
		TOC	3754.760	31.964	3692.013	3817.507
		Fe	131.495	31.964	68.748	194.242
		Mn	4.008	31.964	-58.739	66.755
Spike_4	Wood + Fe	NO3	271.230	31.964	208.483	333.977
		PO4	.640	31.964	-62.107	63.387
		TOC	595.040	31.964	532.293	657.787
		Fe	213.324	31.964	150.577	276.071
		Mn	357.600	31.964	294.853	420.347
	Wood + Fe + Mn	NO3	165.970	31.964	103.223	228.717
		PO4	1.050	31.964	-61.697	63.797
		TOC	1273.300	31.964	1210.553	1336.047
		Fe	11.699	22.602	-32.670	56.068
		Mn	6.276	22.602	-38.093	50.644
	Wood Only	NO3	1330.518	24.515	1282.393	1378.642
		PO4	25.710	22.602	-18.659	70.079
		TOC	3430.482	30.476	3370.655	3490.309
		Fe	80.700	22.602	36.332	125.069
		Mn	2.134	22.602	-42.234	46.503
Spike_5	Wood + Fe	NO3	147.200	24.515	99.075	195.325
		PO4	.530	22.602	-43.839	44.899
		TOC	584.209	30.476	524.382	644.036
		Fe	184.052	22.602	139.683	228.420
		Mn	269.350	22.602	224.981	313.719
	Wood + Fe + Mn	NO3	74.724	24.515	26.599	122.848
		PO4	.850	22.602	-43.519	45.219
		TOC	1242.973	30.476	1183.146	1302.800

1.2 Significance difference between nitrate pre-conditioning stages

Post Hoc Tests

Spike

Multiple Comparisons

Dependent Variable: Score

Tukey HSD

(I) Spike	(J) Spike	Mean Difference (I-J)	Std. Error	Sig.	95% Confidence Interval	
					Lower Bound	Upper Bound
Spike_1	Spike_2	-9.6257	12.17127	.933	-42.9055	23.6542
	Spike_3	-34.1243*	11.85630	.033	-66.5430	-1.7057
	Spike_4	-79.3839*	11.85630	.000	-111.8025	-46.9653
	Spike_5	68.3226*	10.54323	.000	39.4943	97.1509
Spike_2	Spike_1	9.6257	12.17127	.933	-23.6542	42.9055
	Spike_3	-24.4987	11.99134	.247	-57.2865	8.2892
	Spike_4	-69.7582*	11.99134	.000	-102.5461	-36.9703
	Spike_5	77.9483*	10.69487	.000	48.7053	107.1912
Spike_3	Spike_1	34.1243*	11.85630	.033	1.7057	66.5430
	Spike_2	24.4987	11.99134	.247	-8.2892	57.2865
	Spike_4	-45.2595*	11.67151	.001	-77.1729	-13.3462
	Spike_5	102.4469*	10.33500	.000	74.1880	130.7059
Spike_4	Spike_1	79.3839*	11.85630	.000	46.9653	111.8025
	Spike_2	69.7582*	11.99134	.000	36.9703	102.5461
	Spike_3	45.2595*	11.67151	.001	13.3462	77.1729
	Spike_5	147.7065*	10.33500	.000	119.4475	175.9654
Spike_5	Spike_1	-68.3226*	10.54323	.000	-97.1509	-39.4943

	Spike_2	-77.9483*	10.69487	.000	-107.1912	-48.7053
	Spike_3	-102.4469*	10.33500	.000	-130.7059	-74.1880
	Spike_4	-147.7065*	10.33500	.000	-175.9654	-119.4475

Based on observed means.
The error term is Mean Square(Error) = 10216.817.
*. The mean difference is significant at the .05 level.

Treatment

Multiple Comparisons

Dependent Variable: Score
Tukey HSD

(I) Treatment	(J) Treatment	Mean Difference (I-J)	Std. Error	Sig.	95% Confidence Interval	
					Lower Bound	Upper Bound
Wood Only	Wood + Fe	652.5058*	8.54267	.000	632.4452	672.5664
	Wood + Fe + Mn	481.0922*	8.54267	.000	461.0316	501.1528
Wood + Fe	Wood Only	-652.5058*	8.54267	.000	-672.5664	-632.4452
	Wood + Fe + Mn	-171.4136*	8.54267	.000	-191.4742	-151.3530
Wood + Fe + Mn	Wood Only	-481.0922*	8.54267	.000	-501.1528	-461.0316
	Wood + Fe	171.4136*	8.54267	.000	151.3530	191.4742

Based on observed means.
The error term is Mean Square(Error) = 10216.817.
*. The mean difference is significant at the .05 level.

Homogeneous Subsets

Score

Tukey HSD[a,b]

Treatment	N	Subset		
		1	2	3
Wood + Fe	280	157.1014		
Wood + Fe + Mn	280		328.5150	
Wood Only	280			809.6071
Sig.		1.000	1.000	1.000

Means for groups in homogeneous subsets are displayed.
Based on observed means.
The error term is Mean Square(Error) = 10216.817.
a. Uses Harmonic Mean Sample Size = 280.000.
b. Alpha = .05.

Factor

1.3 Significance difference between the variables

Multiple Comparisons

Dependent Variable: Score

Tukey HSD

(I) Factor	(J) Factor	Mean Difference (I-J)	Std. Error	Sig.	95% Confidence Interval	
					Lower Bound	Upper Bound
Fe	Mn	-12.5278	10.83673	.776	-42.1586	17.1030
	NO3	-220.1253*	10.93306	.000	-250.0195	-190.2311
	PO4	85.8970*	10.83673	.000	56.2661	115.5278
	TOC	-1714.2233*	11.26186	.000	-1745.0165	-1683.4301
Mn	Fe	12.5278	10.83673	.776	-17.1030	42.1586
	NO3	-207.5975*	10.93306	.000	-237.4917	-177.7033
	PO4	98.4247*	10.83673	.000	68.7939	128.0555
	TOC	-1701.6955*	11.26186	.000	-1732.4888	-1670.9023
NO3	Fe	220.1253*	10.93306	.000	190.2311	250.0195
	Mn	207.5975*	10.93306	.000	177.7033	237.4917
	PO4	306.0222*	10.93306	.000	276.1280	335.9164
	TOC	-1494.0980*	11.35458	.000	-1525.1448	-1463.0513
PO4	Fe	-85.8970*	10.83673	.000	-115.5278	-56.2661
	Mn	-98.4247*	10.83673	.000	-128.0555	-68.7939
	NO3	-306.0222*	10.93306	.000	-335.9164	-276.1280
	TOC	-1800.1203*	11.26186	.000	-1830.9135	-1769.3270
TOC	Fe	1714.2233*	11.26186	.000	1683.4301	1745.0165
	Mn	1701.6955*	11.26186	.000	1670.9023	1732.4888

NO3	1494.0980*	11.35458	.000	1463.0513	1525.1448
PO4	1800.1203*	11.26186	.000	1769.3270	1830.9135

Based on observed means.

The error term is Mean Square(Error) = 10216.817.

*. The mean difference is significant at the .05 level.

THE UNIVERSITY OF WAIKATO
Te Whare Wānanga o Waikato

Co-Authorship Form

Postgraduate Studies Office
Student and Academic Services Division
Wahanga Ratonga Matauranga Akonga
The University of Waikato
Private Bag 3105
Hamilton 3240, New Zealand
Phone +64 7 838 4439
Website: http://www.waikato.ac.nz/sasd/postgraduate/

This form is to accompany the submission of any PhD that contains research reported in published or unpublished co-authored work. **Please include one copy of this form for each co-authored work.** Completed forms should be included in your appendices for all the copies of your thesis submitted for examination and library deposit (including digital deposit).

Please indicate the chapter/section/pages of this thesis that are extracted from a co-authored work and give the title and publication details or details of submission of the co-authored work.

Elucidating phosphorus removal dynamics in a denitrifying woodchip bioreactor

Nature of contribution by PhD candidate	collaboration on project conception, design and development, sample collection, analysis, interpretation, manuscript writing
Extent of contribution by PhD candidate (%)	90

CO-AUTHORS

Name	Nature of Contribution
Adam Hartland	collaboration on project conception, design and development, interpretation, manuscript editing
Dorisel Torres-Rojas	Collaboration on project conception, design and development, sample collection, manuscript editing
Louis Schipper	Collaboration on design, manuscript editing
Aldrin Rivas	Collaboration on design, sample collection, analysis, manuscript editing
Greg Barkle	Collaboration on design, manuscript editing
Brian Moorhead	Collaboration on design, sample collection, analysis

Certification by Co-Authors

The undersigned hereby certify that:

- the above statement correctly reflects the nature and extent of the PhD candidate's contribution to this work, and the nature of the contribution of each of the co-authors; and

Name	Signature	Date
Adam Hartland		21/11/23.
Dorisel Torres-Rojas	Type text here	14/12/2023
Louis Schipper	Louis Schipper	21/11/23
Aldrin Rivas		21/11/23
Greg Barkle		21/11/2023
Brian Moorhead		21/11/23

THE UNIVERSITY OF WAIKATO
Te Whare Wānanga o Waikato

Co-Authorship Form

Postgraduate Studies Office
Student and Academic Services Division
Wahanga Ratonga Matauranga Akonga
The University of Waikato
Private Bag 3105
Hamilton 3240, New Zealand
Phone +64 7 838 4439
Website: http://www.waikato.ac.nz/sasd/postgraduate/

This form is to accompany the submission of any PhD that contains research reported in published or unpublished co-authored work. **Please include one copy of this form for each co-authored work**. Completed forms should be included in your appendices for all the copies of your thesis submitted for examination and library deposit (including digital deposit).

Please indicate the chapter/section/pages of this thesis that are extracted from a co-authored work and give the title and publication details or details of submission of the co-authored work.

Elucidating phosphorus removal dynamics in a denitrifying woodchip bioreactor

Nature of contribution by PhD candidate	collaboration on project conception, design and development, sample collection, analysis, interpretation, manuscript writing
Extent of contribution by PhD candidate (%)	90

CO-AUTHORS

Name	Nature of Contribution
Rupert Craggs	Collaboration on design, analysis

Certification by Co-Authors

The undersigned hereby certify that:

- the above statement correctly reflects the nature and extent of the PhD candidate's contribution to this work, and the nature of the contribution of each of the co-authors; and

Name	Signature	Date
Rupert Craggs		21/11/23

THE UNIVERSITY OF WAIKATO
Te Whare Wānanga o Waikato

Co-Authorship Form

Postgraduate Studies Office
Student and Academic Services Division
Wahanga Ratonga Matauranga Akonga
The University of Waikato
Private Bag 3105
Hamilton 3240, New Zealand
Phone +64 7 838 4439
Website: http://www.waikato.ac.nz/sasd/postgraduate/

This form is to accompany the submission of any PhD that contains research reported in published or unpublished co-authored work. **Please include one copy of this form for each co-authored work**. Completed forms should be included in your appendices for all the copies of your thesis submitted for examination and library deposit (including digital deposit).

Please indicate the chapter/section/pages of this thesis that are extracted from a co-authored work and give the title and publication details or details of submission of the co-authored work.

Iron–based composites for in–field phosphorus removal from agricultural drainage

Nature of contribution by PhD candidate	Collaboration on project conception, design and development, analysis, interpretation, manuscript editing
Extent of contribution by PhD candidate (%)	90

CO-AUTHORS

Name	Nature of Contribution
Adam Hartland	Collaboration on project conception, design and development, interpretation, manuscript editing
Dorisel Torres-Rojas	Collaboration on project conception, design and development, interpretation, manuscript editing
Sebastian N. Hoepker	Sample analysis
Greg Olsen	Design and development
Rupert Craggs	Collaboration on project conception, design and development, interpretation, manuscript editing

Certification by Co-Authors

The undersigned hereby certify that:

- the above statement correctly reflects the nature and extent of the PhD candidate's contribution to this work, and the nature of the contribution of each of the co-authors; and

Name	Signature	Date
Adam Hartland	Attached	19/12/23
Dorisel Torres-Rojas	Type text here	14/12/2023
Sebastian N. Hoepker		5/12/23
Greg Olsen		29/11/23
Rupert Craggs		21/11/23

THE UNIVERSITY OF WAIKATO
Te Whare Wānanga o Waikato

Co-Authorship Form

Postgraduate Studies Office
Student and Academic Services Division
Wahanga Ratonga Matauranga Akonga
The University of Waikato
Private Bag 3105
Hamilton 3240, New Zealand
Phone +64 7 838 4439
Website: http://www.waikato.ac.nz/sasd/postgraduate/

This form is to accompany the submission of any PhD that contains research reported in published or unpublished co-authored work. **Please include one copy of this form for each co-authored work.** Completed forms should be included in your appendices for all the copies of your thesis submitted for examination and library deposit (including digital deposit).

Please indicate the chapter/section/pages of this thesis that are extracted from a co-authored work and give the title and publication details or details of submission of the co-authored work.

Phosphorus removal by iron oxides in lab-scale denitrifying woodchip bioreactors with and without manganese dioxide

Nature of contribution by PhD candidate	Collaboration on project conception, design and development, sample collection, analysis, interpretation, and writing
Extent of contribution by PhD candidate (%)	90

CO-AUTHORS

Name	Nature of Contribution
Adam Hartland	Collaboration on project conception, design and development, interpretation, and manuscript editing
Dorisel Torres-Rojas	Collaboration on project conception, design and development, analysis, and interpretation

Certification by Co-Authors

The undersigned hereby certify that:

- the above statement correctly reflects the nature and extent of the PhD candidate's contribution to this work, and the nature of the contribution of each of the co-authors; and

Name	Signature	Date
Adam Hartland	A Hartland	19/12/23
Dorisel Torres-Rojas	Dorisel Torres-Rojas	14/12/2023